Master Thesis

Characterisation of Cold and Isolated Biomolecules

by

Jan Horlebein

born in Erbach (Odenwald)

in the group of

Prof. Dr. Gert von Helden

at the

Department of Molecular Physics
Fritz Haber Institute of the Max Planck Society

Student ID:	5378579
First Examiner:	Prof. Dr. Gert von Helden
Second Examiner:	Prof. Dr. Kevin Pagel
Supervisor:	Maike Lettow, M.Sc.
Date of submission:	10th November, 2021

By three methods we may learn wisdom: first, by reflection, which is the noblest; second, by imitation, which is the easiest; third, by experience, which is the most bitter. - Confucius

Abstract

Gas phase infrared (IR) spectroscopy has emerged as a powerful method to study (bio)molecules in the absence of influences from external factors in the liquid or solid phase. However, the low number density of analytes in the gas phase requires a change in measurement principle. Instead of monitoring the attenuation of IR radiation upon interaction with the analyte, the effect of the irradiation on the analyte has to be monitored. Different concepts to realise this so called *action spectroscopy* have been realised to date.

In this thesis, a novel instrument to perform gas phase IR spectroscopy is introduced. Based on an ion mobility mass spectrometer conceived earlier, the instrument aims to combine the complementary techniques of ion mobility spectrometry and mass spectrometry for a sophisticated selection of ions for IR spectroscopy. After ion mobility and mass selections, ions are rapidly cooled to the temperature of a cryogenic ion trap by collisions with a buffer gas. The loss of energy upon colliding with the buffer gas does not only enable trapping of ions in the cryogenic ion trap, the low temperatures in the cryogenic ion trap also allows for the attachment of molecular tags. These molecular tags serve as messengers for the subsequent messenger tagging IR spectroscopy. A pulsed beam of cooled and tagged ions will be created upon ejection from the cryogenic ion trap and is subsequently overlaid with the IR radiation provided by the Fritz Haber Institute Free Electron Laser (FHI FEL). By scanning the wavelength of the FEL, the different vibrational modes of the ions can be probed. Excitation of vibrational bands in the analyte can be detected as the depletion of a messenger tag: absorption of a resonant photon is dissipated throughout the molecule by intramolecular vibrational energy redistribution and subsequently to the surrounding by the loss of an attached messenger. The ratio of messenger tagged and messenger tag depleted ions can be determined from using time-of-flight mass spectrometry.

In this work, individual parts of *iMob 2.0* are explained in detail. The systematic characterisation of the cryogenic ion trap as a central part of the machines initial commissioning will be highlighted. Furthermore, the performance and potential of messenger tagging IR spectroscopy will be evaluated using the pentapeptide leucine-enkephalin (LEK). In comparison to IR spectra obtained by two different types of action spectroscopy, namely IR multiphoton dissociation (IRMPD) spectroscopy and infrared (IR) spectroscopy using helium nanodroplets, the IR spectrum obtained from the messenger tagging approach can be benchmarked. In addition to LEK, two isomeric trisaccharides of the Lewis antigen class will be subject to IR spectroscopic experiments. The migration of inherent fucose moieties in these biologically relevant molecules remains puzzling and the ability to distinguish ions of the same mass by ion mobility spectrometry holds the promise to selectively shed light onto the observed rearrangement.

Zusammenfassung

Infrarot (IR) Spektroskopie in der Gasphase etabliert sich zunehmend auch in der Analyse von großen (Bio)Molekülen. Dabei liegt der Vorteil gegenüber IR Spektroskopie in Lösung oder am Feststoff darin, dass externe Störeinflüsse besser vermieden werden können. Ein inhärentes Problem von Gasphasen IR Spektroskopie ist jedoch die geringe Teilchendichte. Zur Überwindung dieser Problematik hat sich das Prinzip der Wirkungsspektroskopie durchgesetzt. Dabei wird nicht der Einfluss der Probe auf das eingestrahlte Licht verfolgt, sondern es wird beobachtet welchen Einfluss das Licht auf die Strahlung hat.

Im Rahmen dieser Arbeit wird ein Gerät beschrieben, das eine Umsetzungsmöglichkeit zur Wirkungsspektroskopie realisiert. Dabei wurde ein schon bestehendes Messgerät für Ionenmobilitäts- und Massenspektrometrie dahingehend erweitertet, dass es für Reporter Spektroskopie geeignet ist. Die Selektion von Ionen mittels Ionenmobilitäts- und Massenspektrometrie ist dabei komplementär und erlaubt Spektroskopie an sehr selektierten Ionen. Dafür werden diese in einer kalten Ionenfalle durch die Kollision mit einem Puffergas abgebremst und auf die Temperatur der Falle gekühlt. Dabei ermöglichen die niedrigen Temperaturen in der Ionenfalle das nicht-kovalente Anlagern von inerten Reportermolekülen, welche für das Messprinzip essentiell sind. Durch gepulste Ejektion aus der Ionenfalle entsteht ein Ionenstrahl, welcher mit der IR Strahlung des Freien Elektronen Lasers (FEL) des Fritz Haber Instituts (FHI) überlagert werden kann. Dabei führt das resonante Anregen von Schwingungsbanden in den Molekülionen dazu, dass, durch Umverteilung der Schwingungsenergie, das Reportermolekül abgelöst wird. Dieser Verlust des Reportermoleküls lasst sich in einem Flugzeitmassenspektrometer detektieren und erlaubt aus dem Verhältnis zwischen Ionen mit und ohne Reportermolekül bei einer definierten Wellenzahl ein IR Spektrum zu ermitteln.

In dieser Arbeit werden die einzelnen Bauteile des *iMob 2.0* beschrieben und in das Experiment eingeordnet. Es folgt eine systematische Evaluation einiger Parameter der kalten Ionenfalle, die sozusagen das Herzstück der Apparatur darstellt. Um das Potential der IR Spektroskopie am iMob 2.0 abschätzen zu können, wird das Pentapeptide Leucin-Enkephalin benutzt, welches bereits mit zwei anderen Varianten der Wirkungsspektroskopie, IR Vielphotonen-Dissoziation Spektroskopie und IR Spektroskopie in Helium Nanotröpfchen, untersucht wurde. Außerdem werden Trisaccharide aus der Gruppe der Lewis Antigen hinsichtlich der beobachteten Umlagerung von Fucose-Einheiten untersucht. Da noch nicht verstanden ist, wie diese Migration im Detail funktioniert, ist das iMob 2.0 durch IR Spektroskopie nach Selektion isomerer Verbindungen aufgrund unterschiedlicher Ionenmobilitäten dazu prädestiniert das Verständnis dieses Phänomens zu erweitern.

Contents

List of Figures

Abbreviations

ATD	arrival time distribution
BG-H2	blood group human 2
CAD	computer-aided design
CCS	collision cross section
CID	collision-induced dissociation
CT	cold trap
DC	direct current
DNA	deoxyribonucleic acid
ESI	electrospray ionisation
nESI	nano-electrospray ionisation
FEL	free-electron laser
FELIX	Free-Electron Laser for Infrared eXperiments
FHI	Fritz Haber Institute
FWHM	full width at half maximum
HED	high energy dynode
HPLC	high pressure liquid chromatography
IMS	ion mobility spectrometry
IR	infrared
IRL	internal residue loss
IRPD	infrared photon dissociation
IRMPD	infrared multiphoton dissociation
IUPAC	International Union of Pure and Applied Chemistry
IVR	intramolecular vibrational energy redistribution
LEK	Leucine-enkephalin
Le	Lewis antigen
MALDI	matrix-assisted laser desorption/ionisation
MS	mass spectrometry
MPG	Max Planck Society
m/z	mass-to-charge ratio
nESI	nano-electrospray ionisation
OPO	optical parametric oscillator
PCB	Printed Circuit Board
PEEK	polyether ether ketone
PTFE	polytetrafluorethylen
RF	radio frequency
SNFG	symbol nomenclature for glycans
ToF	time-of-flight
UV	ultraviolet

Adduct ions observed in mass spectrometry experiments are commonly denoted as $[X+M]^{n+}$, where M represents the neutral molecule, X the ion of interest, and n the overall charge of the ion.

1. Towards the Analysis of Isolated Biomolecules

Looking back in history, technological and scientific advances often accompany each other. Refined methodology and increasing abilities to manufacture scientific instruments have allowed mankind to explore phenomena invisible to the human eye before. While this contributed to discoveries in many fields, the shift from a macroscopic to a microscopic and later to a molecular and atomistic perspective has significantly extended the tool box of scientists studying the principles of life. Following discoveries in the late 19^{th} and the 20^{th} century, a variety of methods for the determination of biomolecular structure have evolved and enabled scientists to understand life on a molecular level. To deepen the understanding on the molecular level, knowledge about the structure of molecules involved in biological processes allows for conclusions about the function of the molecule. In this regard, X-ray crystallography has been the working horse for structural biologists for many decades, and is nowadays complemented by magnetic resonance techniques and many flavours of microscopy.[1–3] At about the same time nuclear magnetic resonance emerged as a powerful tool for biologists, instrumentational innovation equally enabled the analysis of biomolecules in the gas phase.

Traditional ion sources did not allow for the transfer of large and delicate biomolecules to the gas phase. Only the advent of soft ionisation sources, namely electrospray ionisation (ESI) and matrix-assisted laser desorption/ionisation (MALDI), has enabled for the study of biomolecules in the absence of external influences in vacuum.[4,5] Under native conditions, low charge states of the molecule may be retained upon transfer from the liquid to the gas phase.[6] These the low charge states usually resemble the biologically important structures and can subsequently be studied in the absence of influences from solvents, ions or the interaction with other molecules.[7]

Out of many, mass spectrometry is the most established experimental method to study biomolecules in the gas phase and has been successfully combined with both, ESI and MALDI sources from their invention.[4,5] While mass spectrometry can already provide a myriad of information about the structure of analytes, it can be easily complemented by orthogonal techniques, such as ion mobility spectrometry (IMS) or high pressure liquid chromatography (HPLC).[8] Thereby, it may enable even more sophisticated insights into structure and function of molecules. Another experimental technique which allows to assess molecular structure or identify structural motifs is vibrational spectroscopy.[9] Despite the challenges involved to conduct IR spectroscopy, one flavour of vibrational spectroscopy, in the gas phase, the combined investigation of biomolecules using mass spectrometry and IR spectroscopy has gained popularity over the last two decades.[10–12] To

overcome the challenges of IR spectroscopy in the gas phase, different instrument designs have been proposed up to date.[13,14]

Here, a report on advances in the instrumentation to conduct molecular experiments in the gas phase is given. An existing ion mobility mass spectrometer was extended using three quadrupolar deflectors, a cryogenic ion trap, a hexapole, and a ToF mass spectrometer as well as various ion optics for an improved ion trajectory. This extension has been implemented with the intention to facilitate messenger tagging IR spectroscopy. By implementing a cryogenic ion trap of novel design, analyte ions are sufficiently cooled and messenger tagged after they have been selected based on their ion mobility and mass. Subsequently, they are interrogated by IR light. The ion trap used in the experimental setup here runs on a continuous duty cycle which favours a more simple mode of operation compared to instrumentation reported earlier.[15,16] High photon flux IR radiation is provided by the Fritz Haber Institute (FHI) free-electron laser (FEL) which enables to scan over a range of wavenumbers in the fingerprint region. Subsequently, the influence of the incoming radiation on the analyte ions is monitored by comparing the messenger tagging pattern of the analyte ions prior to and after IR irradiation using the ToF mass spectrometer.

2. Fundamentals

The experimental approach taken in this work combines several powerful yet complementary techniques to enable the thorough investigation of biomolecules in the gas phase: ion mobility spectrometry (IMS), mass spectrometry (MS) and messenger tagging IR spectroscopy. While IMS and MS are used to select or detect analytes based on their conformation and mass-to-charge ratio (m/z), IR spectroscopy is employed to probe the structural motifs of the analyte. Below, the individual concepts will be explained in greater detail.

Mass spectrometry has its limitations when it comes to distinguishing structures of the same molecular weight. In this regard, it is beneficial to make use of an additional, orthogonal separation step to facilitate the analysis of complex samples. One strategy to achieve this, is the implementation of an IMS separation step prior to MS analysis. Ion mobility allows for an additional separation in the gas phase and can be realised by including a cell or tube filled with an inert gas in the mass spectrometer[17,18]. Applying a weak electric field to the cell lets ion traverse through the cell after ionisation. Once injected into the cell, ions with a small cross section and high charge traverse the cell faster than those with a more extended cross section and lower charge which interact more extensively with the buffer gas and less with the electric field[19].

2.1. Gas Phase Spectroscopy

2.1.1. Ion Mobility Spectrometry

While ion mobility spectrometry (IMS) has gained wider acceptance for the investigation of large biomolecules only recently, its concepts date back to the late 19$^{\text{th}}$ century and experiments by Thomson and Rutherford.[20] The underlying theory has been formulated by Langevin and is still considered as the theoretical foundation of diffusive processes in gases.[19,21]

Today, different concepts to realise IMS are known, of which drift tube IMS is a the simplest implementation. To realise this, a drift tube or cell is filled with an inert buffer gas and injected molecular ions are separated by their different velocities when applying a weak electric field to the drift cell. The drift velocity ν_{D} of a given ion species is directly proportional to the applied electric field E

$$\nu_{\mathrm{D}} = K \cdot E \tag{2.1}$$

using the ion mobility K as constant. Factors contributing to the ion mobility K are rooted in the structure of the molecule, however experimental conditions and the buffer gas play a crucial role, too. Thus, separation of ions in ion mobility spectrometry relies on differences in ion mobilities. In order to consider an electric field weak, the induced velocity ν_{D} must be small compared to the diffusive motion of the molecular ions in the buffer gas. Under the conditions described, ions are in thermal equilibirium with the buffer gas and the ion mobility K can be related to the ion's diffusion coefficient D using Einstein's relation:

$$K = \frac{z \cdot e \cdot D}{k_{\mathrm{B}} \cdot T} = \frac{q \cdot D}{k_{\mathrm{B}} \cdot T} \tag{2.2}$$

where q is the total charge of the ion, k_{B} the Boltzmann constant and T the temperature of the buffer gas.
For increased comparability of ion mobilities under varying environmental conditions, normalisation using standard temperature T_0 and pressure P_0 is common:

$$K_0 = K \cdot \frac{P}{P_0} \cdot \frac{T_0}{T} \tag{2.3}$$

Measuring drift times t_{D} of an ion at different drift voltages of the weak electric field allows to determine the ion mobility of the respective ion. This ion mobility can be correlated to the ion's size using kinetic theory as demonstrated by Revercomb and Mason.[19] This is commonly expressed in the Mason-Schamp equation, allowing the determination of the collision cross section (CCS) Ω as measure of the surface area opposing the drift motion of an ion[19]:

$$K_0 = \frac{3 \cdot z \cdot e}{16 \cdot N} \cdot \sqrt{\frac{2 \cdot \pi}{\mu \cdot k_{\mathrm{B}} \cdot T}} \cdot \frac{1}{\Omega} \tag{2.4}$$

Here, z is the charge of the ion, e the elemantary charge, N the number density of the drift gas and, μ the reduced mass of the ion and the drift gas.

A schematic illustration of the described principles of ion mobility spectrometry is given in Fig. 2.1. A mixture of analytes is separated based on their different mobility in the ion mobility drift cell filled with helium. Recording the arrival time distribution (ATD) of the ions at different drift voltages allows for the collision cross section to be determined as described above.

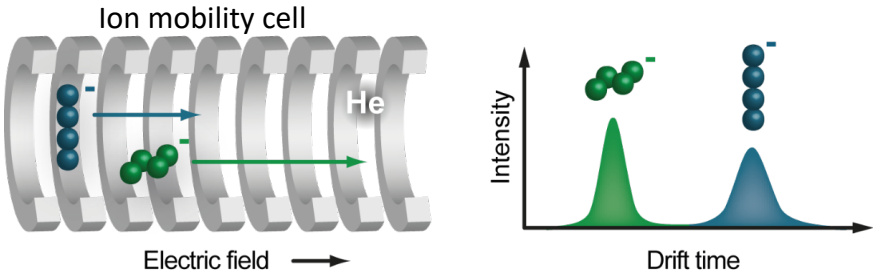

Fig. 2.1.: Schematic illustration of the separation principle in a drift tube ion mobility spectrometer. After ionisation, ions are injected into a buffer gas filled drift tube and traverse the tube under the influence of a constant electric field. Ions with a compact shape traverse the cell faster than those with an extended shape. This results in different drift times for different species.

2.1.2. Infrared Spectroscopy

Infrared (IR) spectroscopy is one flavour of vibrational spectroscopy routinely applied in laboratories to gain insight into the structural elements of unknown samples, identify compounds by their fingerprint or investigate the conformation of a molecule. For a molecule to feature modes of vibration which are IR active, the vibrational mode induces a change in the electric dipole of the molecule. This is commonly referred to as a *selection rule.*[22] The number of vibrational modes of every molecule of N atoms can be deduced from its degrees of freedom: for linear molecules, the number of independent vibrational modes is $3N-5$, for non-linear molecules $3N-6$. If the energy of incoming photons matches the energy of a vibrational transition which is IR active, photons are absorbed and the matching vibrational mode is excited. IR radiation in the regime used for IR spectroscopy is quantified by its wavenumber $\tilde{\nu}$ in reciprocal centimetres (cm^{-1}). In contrast to wavelengths, wavenumbers scale linearly with the energy.

Routinely, IR spectroscopy is performed, either in liquid or solid state in the mid-IR range from 400 to 4000 cm^{-1}, by monitoring the attenuation of an IR light beam before and after traversing a sample of length l, containing molecules at a number density n. Using the Beer-Lambert law, the absorption of the analysed sample can be determined from

$$I(\tilde{\nu}) = I_0(\tilde{\nu}) \cdot e^{-\sigma(\tilde{\nu}) \cdot L \cdot n} \tag{2.5}$$

where $I_0(\tilde{\nu})$ and $I(\tilde{\nu})$ are the intensities of the light before and after interacting with the sample, respectively, and $\sigma(\tilde{\nu})$ is referred to as the absorption cross section of the sample.

In contrast to the liquid or solid state, absorption spectroscopy of gas phase ions is usually difficult because the product $L \cdot n$ is very small following low number densities at the space charge limit $n_{scl} \approx 10^6$ in the gas phase.[23] By changing the observable, this limitation can be overcome when applying *action spectroscopy* rather then absorption spectroscopy. Instead of monitoring

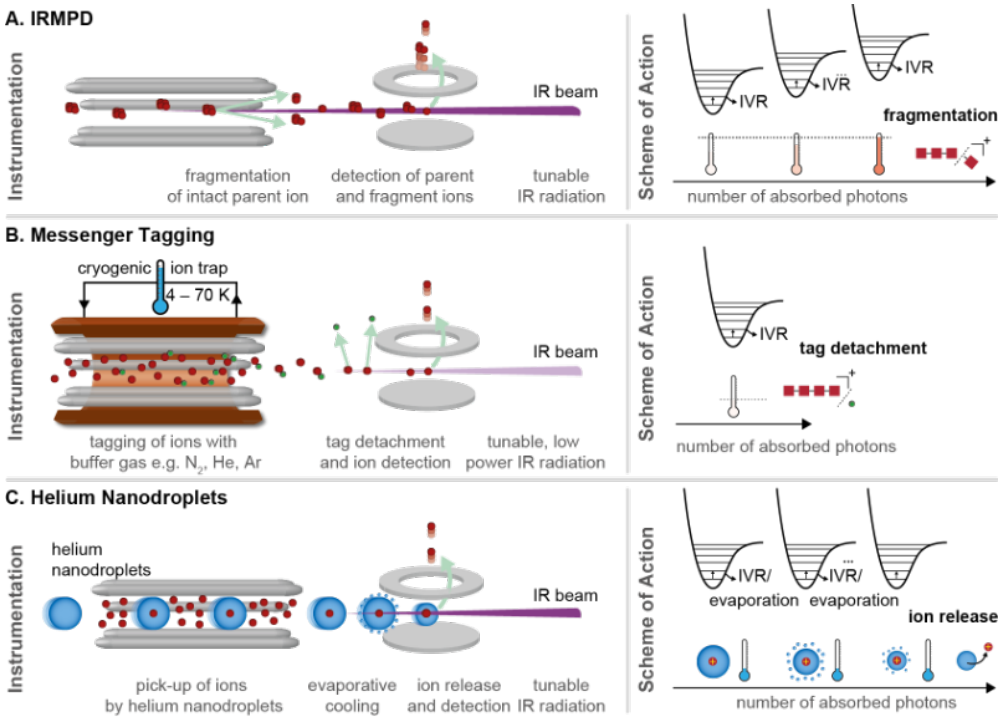

Fig. 2.2.: Different flavours of IR action spectroscopy. a) IR multiphoton dissociation spectroscopy. Multiple resonant IR photons absorbed by a single molecular ion overcome the dissociation threshold of the molecule through energy distribution (intramolecular vibrational energy redistribution (IVR)) and the dissociation fragments are detected in a mass spectrometer. Operational principle of the iMob 1.0 instrument.[13,27] b) Messenger tagging IR spectroscopy. Absorption of a single IR photon leads to the depletion of non-covalently attached messenger tags after IVR. Mass spectrometry allows to monitor the ratio of messenger tagged and messenger tag depleted ions. Measurement principle of iMob 2.0 c) IR spectroscopy in helium nanodroplets. Absorption of resonant IR photons leads to evaporation of the helium matrix as a consequence of energy dissipation after IVR. If the helium nanodroplets become too small, the embedded ion is ejected from the nanodroplet and detected in a mass spectrometer. Realised at the helium nanodroplet machine in the von Helden group. Figure provided by the courtesy of Maike Lettow.

the attenuation of light upon interaction with the sample, the effect of irradiation on the analyte is monitored. In case of resonant IR photons interacting with the molecule, excitation of the molecules can be detected in form of fragmentation, ejection from helium nanodroplets or depletion of a messenger tag.[14,24–26]

One flavour of action spectroscopy applied to biomolecules very early is infrared multiphoton dissociation (IRMPD) spectroscopy (Fig. 2.2 A.).[28,29] During an IRMPD experiment, molecular ions are irradiated with an IR light source and absorb photons if the wavenumber of the photon corresponds to a vibrational mode of the molecule, i.e. is in resonance.[30] In a process known as intramolecular vibrational energy redistribution (IVR) the incoming energy is distributed throughout the molecule on a sub-nanosecond timescale and another photon of the same wavenumber can be absorbed.[31] The sequential absorption of photons will eventually allow the molecule to over-

come the dissociation barrier, and induces the fragmentation of the parent ion.[24] Observing the fragmentation during a wavenumber scan of the IR radiation source by means of mass spectrometry, an IR spectrum can be obtained by recording the number of fragment ions as a function of the wavenumber.

Another realisation of action spectroscopy applied to biomolecules is to monitor the ejection of analyte ions from cryogenic superfluid helium nanodroplets.[11,32,33] After transfer to the gas phase, the analyte ions are embedded into He nanodroplets and rapidly cooled down to the equilibrium temperature of 0.4 K.[14,34] Irradiation with IR light of ions trapped in the He nanodroplets leads to the absorption of a photon which is in resonance to a vibrational mode. As for IRMPD, the energy is redistributed by IVR but is dissipated to the He nanodroplet matrix. This energy dissipation results in helium to evaporate from the nanodroplets until the He nanodroplets are too small to retain the analyte ion which is then ejected and can be detected using mass spectrometry. Similarly, an IR spectrum results as the number of ions ejected from He nanodroplets as a function of the wavenumber.

2.1.3. Messenger Tagging Action Infrared Spectroscopy

This thesis will centre around a third measurement principle for action spectroscopy: messenger tagging infrared spectroscopy. As the name suggests, messenger tagging IR spectroscopy relies on a messenger molecule or atom that is attached to the analyte non-covalently. In the first experiments reported, Lee and co-workers probed the structure of water clusters tagged with H_2 molecules after supersonic cooling *via* IR spectroscopy.[35] Depletion of the tag after interaction with the IR beam could then be observed as a mass shift in a quadrupole mass analyser.[25]
In order to be applicable as messenger tags in vibrational spectroscopy, two inherent properties must be fulfilled. First, they must not be IR active themselves and, secondly, leave a detectable mass shift after IVR and subsequent depletion.[36] While noble gases are certainly the most obvious choice, they require low temperatures for the attachment to the analyte.[37,38]
The absorption of a resonant IR photon matching a vibrational mode of the messenger tagged molecular ion leads to redistribution of the inciding energy *via* IVR. Depletion of the messenger tag subsequently allows the energy to dissipate and can be monitored as a function of the wavenumber in a mass spectrometer, resulting in an IR spectrum. Since this technique resembles an one-photon process, it is also referred to as infrared photon dissociation (IRPD) spectroscopy. Compared to IRMPD and cryogenic IR spectroscopy performed in helium nanodroplets, the major advantage of IRPD is that it relies on the absorption of only one resonant photon. Thereby, the line broadening seen with IRMPD can be avoided. This broadening of vibrational bands results partially from the absorption of multiple photons which causes anharmonicities to contribute significantly, partially from thermal contributions.[24] Compared to spectroscopy performed in helium nanodroplets, less laser power is required for IRPD and optical parametric oscillator (OPO) tabletop laser may be feasible to perform IRPD experiments in the future.[39]

Despite the seemingly complex measurement principle, a two-state model of messenger tagged and untagged ions suffices to describe the depletion of the action spectroscopy. In analogy to Lambert-Beers law, the number of messenger tagged ions $N_{\mathrm{T}}(\tilde{\nu})$ at a wavenumber $\tilde{\nu}$ can be determined from

$$N_{\mathrm{T}}(\tilde{\nu}) = N_0 \cdot e^{-\sigma(\tilde{\nu})\cdot\Phi(\tilde{\nu})}, \tag{2.6}$$

where N_0 is the number of messenger tagged ions before IR irradiation and $\sigma(\tilde{\nu})$ the absorption cross section which can be derived as the product of the mass absorption coefficient μ/ρ and the molar mass of the analyte M. In comparison to Beer-Lambert law, action spectroscopy additionally depends on the number of photons interacting with the sample. This dependency comes into eq. (2.6) by introducing the photon flux $\Phi(\tilde{\nu})$ as function of the wavenumber which describes the number of photons per second and area. In order to determine the number of ions depleted of their tag $N_{\mathrm{NT}}(\tilde{\nu})$, eq. (2.6) can be rearranged to:

$$N_{\mathrm{NT}}(\tilde{\nu}) = N_0 \cdot \left(1 - e^{-\sigma(\tilde{\nu})\cdot\Phi(\tilde{\nu})}\right) = N_0 - N_T(\tilde{\nu}). \tag{2.7}$$

2.1.4. Cryogenic Ion traps

While Lee and coworkers created their molecular beam from laser desorbed molecules and supersonic cooling, this is not a feasible approach to bring biomolecules into the gas phase.[25,35] A more gentle way to handle biomolecules is the application of an ESI or nano-electrospray ionisation (nESI) source.[4,40] However, this continuous ion source does not allow for the formation of messenger tagged ions during ionisation. Therefore, spectroscopists turned to cryogenic ion traps to facilitate messenger tagging of biomolecules after ionisation.[41]

About half a century ago, techniques to trap ions in a radiofrequency Paul trap or a electromagnetic Penning trap have been introduced.[42,43] From these early works, several trap designs have evolved. In this line of work, a three-dimensional design of a Paul trap emerged and has been employed for photoelectron as well as for photodissociation experiments.[44,45] In the early 1990s, Gerlich and co-workers proposed a linear 22-pole ion trap based on the principles of a Paul trap to trap, cool, and store ions while allowing for spectroscopy.[46,47] This multipole design has been successfully implemented by other groups to allow for spectroscopy of cold biomolecules.[48–50] A further implementation of a cryogenic ion trap for IRPD was demonstrated by Asmis *et al.*[51] who used a 16-pole ion guide for trapping of ions on a millisecond/second timescale before irradiation with the Free-Electron Laser for Infrared eXperiments (FELIX). Moving away from the round cross section design of ion traps, Rizzo and co-workers conceived a planar multipole ion trap coupled to a ToF mass spectrometer.[16] This designs allows for higher injection rates and better ejection characteristics compared to conventional Paul trap derived models. First implementations

of a segmented ion trap have been realised by Luca *et al.*[52] and later improved by Goebbert *et al.*[53], and Heine and Asmis[54] to facilitate IRPD spectroscopy on cold ions and eventually focusing of ions from the cryogenic ion trap to an interaction region. In 2016, Gerlich and co-workers proposed a quadrupolar ion trap in which each of the quarter round rods is approximated by six copper wires and allows tagging of ions with helium at temperatures of 3 K.[55] Subsequently, the application of cryogenic ion traps in IR spectroscopy has been extended by including orthogonal techniques, e.g. IMS, recently.[56]

The major advantage of using an ion trap for messenger tagging, i.e. the cluster formation, of ions created by gentle ESI is the fact that the ion trap can be turned into a cryogenic ion trap by attaching it to a cryostat. This allows to separately control the formation of the clusters and to remove not only the kinetic but also the thermal energy from the ions. However, the ion traps introduced above have one major drawback: they require to be operated using a duty cycle. Because the radiation for spectroscopy is sent through the ion trap, the gas mixture for thermalisation and messenger tagging has to be pumped out of the trap before the structure of the ion cloud can be probed by a laser. The ions are then ejected from the trap for detection in a mass spectrometer.

2.2. Free-electron Laser

As introduced in section 2.1.2, action spectroscopy depends not only on the number density of the analyte in the gas phase but in addition requires a high photon flux. Despite recent advances in tabletop light sources, the photon flux achievable remains limited. In contrast, a FEL is able to provide radiation of high power over a wide spectroscopic range. Rather then relying on stimulated emission after excitation, electrons are ejected from an electron gun and accelerated to almost the speed of light in a FEL facility. Conceived for the first time over half a century ago, the free electrons are forced onto a sinusoidally oscillating trajectory which is enforced by strong magnets of an undulator.[57,58] This wiggling motion of the electrons results in the emission of coherent radiation which depends on the energy of the electrons and the magnetic field in the undulator. The interaction of this radiation with the electron bunch causes self-amplification and subsequently leads to coherent high power radiation. The monochromatic nature of this radiation results from the fixed distance of the undulator and can be tuned by changing the gap of the undulator.[58]

The FEL operated at the FHI of the Max Planck Society (MPG) was brought to routine operation in late 2013 and is capable of providing IR radiation from 4 to 50 µm using a mid-IR beamline and is in the progress of being upgraded to also facilitate the far-IR regime.[59,60] A scheme of the instrumentational setup is shown in Fig. 2.3. Electrons ejected from the electron gun are accelerated by two linear accelerators (LINACs) to provide an energy range from 15 to 50 MeV.[60] A 5.4 m long IR FEL cavity is confined by two gold-plated copper mirrors and houses a 2 m long planar hybrid-magnet undulator comprising 50 periods of 40 mm permanent NdFeB magnets.[61]

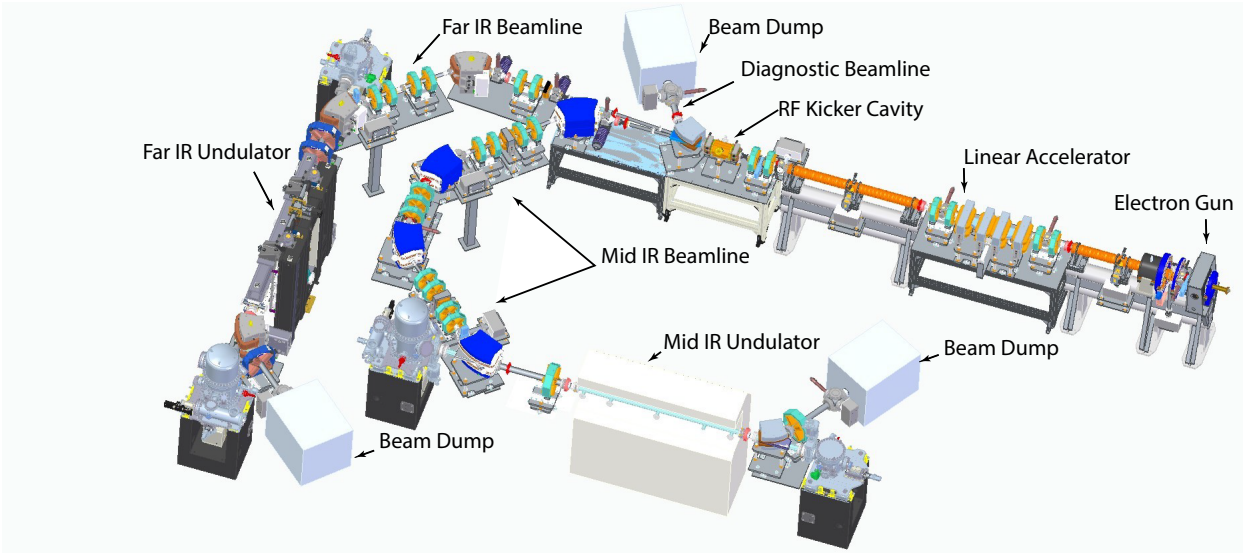

Fig. 2.3.: Arrangement of the FHI FEL infrastructure after the planned upgrade. The undulator for the Far IR regime is still to be implemented and IR light used throughout this thesis is generated by the Mid IR beam line. Adapted from Schöllkopf *et al.* [59].

Resulting IR micro-pulses are 0.5 to 5 ps long and are repeated at a rate of 1 GHz. A single macro pulse is created from 10 000 micro-pulses, repeated with 10 Hz, and can provide energies above 100 mJ at a bandwidth of 0.3 to 0.5 % full width at half maximum (FWHM) of the corresponding wavenumber. [59]

2.3. Chemistry of Glycans

2.3.1. Structure of Glycans

Glycans comprise a large and very diverse class of biomolecules. Often also referred to as carbohydrates or sugars, International Union of Pure and Applied Chemistry (IUPAC) recommendations use the terms *glycan* and *polysaccheride* interchangeably. [62] As such, glycans comprise molecules which in general are made up from more than ten monosaccharide building blocks connected by glycosidic bonds. [63]

Partially, the diversity of glycans results from the myriad of different monosaccharides, which they are made up from. Depending on the position of the carbonyl moiety, they belong either to aldoses with the carbonyl group at the first carbon atom of the carbon backbone or to ketoses with the second carbon atom carrying the carbonyl moiety. Carbon atoms are enumerated so that number of the carbonyl moiety carrying carbon atom is minimised. In addition to the position of the carbonyl moiety, monosaccharides are grouped by the number of carbon atoms they comprises. This leads to monosaccharides to belong to either trioses, tetroses, pentoses, hexoses, or heptoses,

repsectively.

Structural diversity of monosaccharides is further increased by the different orientation hydroxyl groups can have. Based on the orientation of the hydroxyl group furthest apart from the carbonyl moeity, it is possible to differentiate between two chiral configurations of monosacchrides. This renders monosaccharides to be either in L-/ or D-configuration. The presence of a hydroxyl groups and a prochiral carbonyl moiety favours the formation of intramolecular cyclic hemiacetals or hemiketals, depending on the position of the carbonyl group. Upon cyclisation, an additional stereocenter is created. The formation of anomers of either α- (*cis*-) or β- (*trans*-)configuration results from the orientation of the resulting hydroxyl group. Depending on the hydroxyl group which participates in the hemiacetal formation, five- or six-membered rings can be formed which are referred to as furanose and pyranose, respectively.

Furthermore, not every monosaccharide is following the sum formula $C_n(H_2O)_m$, which was thought to be universal for monosaccharides. Today, it is known that several exceptions to this rule exist: 2-deoxyribose is a major building block of deoxyribonucleic acid (DNA) and the deoxyhexose fucose plays a prominant role in biological systems as is laid out below.

Based on the structural diversity of the building blocks, the structure of oligo-, polysaccharides, i.e. glycans, is complex itself. In addition to the points raised above, the connectivity of the individual subunits with respect to one another as well as branching contribute to the diversity. Once an acetal or ketal is formed by linking two monosaccharides covalently, opening of the ring is not possible anymore and the configuration of the anomer is preserved. Since monosaccharides usually contain more than one hydroxyl group at different carbon atoms, different connectivities are conceivable as is branching when two hydroxyl groups of one monosaccharide react to form an acetal or ketal.

Despite the very detailed and precise representation achievable, depicting glycans using their chemical structure will be too complex to retrieve information quickly and sufficiently. Using the symbol nomenclature for glycans (SNFG) proposed in 2015, this standardised nomenclature allows for an easier graphical representation of glycans while taking their structural diversity into account.[64] An overview of the SNFG used in this work is given in Fig. 2.4. Different shapes and colours are used to represent the plethora of monosaccharides and their modifications. To distinguish the configuration of the glycosidic bond solid or dashed lines are used for α- and β-configuration respectively and different connectivity is depicted using different positions at the sugars at different angles.

2.3.2. Biological Importance of Glycans

The best known function of polysaccharides is to provide nourishment in form of starch for the majority of the global population. Furthermore, they act as scaffold structures in plants in form of

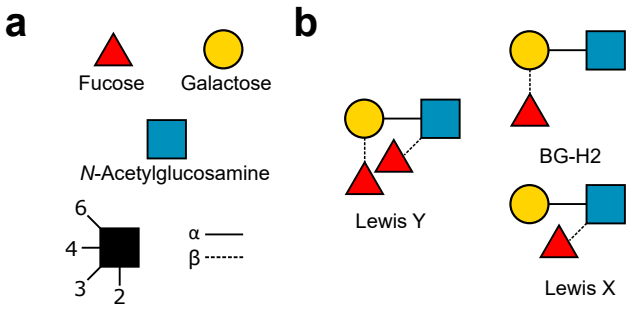

Fig. 2.4.: Symbol Nomenclature for Glycans exemplary for Lewis antigens. a) Sugars are depicted by a set of shapes filled with a distinct colour. α- and β-Configuration of the glycosidic bond is differentiated by solid or dashed lines. Connectivity is depicted by the position of the connection. b) Lewis antigens discussed in section 2.3.2.[64]

cellulose. However, the biological roles of glycans are much more divers when focusing on the molecular level. Glycan structures are involved in almost all molecular processes, may it be in health or malfunction. Often, glycans are attached to proteins after translation in the endoplasmatic reticulum or at the Golgi apparatus and thereby represent the most common translational modification.[65,66] In addition, lipids can also be modified by glycosylation.[65] Despite their abundance in biological systems, the importance of glycans has been realised late compared to proteins or nulceic acids. In this regard, glycans attached to proteins or peptides can facilitate protein folding, but are also used by viruses to mask parts of their capsid proteins to evade the recognition of the immune system as it is also seen with the currently circulating severe acute respiratory syndrom corona virus 2 (SARS-CoV-2).[67–69]

Another example highlighting the importance of glycans in a medicinal context for humans is the AB0 blood group classification. It describes the presence of trisaccharides on the surface of red blood cells. Blood groups can then be assigned on the trisaccharides present. If only one of the two, trisaccharide A or be B is present, the patient has blood group A or B respectively. In case both of the trisaccharides are present, the blood group is AB, in the absence of a trisaccharide it is 0.[70] Benefits from knowing about oligosaccharides present on cell surfaces are not only restricted to the prevention of complications for patients when receiving a blood transfusion but might prove valuable for diagnostics in cancer treatment, too. Structurally related glycans are commonly found in the human body and grouped as Lewis antigens. Healthy cells present a tetrasaccharide, Lewis b (Le^b), on their surface, whereas cancer cells present the isomeric Lewis y which could be used as an early biomarker for cancer development.[71,72] A monosaccharide ubiquitous in Lewis antigens is fucose (see Fig. 2.4). And while most monosaccharides present in nature occur in D-configuration, fucose is one of the few L sugars and furthermore lacks a hydroxyl group at C-6, making it a deoxy sugar. Fucose may only be the fifth most frequent monosaccharide but it is a terminal monosaccharide in almost a quarter of all glycans.[73] Lewis Y contains two isomeric substructures, Lewis X (Le^x) and blood group human 2 (BG-H2), which only differ in the position of the fucose building block as it is shown in Fig. 2.4b.

2.3.3. Fucose - The Wanderer

An inherent problem during the analysis of glycans is their structural diversity.[74] This diversity has been addressed best by employing MS approaches in combination with orthogonal techniques, for example IMS or chromatography.[8,75,76] Information about the structure and sequence of glycans can be gained upon fragmentation during tandem MS experiments.[74] To sufficiently understand the resulting but often crowded fragmentation spectra profound knowledge about the fragmentation reactions and possible rearrangements is necessary. One rearrangement which can render the interpretation of fragmentation spectra of sugars challenging is the so called *fucose migration.*[77] It describes an intramolecular rearrangement reaction during which terminal fucose units are transferred to adjacent or a more remote monosaccharide units and is often indicated by the presence of unexpected fragment ions after collision-induced dissociation (CID) fragmentation experiments.[77]

However, migration of monosaccharides is not limited to fucose alone but has been reported for different hexoses, in peptide mass spectrometry and for other species before.[77–80] Intramolecular rearrangement reactions were indicated by fragment ions that could not be rationalised but by assuming a transfer of monosaccharide subunits and is referred to as internal residue loss (IRL) today.[81] Although the name might suggest that IRL necessarily includes the loss of a monosaccharide during the fragmentation, it is used interchangeably with hexose migration and explicitly also describes the migration of a hexose unit without a loss.[82] Later on, different studies have been published, all reporting misleading or hard to interpret fragmentation patterns associated with the migration of glycan substructures.[83–85] An early study reporting the migration of fucose was published in 1997 observing the migration of fucose units in sialyl-Lewis tetrasaccharides.[86] While the mechanism underlying the rearrangement of protein fragments during mass spectrometry experiments has been elucidated, the mechanism of hexose migration remains unclear in most parts.[80,87,88] Different attempts to shine light onto the details of fucose migration have been made but most of the insights gained have been refuted in subsequent studies. However, one observation can be agreed upon by all studies: only proton- or ammonium adducts ($[M + H]^+$ or $[M + NH_4]^+$) facilitate migration and thus, protons are considered crucial for a hexose subunit to migrate.

Mucha *et al.*[12] assessed the phenomenon of fucose migration in Lewis derived fragment ions by cryogenic IR spectroscopy using a previously described experimental approach.[14] They used sodiated adduct ions of the fucosylated precursor ion Lewis antigen $(Le)^Y$ as their reference and subsequently investigated the protonated species of Le^y before and after fragmentation. Commercially available Le^x and BG-H2 were investigated in order to identify the product created upon fragmentation of Le^y. They could show that the IR spectrum measured after the fragmentation of Le^y can be nicely resembled by a linear combination of the two commercially available Le^x and BG-H2 measured stand alone. Even though IRL is frequently observed after CID, their findings show that CID is not a prerequisite for fucose to migrate. Further, their results show no preference

in ions being formed during fragmentation. This finding is in agreement with an earlier study by Hofmann *et al.*[89] who found that fragmentation of Le^y as sodiated adduct prior to IMS leads to two distinct signals in the ATD of same m/z ratio. This points to the two different substructures, Le^x and BG-H2, which cannot inter convert in the absence of a proton.
In a follow-up study, Lettow *et al.*[90] investigated the role of protons in fucose migration further by cryogenic IR spectroscopy.[14] Their results underline the necessity of having a mobile proton to facilitate fucose migration in Le^x and BG-H2 to the same but not yet known structure. Furthermore, they propose that ammonium adducts of either Le^x or BG-H2 are not strict $[M + NH_4]^+$ ions but rather adducts of ammonia and a protonated glycan ($[MH + NH]^+$). They can confirm this hypothesis by investigating the structure of alkylated ammonium adduct ions for Le^x. The higher proton affinity of trimethylammonia and triethylammonia results in IR spectra which are significantly different from the spectrum seen for the two protonated trisaccharides, Le^x or BG-H2 and therefore rule IRL out. In addition, they were able to show how altering of the proton affinity upon introduction of functional groups can affect the phenomenon fucose migration.

3. Objective of this Thesis

In recent years, the investigation of large biomolecules by IR spectroscopy has gained increased interest. By analysing the structure of these molecules in the gas phase, the solvated structure can be retained while disrupting influences by different factors can be avoided. In order to sufficiently achieve IR spectroscopy in the gas phase, instrumentation for action spectroscopic approaches is needed.

The aim of this thesis is to put instrumentation for messenger tagging IR spectroscopy using a novel cryogenic ion trap setup into operation. Furthermore, cryogenic IR spectra of trisaccharides comprising fucose residues will be recorded to unravel mechanistic details of fucose migration.

In this work, a set of powerful techniques will be combined: ion mobility spectrometry, mass spectrometry and IR spectroscopy. The combination of the different experimental techniques allows for a high controllability of the ions probed by IR spectroscopy. The experimental setup used here consists of an ion mobility spectrometer conceived and built by Stephan Warnke.[13,27] This spectrometer has been extended with several quadrupolar deflectors, a cryogenic ion trap of novel design, a hexapole interaction region, and a ToF mass spectrometer.

While the principles of messenger tagging IR spectroscopy have been explained above, the subsequent chapter will describe the implementation chosen in our research group. After a brief overview, the key components, quadruplar deflector, cryogenic ion trap as well as the interaction region and ToF mass spectrometer will be subject of section 4.3, section 4.4, and section 4.5 respectively. In order to achieve a good ion transmission through the whole instrument, the voltages affecting the ion trajectory require tuning (see section 4.6). Furthermore, suitable conditions for messenger tagging in the cold trap need to be found (refer to section 4.8). Section 4.10 will focus on the timing necessary to release ions from the cryogenic ion trap, overlay the ion beam with the IR beam and finally detect ions in the ToF mass spectrometer. The instrument will be tested and tuned using the pentapeptide leucine-enkephalin (Fig. 4.12), a neurotransmitter present in mammals, and subsequently more challenging samples will be investigated. In this regard, trisaccharides of the Lewis family carrying fucose residues are of particular interest and will be investigated to elucidate the phenomenon of fucose migration further.

4. The iMob 2.0 Experiment

The following chapter will highlight the experimental details of an approach for messenger tagging IR spectroscopy using novel a cryogenic ion trap design. While parts of the instrumentation have been reported earlier, the cryogenic ion trap and the spectroscopy section have been put into operation only recently.[27,91] The instrument will be referred to as *iMob 2.0* evolving the name introduced with the ion mobility spectrometer, *iMob*, in its first implementation.

4.1. Overview

The first iMob machine was conceived as an ion mobility spectrometer for the selection of molecular conformers.[27] Subsequently, it was extended to perform photodissociation experiments by means of IRMPD or ultraviolet (UV) dissociation spectroscopy using the instrumentation depicted in Fig. 4.1.

Briefly, gas phase ions are created *via* a nESI source using PdPt coated glass capillaries and transferred to the light vacuum inside the entrance funnel chamber using a heatable capillary (75 mm long, inner diameter: 0.25 mm) and a voltage gradient between 500 and 1200 V with respect to the entrance. Ions created in this manner are guided to the drift tube using an hourglass shaped radio frequency (RF) funnel.[92] The three sections of this entrance funnel serve different purposes; the first section is used to focus the ion cloud, the second resembles a differential pressure aperture to allow for the transfer to the millibar regime and the third section of increased radius allows for trapping of ions prior to pulsed injection into the drift tube. The drift tube is comprised of four segments of lead glass connected using polyether ether ketone (PEEK) adaptors. A constantly declining electric potential over the drift tube is achieved by connecting the different segments with a resistor chain. Upon injection into the drift tube of 80.55 cm length, the ions are separated based on their ion mobility as outlined in section 2.1.1. After ion mobility separation, the ion cloud is transferred from pressures in the millibar regime to high vacuum using a second RF funnel and subsequently transmitted to two subsequent ion guides. A gating lens following the ion guides just before the quadrupole mass filter allows for ion mobility selection of a slice of the ion cloud emerging from the drift tube. Thereafter, two quadrupole mass filter are built into the iMob apparatus: the first allows for $^{m}/_{z}$-selection of ions contained in the IMS selected ion cloud slice. Following mass selection, the ions are transferred to the interaction region made up from the second quadrupole ion guide in which the ion beam is overlaid with a laser beam providing either

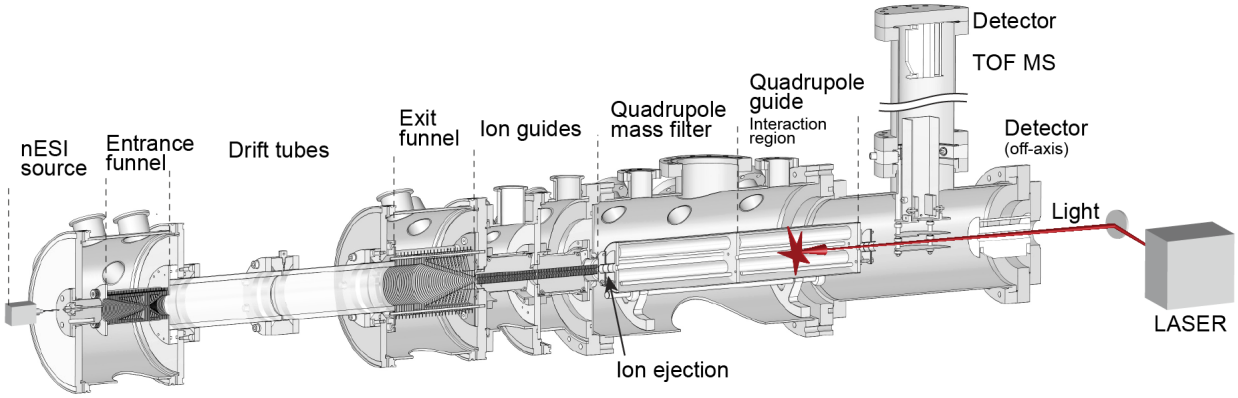

Fig. 4.1.: iMob - Schematic principle of the experimental setup for infrared multiphoton or ultraviolet dissociation experiments. Ions transferred to the gas phase *via* nano-electrospray ionisation are separated based on their ion mobilities using a drift tube spectrometer. After ion mobility and mass selection of the ions of interest, they are investigated by dissociation spectroscopy. Detection of corresponding fragments is achieved with time-of-flight mass spectrometry. Figure adapted from [13].

IR or UV radiation. Fragments generated during the dissociation of the analyte after irradiation can be detected perpendicular to the instruments axis using a ToF mass spectrometer.

4.2. Overview iMob 2.0

Prior to the start of this thesis work, the iMob setup has been modified substantially. After a short overview on the changes implemented, the subsequent sections will explain the extension in greater detail.

The IMS part of the instrument remained largely unaffected by the upgrade. Only the drift tube, originally consisting of four lead glass segments and a total length of 80.55 cm, has been doubled in length to 161.1 cm using four additional glass segments of same fabrication. The ToF mass spectrometer following the quadrupolar ion guide as well as the window on axis have been removed and replaced by a quadrupolar deflector (details see section 4.3) which deflects the ion beam by 90°[1] into the cryogenic ion trap. In order to record arrival time distributions, the ion beam is not deflected by the quadrupolar deflector if 0 V are applied to both pairs of quarter round rods. Instead, it can be characterised using a high energy dynode (HED) multiplier (ETP ion detect DM283, Adaptas™, USA) on line of the IMS stage. In order to operate the dynode more effectively for high mass ions, a voltage of −10 kV is applied to the HED to accelerate the positive ions before they hit the dynode surface, the detector itself is operated at −1.3 kV. The detected current signal is converted to a voltage using an amplifier (model DHPCA-100, FEMTO, Germany). An analog-to-digital converter (PXI 6361, National Instruments, USA) is used to digitise the signal.

[1] counterclockwise angles are given as positive values, clockwise angles as negative values

A set of ATDs for an ion of interest can be recorded after IMS and mass selection. IMS selection is achieved using a gating lens which allows for transmission of only one slice of the ATD. This is realised by switching the applied high voltage (200 V) to a voltage just below the ion energy ($\approx$ 15 V), for a duration of 150 to 500 µs. Temporal control of the IMS selection is facilitated by a delay generator which is used to operate the whole IMS stage at a given frequency (for details see section 4.10).

If voltages are applied to the deflector rods, the ions are deflected into the cryogenic ion trap, thermalised and tagged using He as buffer gas which can be doped with messenger tagging gas as explained in section 2.1.3. Using a voltage ramp, ions are then ejected from the cryogenic ion trap, accelerated, focused, and bend around 90° by a second quadrupolar deflector. Without voltages applied to the quadrupolar deflector, a second ATD detector can be used to diagnostically monitor the ions which are ejected from the cryogenic ion trap. If the cold tagged ions are deflected, they then enter the interaction region where they are overlapped with the FEL IR beam which enters the machine through a KBr window anti-parallel to the IMS stage. The interaction region is comprised of a hexapole which confines the ions radially and stabilises their trajectory. After traversing this guide, the ion beam is deflected by −90° using a third quadrupolar deflector and detected in the in a ToF mass spectrometer.
Throughout the instrument, a plethora of Einzel lenses and steering lenses is employed to focus the molecular ion beam and correct for minor misalignment.

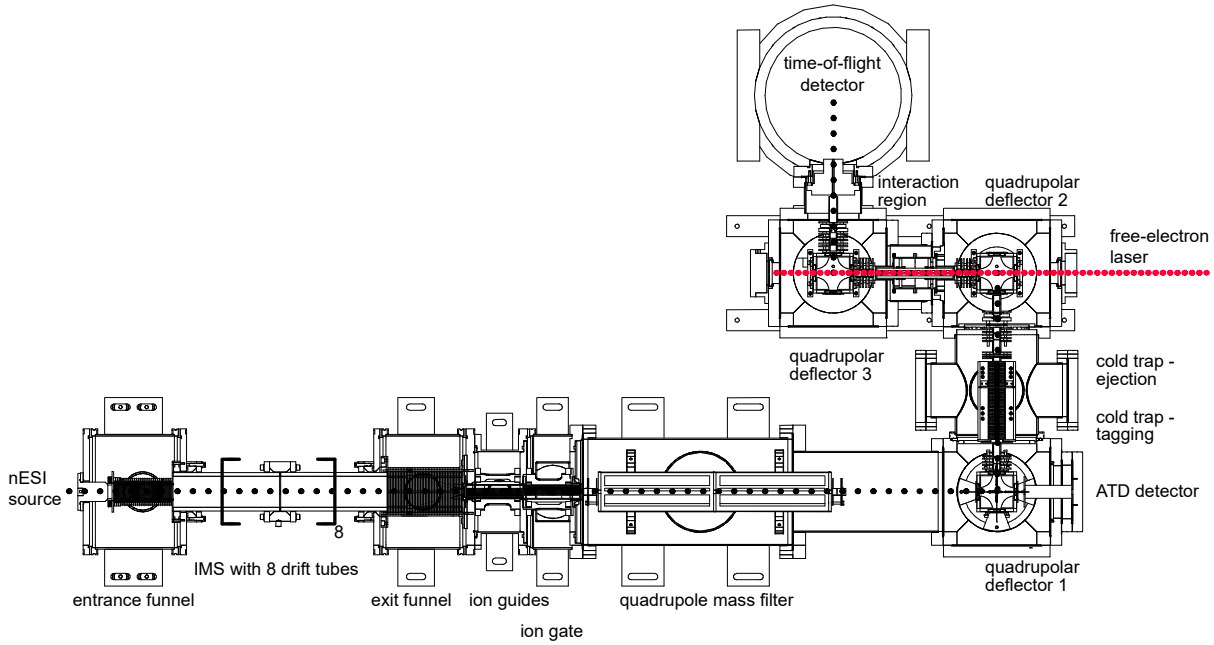

Fig. 4.2.: iMob 2.0 - Overview of the Instrumentation. Shown is a computer-aided design (CAD) model cut open horizontally. The linear ion mobility stage conceived earlier (see Fig. 4.1[27]) was extended using four additional lead glass segments. Three quadrupolar deflectors, a cryogenic ion trap, the interaction region and a time-of-flight mass spectrometer to perform messenger tagging IR spectroscopy replace the ToF mass spectrometer in Fig. 4.1. The IR radiation provided by the free-electron laser is depicted in red, while the ion trajectory is depicted in black.

4.3. Quadrupolar Deflector

The theoretical basis for the quadrupolar deflectors employed in this experiment was explored by Randall E. Pedder in his dissertation in great detail.[93] Deflection of an ion beam by ±90° is facilitated by injecting ions off-axis into a quadrupolar device.

Per se, a quadrupole is a rather simple construct consisting of four round rods arranged in parallel to form a square area. The rods are operated by applying the same direct current (DC) voltage to opposite rods which are electrically connected, while neighbouring rods are of opposite polarity. The application of DC quadrupoles as a deflector was explored by Zeman[94] and have been thoroughly studied by Randall E. Pedder.[93] In theory, rods should be of hyperbolic profile but round rods or even quarter round rods approximate hyperbolic fields in the center of the quadrupole

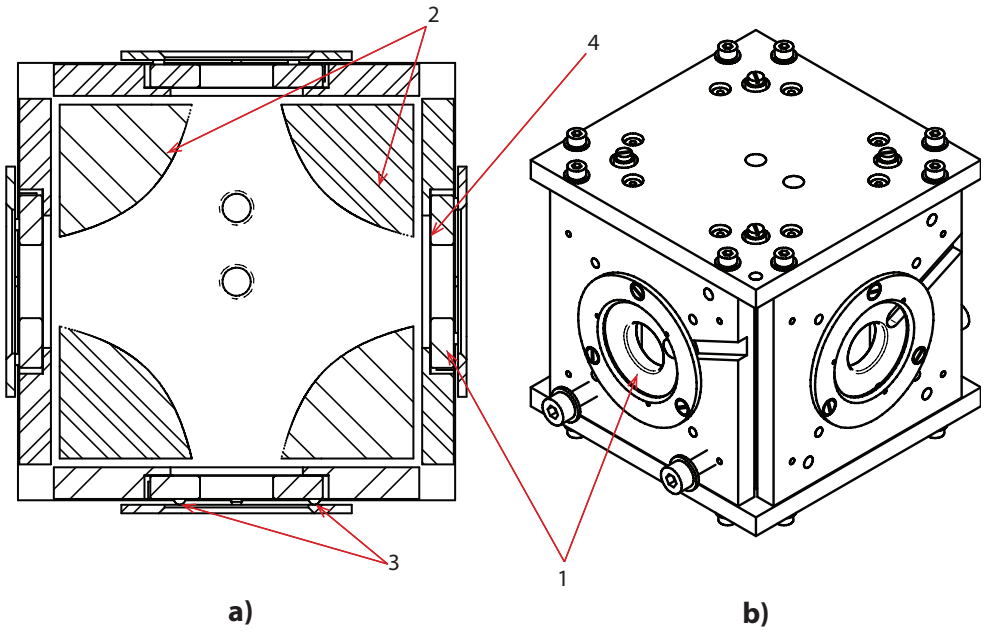

Fig. 4.3.: Computer-aided design of a Quadrupolar Deflector. a) Shows a horizontally cut CAD model of the deflectors used in the iMob 2.0 experiment. b) Quadrupolar Deflector as CAD model. Ions enter and exit the defletor through ion lenses (1). These lenses are isolated from the deflector housing using ruby spheres (3) and Kapton™ foil (4). The quadrupole used for deflection is made up from four quarter round rods (2).

sufficiently.[93] Using static electric fields, i.e. DC voltages, a low resolution energy analyser is implemented reducing the overall ion transmission. This discriminating effect can be circumvented by increasing the distance between diagonally arranged rods above the ideal distance.[93,95] Further, the missing capability of the deflector to focus ions in the plane perpendicular to the rods creates the necessity to employ focusing elements. This drawback is corrected by including four sets of Einzel lenses into the ion trajectory, focusing the ion beam after exiting every quadrupolar deflector. A fourth Einzel lens is used to focus the ion beam after exiting the interaction region before deflector 3.

The four quarter round rods which make up the central part of the deflector are embedded into a stainless steel chamber from which they are electrically insulated. Two opposing quarter round rods are electrically connected and provided with the same voltage. Every side face of the cubic chamber carries a lens insulated from the chamber using polyimide (Kapton®) foil but hold in place by stainless steel spheres (as an upgrade, the stainless steel spheres have been replaced by saphire spheres, see section 5.1.1). Voltage supply is achieved using Kapton® insulated copper wires and a multi-pin feed-through through the vacuum chambers. For further manufacturing details, the interested reader may study the documentation of quadrupolar deflectors or cross beam ionizers as commercially available from Ardara Technologies L.P.. The deflector design employed here has been adapted from their design.

To deflect the ion beam, the inner pole, i.e. the pole around which the ions are to be bend, is set to an arbitrary voltage of opposing polarity to the ion beam. The voltage applied to the quarter rods of opposing polarity has to be tuned for every arbitrary value chosen before. For practical reasons, the voltage of deflector 1 is tuned using the ATD detector on deflector 2 on line from the cryogenic ion trap. Both, the voltages of deflector 2 and deflector 3 are tuned using the ion signal in the ToF mass spectrometer. In a first implementation, the chamber housing the quadrupolar deflector as well as the lenses on its faces were grounded, i.e. their potential could not be adjusted.

4.4. Cryogenic Ion Trap

Many different technical implementations for messenger tagging spectroscopy which make use of ion traps have been reported up to date (compare section 2.1.4). Here, a novel design of segmented ion trap comprising two separate compartments is introduced. The trap itself is attached to a cryocooler head (RDK-408D2 4K Cryocooler Series, Sumitomo Heavy Industries, Ltd., USA) *via* its top and sits in a vacuum chamber, thereby combining installation and cooling. The cryocooler is run using a compressor (Compressor Unit CSW-71D, Sumitomo Heavy Industries, Ltd., Japan). Adjustment of the traps position can be achieved with a three point leveling plate. Alignment of the trap was achieved using a self-leveling crossline laser and the center of the two quadrupolar deflectors 1 and 2 as reference points. After being deflected in bender 1, the molecular ion beam is focused into the cryogenic ion trap through an entrance lens with an aperture diameter of 3 mm using an Einzel lens. The ions are thermalised upon collision with the messenger tag doped buffer gas and are trapped in a potential well confined by in the trapping compartment the entrance and the cold trap gate lens. Radially, the ions are confined by a hexapole which is made up from 36 Printed Circuit Board (PCB) elements. The PCB elements are electrically connected using a resistor chain and voltages are applied to the front and the rear PCB element. In order to further stabilise the ions in the hexapole, a RF voltage ($\nu = 1.32\,\mathrm{MHz}$) is applied to the PCB elements. The radio frequency generator was conceived and constructed by the FHI E-Lab. The trapping compartment is fully enclosed by copper plates, of which the lid is connected to the cold head and carries two holes which serve as inlet for the buffer-tagging gas mixture. The gas mixture is let through milled loops in the cold head connector and enters the trapping compartment pre-cooled. Even though, the ions will already loose their kinetic energy upon collision with the buffer gas, low temperatures are required for the messenger tagging of the ions. Thermalised and messenger tagged ions are transferred to the ejection compartment by lowering the potential applied to housing of the cold trap and therefore also to the cold trap gate element which makes for the back end of the trapping compartment. The ions diffuse over to the ejection compartment through an aperture of 6 mm in diameter. The ejection compartment is made up of 17 additional PCB elements, which are electrically connected by a second resistor chain which facilitates the voltage ramp of the ejection mechanism. This ejection voltage ramp is supplied with the same radio frequency as the the trapping compartment. The voltages used to operate the whole iMob 2.0 setup and the

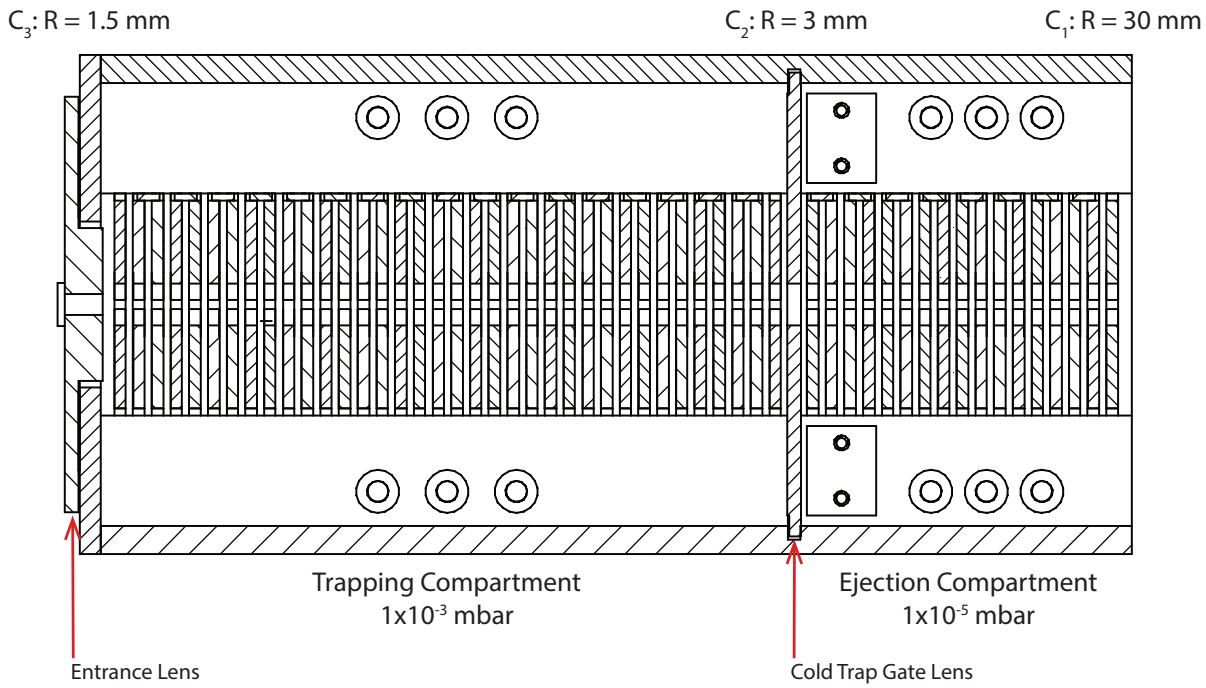

Fig. 4.4.: Computer-aided design of the Cryogenic Ion Trap of the iMob 2.0 instrument. The CAD model is cut open horizontally to reveal the printed circuit boards which make up for the hexapole design of the ion trap. Labels include the three orifices limiting the conductance C_{1-3} as discussed in section 4.8 and the two high pressure compartments separated by the *cold trap gate lens* for transfer of ions from the trapping to the ejection compartment. The segmented design of the cryogenic ion trap results from the two separated compartments. The entrance lens is used to confine the trap in the front and trap ions between the entrance and the cold trap gate lens.

cryogenic ion trap in particular will be explained in greater detail in section 4.6. The back of the cryogenic ion trap is not covered by an additional copper plate and thus a large conductance limit for the gas flow of 60 mm in diameter is used as an approximation. The rectangular cross section of the trap is 64 mm by 52 mm. After ions have been ejected from the ejection compartment of the cryogenic ion trap, they are accelerated towards quadrupolar deflector 2 by a stack of four different acceleration lenses and focused with an Einzel lens. A set of two steering lenses allows for horizontal and vertical correction of the molecular ion beam. The ions coming form the cryogenic ion trap can be monitored using a second, diagnostic electron multiplier detector (ETP ion detect, Adaptas™, USA) on the chamber of deflector 2. It can be used to estimate the amount of ions coming from the cryogenic trap. The detected current signal is converted to a voltage using an amplifier (model DHPCA-100, FEMTO, Germany). An analog-to-digital converter (PXI 6361, National Instruments, USA) is used to digitise the signal.

(a) **(b)** **(c)**

Fig. 4.5.: Photos of the Cryogenic Ion Trap taken prior to the installation in the iMob 2.0 instrument a) Cryogenic Ion Trap pictured upside down from the ejection side. The printed circuit board (PCB) elements confining the hexapole are visible. Voltages to the trap are provided *via* the polytetrafluorethylen (PTFE) voltage divider on the bottom. b) The ejection compartment in the front is separated from the trapping compartment in the back the *cold trap gate lens* (aperture diameter: 6 mm, compare Fig. 4.4). c) Trapping compartment with the copper gate lens in the back, voltages are feed through to the hexapole from the side. The resistor chain governing the voltages is visible on side of the PCB boards in b) and c). Photos taken by Eike Mucha.

4.5. Interaction Region and Time-of-Flight Mass Spectrometer

The pulsed molecular ion beam enters the high vacuum spectroscopy region through an orifice of 12 mm in diameter in a flange separating the vacuum chambers of the cryogenic ion trap and quadrupolar deflector 2 from one another. Upon deflection by 90° in the second quadrupolar deflector, the molecular ion beam is overlaid with the IR beam of the FHI FEL. This part of the instrument is denoted as *interaction region* and depicted in Fig. 4.6.

The FEL radiation is provided to the experimental setup through an evacuated beamline running along the experimantal hall. An optical table consisting of a pneumatic mirror of varying focal lenght, a mirror of fixed focal length and a mirror is used to focus the IR radiation into the iMob 2.0 instrument through a KBr window. Flushing of the table housing with a constant N_2 flow reduces absorption of IR radiation by humidity in the surrouding air. The focal length of the pneumatic mirror can be controlled using voltages from 0 to 10 V and allows to shift the focus of the FEL over the length of the interaction region. The optical path of the IR radiation through the instrument ends at a diagnostic window attached to the vacuum chamber of quadrupolar deflector 3. For safety reasons, this window is covered by a lathed aluminium which can be removed for alignment of the laser beam through the instrument or to measure the power of the laser after traversing the interaction region.

After deflection of the molecular ion beam, the ions are focused using an Einzel lens and enter a custom build hexapole which radially confines and stabilises the ion's trajectory through an applied radio frequency of 1.03 MHz (radio frequency generator taken from a Waters™ /Micromass QToF Ultima, Waters Corporation, UK). While it is possible to apply a DC offset to the hexapole,

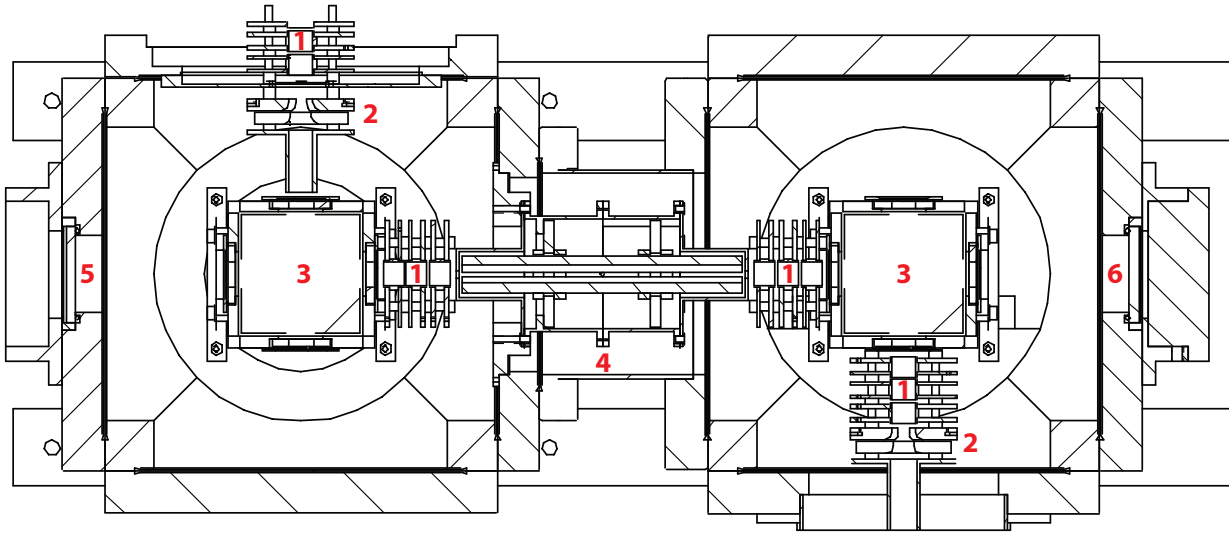

Fig. 4.6.: Computer-aided design of the interaction region of the iMob 2.0 experiment. The CAD model is cut open horizontally. The molecular ion beam enters the second quadrupolar deflector (3) through a set of Einzel lenses (1) and a set of steering lenses (2) from the ion trap on the top left of the figure and exits the interaction region upon deflection in the third quadrupolar deflector (3) on the right. An additional set of Einzel lenses and steering lenses is used to guide the ions into the extraction region of the ToF mass spectrometer. The IR radiation enters the KBr window (5) on the left and is overlaid with the molecular ion beam which is focused colinear through the interaction region using the two Einzel lenses (1). The hexapole (4) is used to stabilise the ions further and is operated in RF only mode. A diagnostic window at the end of the interaction region (6) can be used to align the optical path through the instrument or measure the laser power after traversing the instrument.

it is routinely operated at ground potential. The molecular ion beam is focused into the third quadrupolar deflector using yet another Einzel lens, deflected by $-90°$ and focused into the ToF mass spectrometer by another Einzel lens, a set of horizontal and vertical steering lenses, and a ToF focus lens. The ToF mass spectrometer has been taken from a Waters™ /Micromass QToF Ultima ((Waters Corporation, UK)).

The ions enter the ToF region and are guided by a voltage, V1, towards a pair of extractor plates denoted as pusher and puller. These two extractor plates allow for the pulsed mode operation following the same frequency which is used to control the ejetion of ions from the cryogenic ion trap. In positive ion mode, a high positive voltage pulse is applied to the pusher and a high negative voltage pulse applied to the puller electrode, respectively. In order to accelerate the ions, applied voltage pulses are only of short duration. This is facilitated by two fast high-voltages switches (HTS 31-03-GSM, Behlke, Germany). The ions are accelerated through over the length of the ToF chamber by applying another high voltage. In practice, the ToF spectrometer used here is operated in *V mode* (single reflectron mode). This V mode is enabled by employing a reflectron with a constant voltage of same polarity as the ions thereby deflecting the ions back into the ToF

chamber. Ions coming from the reflectron are then detected using micro-channel plates which serve as electron multiplier. A connected preamplifier converts the current to a voltage (model VT120, Ortec, USA) and the ion signal is subsequently digitised using a analog-to-digital converter (PXIe 5160, National Instruments, USA).

As will be explained in section 4.10, well coordinated temporal control of switchable voltages is crucial for the successful operation of the instrument. Both, the IR and the molecular ion beam arrive in the interaction region pulsed at a rate of 10 Hz and the interaction region allows for the spatial and temporal interaction between IR photons and the molecular ions. If the wavelength of the IR photons is resonant with an IR active vibrational mode of the molecular ion beam, vibrations are induced upon absorption of one photon and IVR leads to the depletion of one messenger tag. The ToF mass spectrometer serves as detector to distinguish between molecular ions which still carry a messenger tag and those which have been depleted of their tag. Recording this ratio for a range of wavenumbers allows to calculate an IR spectrum.

4.6. Operation Mode iMob 2.0 - Voltages

Guiding a molecular ion beam stably through the iMob 2.0 apparatus requires a defined potential surface. Fig. 4.7 and Fig. 4.8 illustrate the potentials which facilitate the ion's trajectory throughout the instrument. Fig. 4.7 takes into account only the voltages up to the first quadrupole deflector, whereas Fig. 4.8 shows all potentials for the IR spectroscopy section starting with the cryogenic ion trap and finally reaching the ToF mass spectrometer. The voltage values noted in the diagram are exemplary values which will vary for individual samples. Values found in practice may differ slightly depending on radio frequency amplitudes and the acceleration voltages after the cryogenic trap. Also, since the quadrupolar deflectors can function as an energy filter, values for the tuned quarter round rods may vary slightly for different molecules. A list of exemplary voltages used during routine operation of iMob 2.0 can be found in section 5.2 and a profound description of the voltages in the IMS part of iMob 2.0 is given in the diploma thesis by Stephan Warnke.[27]

The manifold voltages are supplied mostly by voltages sources built in-house by the FHI E-Lab. In addition, two voltages, *ejection front* and *ejection end high*, are currently supplied by Delta Elektronika DC power supplies (Delta Elektronika B.V., Netherlands). The high voltage required for the operation of the drift tube is provided by a iseg NHQ205 supply (iseg Spezialelektronik GmbH, Germany). Both ATD detectors accept −10 kV for deflection from a CAEN N1570 voltage source (CAEN S.p.A., Italy) and −1.3 kV for detection from a second iseg NHQ205. Most RF supplies are of custom design as well. Only the RF supply for the hexapole interaction region has been taken from a commercial Q-Tof Ultima (Waters Corporation, UK) and is operated at 1.03 MHz.

An upgraded voltage supply scheme has been implemented for the three quadruoplar deflectors in the course of this thesis work and the details are described in section 5.1.1. All Einzel lenses used throughout the lately implemented parts of the instrument are supplied with one voltage to the central lens. The two outer lenses are electrically connected and float on the centerline potential of the quadrupolar deflector housings and in case of the Einzel lens between the cryogenic ion trap and quadrupolar deflector 2 on ground potential. The cryogenic ion trap is supplied with several voltages to be fully functional. The aforementioned entry lens is supplied with a voltage just under the energy of the ions and serves to prevent ions from trickling out of the trap again. The first and the last PCB element of the trapping compartment are supplied with a voltage to provide the hexapole defined by the 36 PCB elements forming the hexapole. PCB elements in between are supplied using a chain of electrical resistors.

The voltages involved in the transfer of ions from the trapping compartment to the ejection compartment is depicted in Fig. 4.9. The mechanism by which ions are ejected from the cryogenic ion trap comprises three steeps which are cycled at a frequency of 10 Hz when operating the instrument routinely. Ions are trapped in the hexapole made up of the PCB elements and confined by the cold trap entry lens and cold trap gate. A potential of $\sim 18\,\mathrm{V}$ and a radio frequency of 1.32 MHz are used to stabilise the ions while they are being thermalised and tagged with a messenger. Transfer of thermalised and messenger-tagged ions is facilitated by a gating voltage, cold trap gate, which is set to a high voltage, prohibiting ions from traversing most of the time. Only when the applied voltage is lowered, ions trickle into the ejection compartment (Fig. 4.9 center). Subsequently, the ions are expelled from the cryogenic ion trap, by lowering the ejection voltage ramp to invert its slope (Fig. 4.9 right). This duty cycle of ejecting ions from the cryogenic ion trap is advantageous, because it allows for a continuous filling of the ion trap while emptying the trap independently.

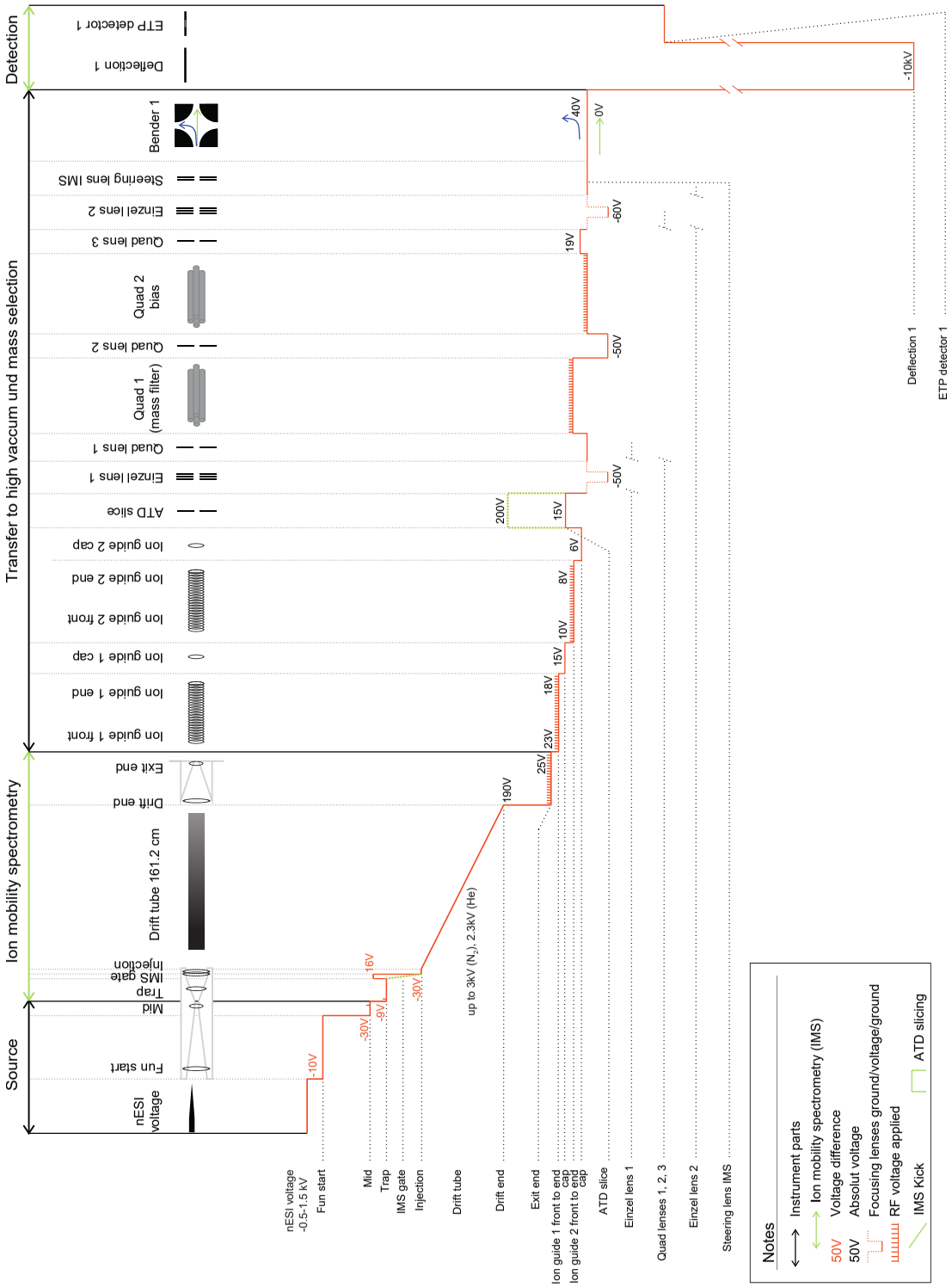

Fig. 4.7.: iMob 2.0 Voltage Diagram - Ion Mobility Spectrometry Part

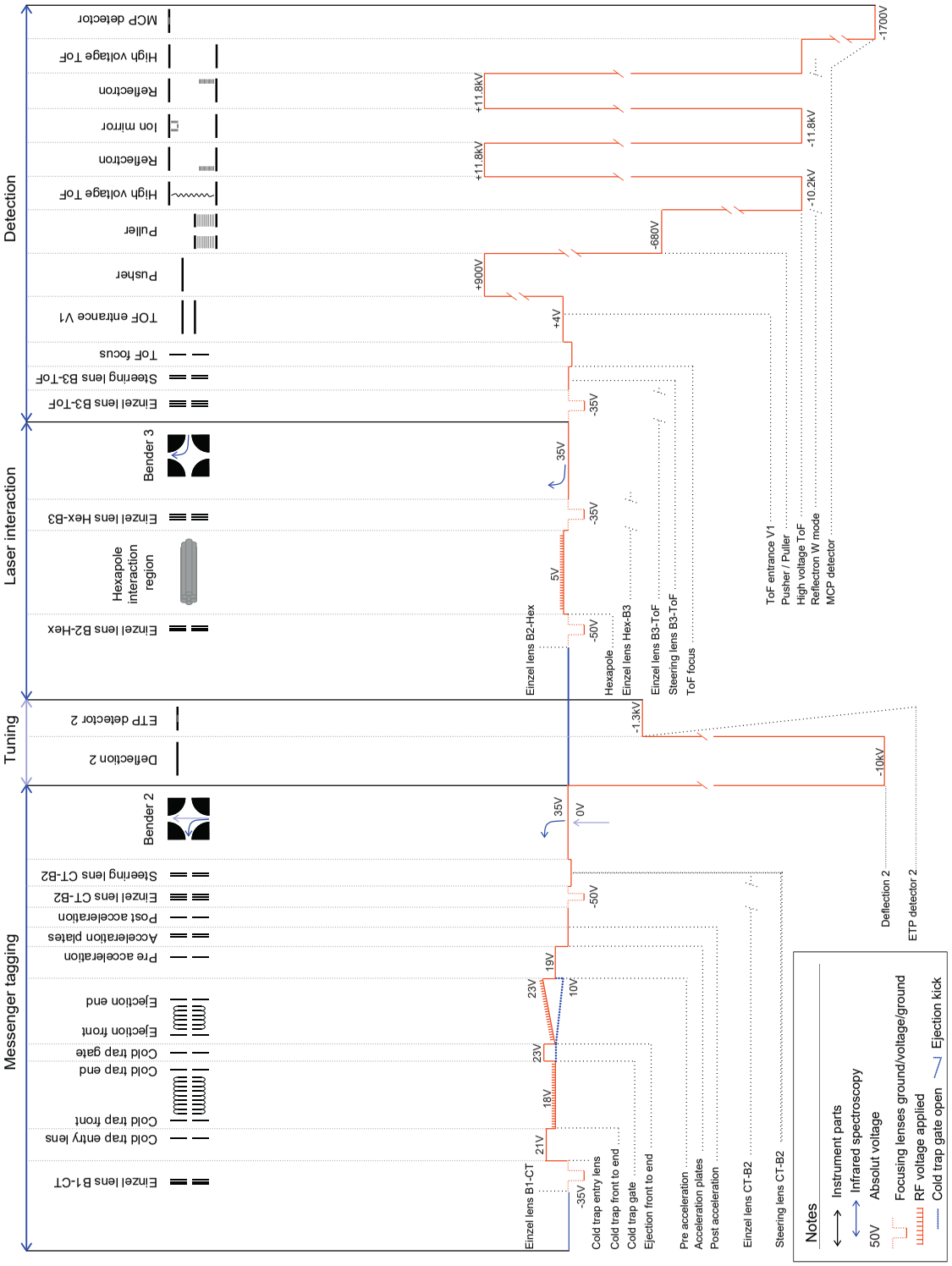

Fig. 4.8.: iMob 2.0 Voltage Diagram - IR Spectroscopy Part

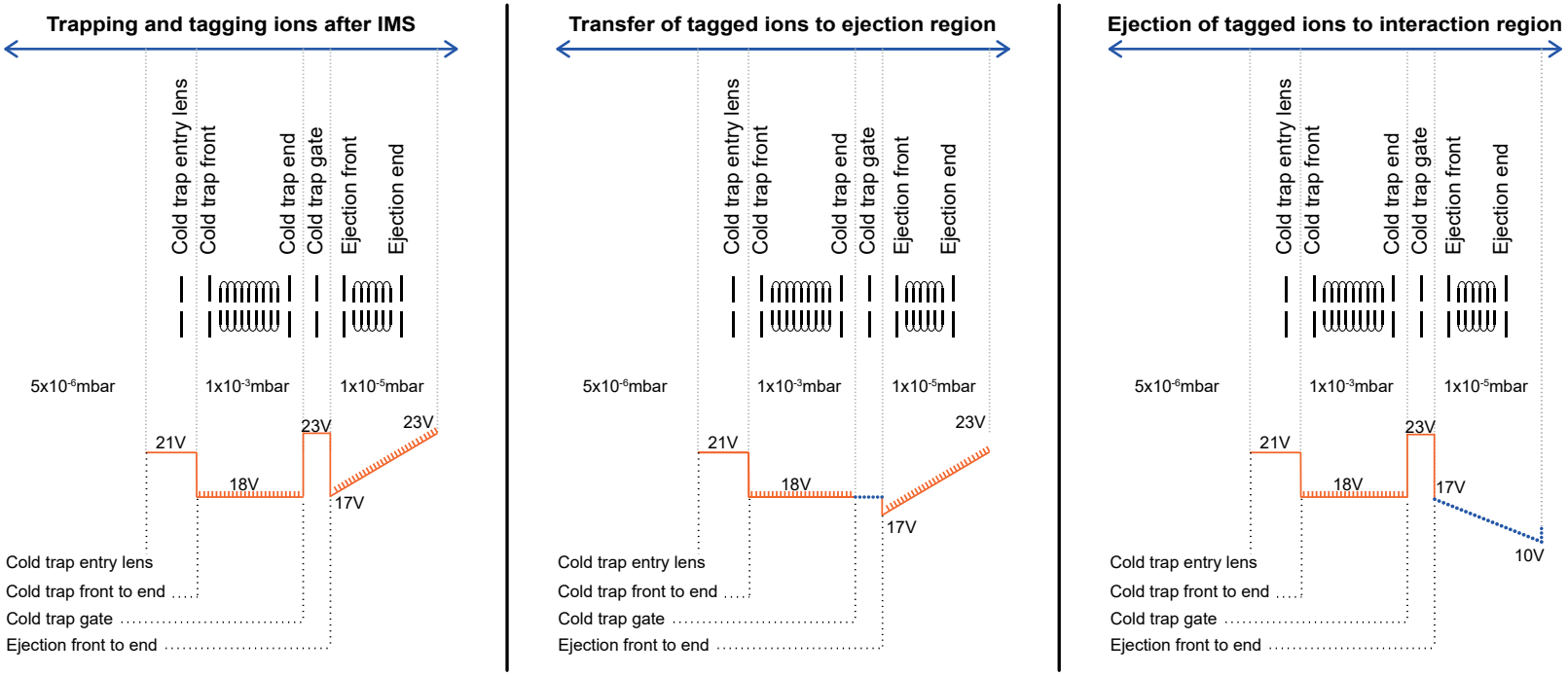

Fig. 4.9.: iMob 2.0 Cryogenic Ion Trap Voltages - Ion transfer and ejection. Ejection of ions from the cryogenic ion trap is facilitated by a three step cycle of accumulating, trapping, and tagging ions in the trapping compartment of the trap (left), transferring ions to the ejection region by lowering the cold trap gate voltage (center), and ejecting ions from the ejection compartment by inverting the ejection voltage ramp (right).

4.7. Gas Supply to the iMob 2.0 Instrument

For the full operation of the iMob 2.0 instrument, two parts of the instrument require a continuous gas supply: the drift tube for IMS experiments is operated by a small flow of either helium or nitrogen from the exit funnel towards the entrance funnel (differential pressure during operation in helium: 0.6 mbar). Similarly, the cryogenic ion trap has an inlet for a buffer gas (mixture). For sophisticated supply to both of these parts, a gas mixing plate, colloquially referred to as *Gasbahnhof*, was purchased from Swagelok (Leipzig Berlin, Germany).

A schematic representation of the Gasbahnhof is given in Fig. 4.10. The mixing plate itself has three possible inlets of which two are designated for helium and nitrogen. A third spare supply is currently used to release high pressure but can be used for exotic messenger tagging gases if needed. Nitrogen supply is ensured through the nitrogen supply at the Molecular Physics department of the FHI, for helium a 50 L gas bottle is used.
To achieve independent operation of both gas supply to the instrument, two separate loops are assembled on the mixing plate. The loop supplying drift gas makes use of a pressure reducer to lower the pressure of the supplied gas to safely operate the drift tube pressures. Drift gases are changed on the mixing plate using the respective valves.
The second loop used to provide the buffer gas (mixture) is depicted on the right of the Gasbahnhof. It is separated from the first loop using a finely adjustable bellows sealed valve. All other valves are less delicate diaphragm-sealed valves. A digital pressure transducer allows to monitor the pressure in this second loop and vacuum pump connected to the mixing plate to evacuate it. A bypass to the second pressure reducer allows to evacuate the pipe connected to the inlet valve on the vacuum chamber and thereby protects the pressure reducer. Both pressure reducers can further be protected while mixing buffer gas or switching the drift gas using a diaphragm-sealed valve.
The sample cylinder at the bottom of the Gasbahnhof allows for the preparation of buffer gas doped with a gas for messenger tagging. A defined gas mixture is prepared using partial pressures monitored *via* the pressure transducer. The bellows sealed valve is used to let the gas of smaller fraction flow into the buffer gas loop and the sample cylinder, before the cylinder valve is closed, everything is evacuated and the main component of the buffer gas mixture, i.e. helium, is dosed to the desired final pressure.

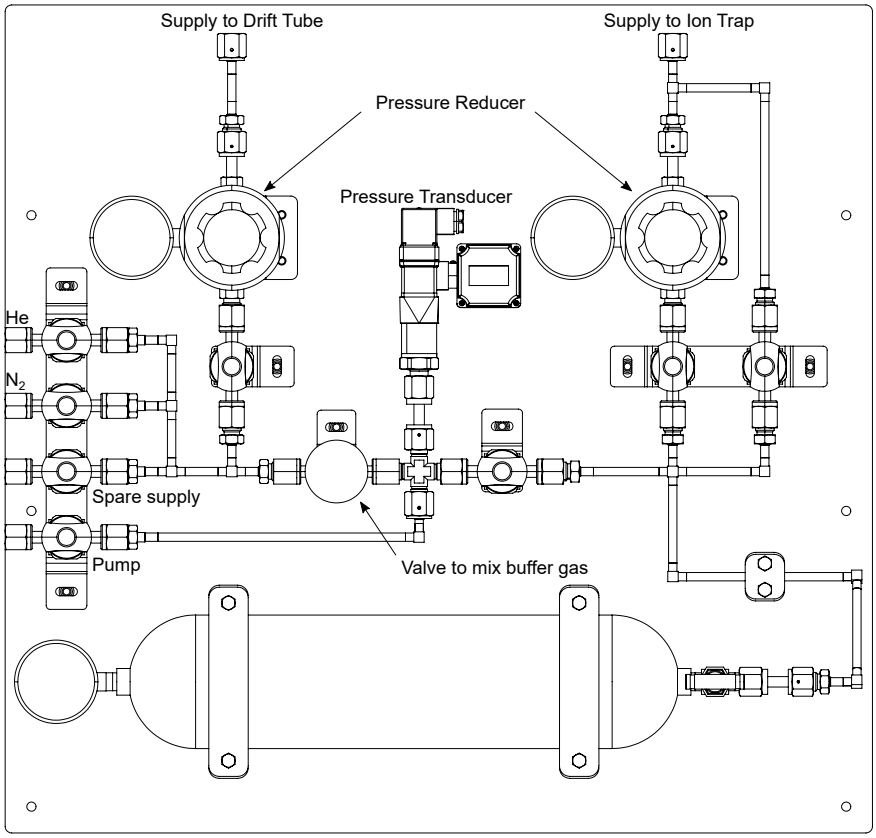

Fig. 4.10.: The Gasbahnhof - Combined Gas Supply for the iMob 2.0 instrument. Gas supply and mixing plate used to supply drift and buffer gas independently. The left side of the plate supplies the drift gas after high pressures have been reduced. The right sight is dedicated for the mixing of buffer gas with messenger tagging gas and supplies the cryogenic ion trap.

4.8. Operation Mode iMob 2.0 - Pressure in the Cryogenic Ion Trap

Throughout the iMob 2.0 instrument, different pressures are applied in order to sufficiently operate the experiment. While the ionisation *via* nESI is achieved at ambient pressure, pressures in the millibar regime are applied in the IMS stage. For the quadrupolar mass spectrometer to be operated, high vacuum is required. For an in-depth documentation of the pressures in the first implementation of the iMob the interested reader may be referred to the theses work of Stephan Warnke.[13,27]

Since the newly implemented section of iMob 2.0 is directly connected to the chamber of the quadrupole mass filter, the ions have already been transferred to high vacuum and the pressure regime. While pressures are elevated in the cryogenic ion trap, it drops to the mid to low 10^{-7} mbar regime in the interaction region and the ToF mass spectrometer during normal operation.

In order to maintain the high vacuum in the recently added parts, four turbomolecular pumps are connected to the vacuum chambers of the cryogenic ion trap, the two quadrupolar deflector housings and the ToF mass spectrometer (2× Pfeiffer HiPace300 TC400 (Pfeiffer Vacuum), 2×

Edwards EXT255H (Edwards Vacuum)). A dry scroll pump (Edwards nXDS10i, Edwards Vacuum) is employed to maintain low vacuum. In addition, two penning gauges are used to monitor the high vacuum, one on the chamber of deflector 2 and one on the ToF mass spectrometer (both Pfeiffer Penning gauge PTR225, Pfeiffer Vacuum).

The conductance between the vacuum chamber housing the cryogenic ion trap and the chamber housing the quadrupole mass filter is not restricted and the pressure measured at the pressure gauge at quadrupole should correspond to the pressure in the chamber around the cryogenic ion trap. The orifice connecting the chamber of the cryogenic ion trap and the chamber of the second quadrupolar deflector has a diameter of 12 mm, hinders gas influx into the deflector chamber and therefore complicates monitoring of the pressures using the gauge on the chamber of deflector 2. The closed and compartmentalised design of the cryogenic ion trap (see Fig. 4.4) allows for different pressures in the different two compartments. In the trapping compartment of the ion trap, the ions are to be thermalised, i.e. they are to loose their kinetic energy upon collision with the buffer gas. In contrast, the pressure out of the cryogenic ion trap should be low enough to avoid a reduction in transmission. Because the mean free path of gas in the ion trap is much larger then the dimensions of the vacuum, the molecular conductance C in $\mathrm{L{\cdot}s^{-1}}$ through the circular apertures of the cryogenic ion trap can be determined from

$$C = 3.7 \times 10^{-2} \cdot \sqrt{\frac{T}{M}} \cdot A \tag{4.1}$$

Where M is the molecular weight of the gas of interest in amu, T the temperature in Kelvin and A the aperture area in $\mathrm{mm^2}$. The radius of the two orifices relevant to determine the conductance is given in Fig. 4.4. Since there is no lens covering the end of the cryogenic ion trap, the area of the cryogenic ion trap itself is used to calculate the conductance and a radius of 30 mm is approximated. Conductance adds up analogous to capacitors in electric networks. Subsequently, the conductance of two apertures in series is calculated as the sum of the two reciprocal conductances. For conductances in parallel, the conductances add up. In case of nitrogen, $M = 28\,\mathrm{g\,mol^{-1}}$, the conductance C_n of the orifices n shown in Fig. 4.4 in the trap at $T = 40\,\mathrm{K}$ is shown in table 4.1.

Tab. 4.1.: Cryogenic Ion Trap - Conductance. See Fig. 4.4 for orifice nomenclature.

Orifice n	C_n [L $\mathrm{s^{-1}}$]
1	125.04
2	1.25
3	0.31
1+2	1.24
(1+2)+3	1.55

Assuming a pressure of $p_{\text{CT -Trapping}} = 1 \times 10^{-3}$ mbar in the trapping compartment of the cryogenic ion trap, the combined conductance of buffer gas out of the cryogenic ion trap leads to a mass rate flow of $Q = 1.6 \times 10^{-3}\,\text{mbar}\,\text{L}\,\text{s}^{-1}$. With a pumping speed of $S = 300\,\text{L}\,\text{s}^{-1}$ the turbomolecular pump connected to the bottom of the cryogenic ion trap vacuum chamber is able to maintain a pressure pressure of $p = 5 \times 10^{-6}$ mbar in the chamber. This pressure can be monitored using the pressure gauge, colloquially referred to as *L3*, mounted to the chamber of the quadrupolar mass filter. In fact, monitoring this pressure allows to reversely conclude the pressure in the cryogenic iron trap. Further, the pressure in the ejection compartment $p_{\text{CT - Ejection}}$ of the cryogenic ion trap can be calculated from the mass flow through orifices 1 and 2, $Q_{1+2} = 1.2 \times 10^{-3}\,\text{mbar}\,\text{L}\,\text{s}^{-1}$, and the conductance through orifice 2 as follows:

$$p_{\text{CT - Ejection}} = p_{\text{CT - Trapping}} - \frac{Q_{1+2}}{C_2} \tag{4.2}$$

Subsequently, the pressure in the ejection compartment of the cryogenic ion trap is $p = 1 \times 10^{-5}$ mbar.

4.9. Tagging conditions

Due to the low number density in the gas phase, absorption IR spectroscopy is not feasible. In order to obtain IR spectra of analytes in the gas phase, action spectroscopy can be applied to circumvent the limitation of a low number density if high photon flux can be achieved. One strategy to implement action spectroscopy is messenger tagging IR spectroscopy (compare section 2.1.3). Messenger tagging of ions of interest is achieved using the cryogenic ion trap outlined before. Using a buffer gas - primarily helium - ions which enter the ion trap are cooled to the temperature of the cryogenic ion trap. The low temperatures are achieved by mounting the cryogenic ion trap on the second stage of a closed cycle cryostat (Sumitomo RDK-408D2, SHI Ltd., Japan). A compressor unit (Sumitomo CSW-71D, SHI Ltd., Japan) is employed to operate the cryostat.

Reproducible tagging of the ions is achieved by combinations of low temperature, a defined pressure in the ion trap, usually in the 10^{-6} mbar regime at the quadrupole, and a low fraction of messenger gas mixed with the buffer gas which flows into the trap. The influence of the different parameters involved in messenger tagging is assessed in section 5.3. Section 4.8 introduced how the pressure in the ion trap can be determined.
Tagging with helium as messenger tag is not possible because the ion trap cannot be cooled low enough for helium tagging to be achieved. In practice, the cryogenic ion trap cannot be cooled below 26 K. A Lake Shore 340 temperature controller (Lake Shore Cryotronics, Ohio, USA) allows for temperatures between 25 and 150 K to be reached using a 25 W heater attached to the cryogenic ion trap. The heater is controlled in steps of 0.1 % of 25 W and the temperature of the cryostat and the ion trap is monitored with three temperature diodes. One is attached directly to the

cryostat, one to the adapter stage used to attach the cryogenic ion trap to the cryostat and one to the bottom of the cryogenic ion trap itself.

4.10. Timing and Data Acquisition

To sufficiently run the iMob 2.0 experiment, some ion optics need to be operated in a given order and at a relative time dependency: for example, it would not work to have the gate for IMS selection (denoted as *ATD Slice* in Fig. 4.11) to change from high to low state at the same time as ions are injected into the drift tube. Therefore, two delay generators are employed to allow for the introduction of time dependencies. The first delay generator controls the aforementioned time dependency of the IMS section of the instrument and is depicted in the upper panel of Fig. 4.11. Driven by an internal clock, frequencies up to 200 Hz can be set to allow for the injection of ions into the drift tube by the *IMS Gate*. This gating is necessary, as a continuous trickling of ions into the drift tube would prevent from recording arrival time distribution on the detector on line of the drift tube. A second set of ion optics with a time dependency to it is the so called *ATD Slice*. In basic operation, this lens is set to its low voltage and allows ion transmission. If in use, the lens is at its high voltage most of the time and only switches to the low voltage to allow a certain fraction of the ATD to pass, i.e. it allows for IMS selection. The delay used to realise this IMS selection is denoted as $t_{\text{ATD slice}}$ in Fig. 4.11 and references to the injection of ions into the drift tube.

In order to allow for an independent operation of the IR spectroscopy section of iMob 2.0, a second delay generator is employed. While also a second internal clock can be used for running the experiment during tuning and setup, the trigger signal of the electron gun of FEL laser is used during beam times to control ion transfer in and ejection from the cryogenic ion trap as well as pulsing of the pusher and puller plates of the ToF mass spectrometer. This allows for a well timed overlapping of the molecular ion and the laser beam at a spatial point in the interaction region which can be adjusted by shortening or elongating the delay t_{FEL} seen in Fig. 4.11. This delay can be estimated by

$$t_{\text{FEL}} = 700\mu s - (l_{\text{CT Gate}} + t_{\text{TOF}}/2)$$

where $l_{\text{CT Gate}}$ is the duration of the CT Gate trigger, enabling the transfer of ions from the trapping to the ejection compartment, and t_{TOF} is the time ions require to travel from the ejection region of the cryogenic ion trap to the ToF mass spectrometer. The $-700\,\mu s$ is the negative delay after which the FEL laser should approximately arrive to the instrument and can be set by the FEL operator depending on the preferences of the individual experiment. However, the 700 µs contain an uncertainty. Because the electron gun trigger is used, a delay in the order of a few microseconds has to be added in order to obtain the time at which the laser arrives to the experiment. Here, the trigger signal which arrives as a lead before the laser is used as reference point for the timed control of the switchable ion optics. t_{TOF} is a variable for different samples, as the energy gained by the ions upon ejection and acceleration should remain the same for all samples. The resulting

velocity, however, depends on the m/z ratio of the sample, and higher m/z values result in lower velocities, i.e. longer t_{TOF}. The trace *Data Sync* in Fig. 4.11 refers to the limited time for saving a spectrum before a new spectrum is acquired.

Toggle Mode for Background Acquisition

As laid out before, the trigger signal of the FEL laser with a frequency of 10 Hz is used to control the ion optics in a time-dependent manner to guide ions through the instrument and synchronise the laser and molecular ion beam. In order to acquire a background spectrum without IR irradiation, a digital toggle mode was implemented (see Fig. 4.11). This toggle mode allows to bisect the trigger signal provided with the FEL and acquire a background signal at a rate of 10 Hz shifted by 50 ms compared to the spectrum acquired immediately after IR irradiation. This toggle mode is controlled by the same delay generator used for the control of the instrument with lasing. In fact, the toggle trigger references to the triggering with lasing with a 50 ms delay and a duration of 49.5 ms to avoid overlapping with the subsequent data acquisition during laser irradiation. The toggle trigger signal then mediates which input channel of the oscilloscope for monitoring the ToF signal is active and as such allows to write data with lasing and the background data in two alternating channels.

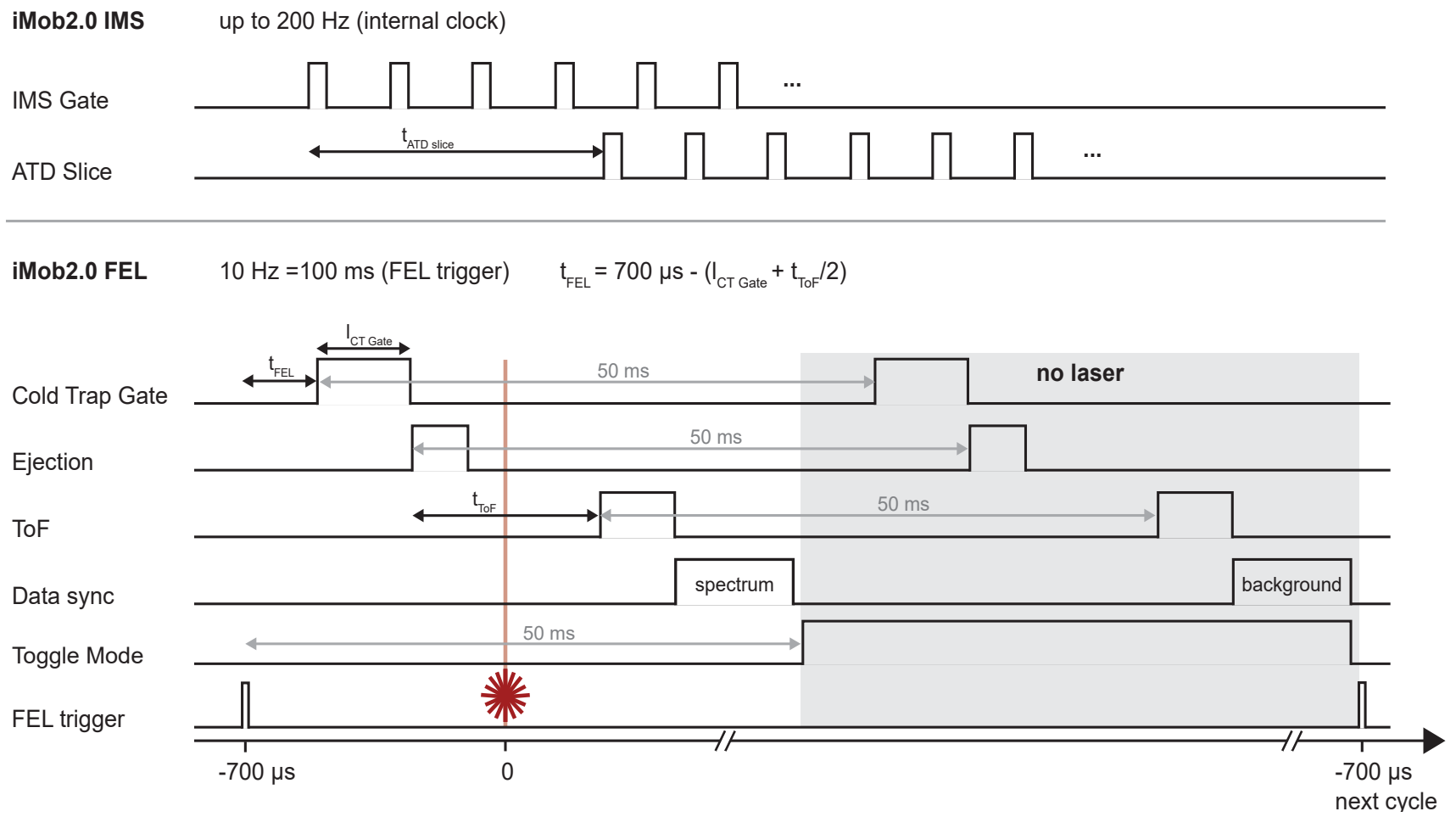

Fig. 4.11.: iMob 2.0 Timings and Pulse Sequence. The ion mobility spectrometry (IMS) trigger pulse controls the injection of ions into the drift tube (IMS Gate) and the selection of a fraction of the ion cloud after ion mobility separation (ATD slice). The trigger pulse of the electron gun of the Fritz Haber Institute Free Electron Laser (FHI FEL) controls the new messenger tagging IR spectroscopy section. The approximately −700 µs lead of the triggers over the laser beam suffices for the ions to reach the interaction region. The equation given is an empirical rule of thumb to estimate the time between ion ejection from the cryogenic ion trap and the overlay with the laser.

4.11. Materials

Solvents used throughout this work were of HPLC grade and purchased from Sigma-Aldrich.

4.11.1. Leucine-enkephalin

Leucine-enkephalin (LEK) was purchased from Sigma Aldrich, Switzerland, and used without further purification. For experiments, a 50 µM LEK solution in water/methanol (v/v: 1/1) was prepared. Fig. 4.12 shows the amino acid sequence of protonated LEK ($[LEK + H]^+$).[96]

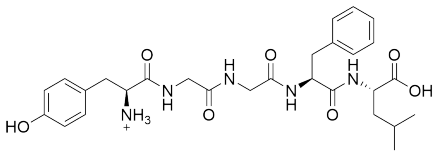

Fig. 4.12.: Structure of protonated leucine-enkephalin

4.11.2. Lewis X and Blood Group type 2 sugars

Lewis X and Blood Group H type 2 trisaccharides were purchased from Elicityl SA, France. The trisaccharides were dissolved to yield 1 mM stock solutions using water. For measurements, sample solutions were prepared freshly by diluting the stock to 500 µM with water/methanol (v/v: 1/1).

4.11.3. Cytochrome C

Bovine cytochrome C was purchased from Sigma Aldrich, USA, and used without further purification. For the preliminary testing of the instrument, a 50 µM solution in 10 mM NH_4COO was used.

5. Results and Discussion

5.1. Technical Improvements of the iMob 2.0 Experiment

5.1.1. Upgrading Quadrupolar Deflector

In the first realisation, the quadrupolar deflectors were constructed and operated with the chamber and the lenses on the side faces being connected to ground. Comparing the signal intensity of the ATD signal at deflector 1 on axis of the IMS section with the signal on the detector on deflector 2 after the cryogenic ion trap, a loss in signal intensity by a factor of 50 could be observed. Given the pulsed ejection out of the cryogenic ion trap, the loss in signal intensity was expected to be lower. To increase the deflection efficiency, the electrical insulation of the quadrupolar deflector 1 was explored. Electrical insulation was achieved using four PEEK feet for the chamber housing and replacement of the stainless steel spheres holding the side face lenses in the ion's trajectory in place with ruby spheres (see Fig. 4.3 for details). Additional wires connecting the two lenses on the trajectory to the cryogenic ion trap and the chamber separately with a voltage source have been added. For simplicity, theses three elements are not supplied with individual voltages. Instead, they are supplied using the centerline potential of the two deflector voltages. The voltages are averaged using a simple voltage divider consisting of two resistors of same resistance as depicted in Fig. 5.1.

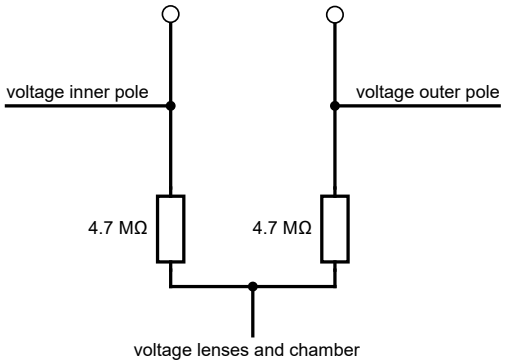

Fig. 5.1.: Voltage Divider for Deflector Chamber and Lenses. The voltages applied to the two pairs of quarter round rods are averaged using two resistors of same resistance to operate the deflector chamber and the lenses on the side faces on the centerline potential of the quarter round rods.

5.1.2. Improved Referencing for the Temporal Control of the Spectroscopy Part

Section 4.10 introduced the time dependent operation of ion optics in the IMS and the spectroscopy stage of iMob 2.0. It was layed out, that the 700 µs lead of the trigger over the arrival of the FEL laser in the instrument was used for referencing of the gate for ion transfer in and ejection from the cryogenic ion trap as well as for pulsing of the puller ans pusher plates in the ToF mass spectrometer.

Since this referencing scheme is not intuitive and the rule of thumb introduced to calculate the delay after arrival of the FEL trigger is an empirical estimation, the referencing was updated after the initial commissioning. The relative dependency of the trigger signals for the individual switchable ion optics remains the same, but $t = 0$, i.e. the arrival of the FEL laser pulse to the instrument, is the new reference point. Negative delays, i.e. leads, are used to reference back from $t = 0$. As such, t_{delay} is the point in time at which the ejection ramp switches back from ejecting to trapping and the duration of the ejection trigger itself is a negative value ending at t_{delay}. Same principle applies to the timing of the cold trap (cold trap (CT)) gate; the end of its trigger references to the beginning of the ejection trigger and it as a 'negative' duration starting at the end of CT gate. The ToF puller and pusher are pulsed with respect to the beginning of the ejection trigger as before. This updated referencing scheme has a major advantage: By adjusting t_{delay}, the train of trigger signals is shifted with respect to the arrival of the FEL laser pulse and allows for easier adjustment of the spatial and temporal point of the overlay between molecular ion and laser beam.

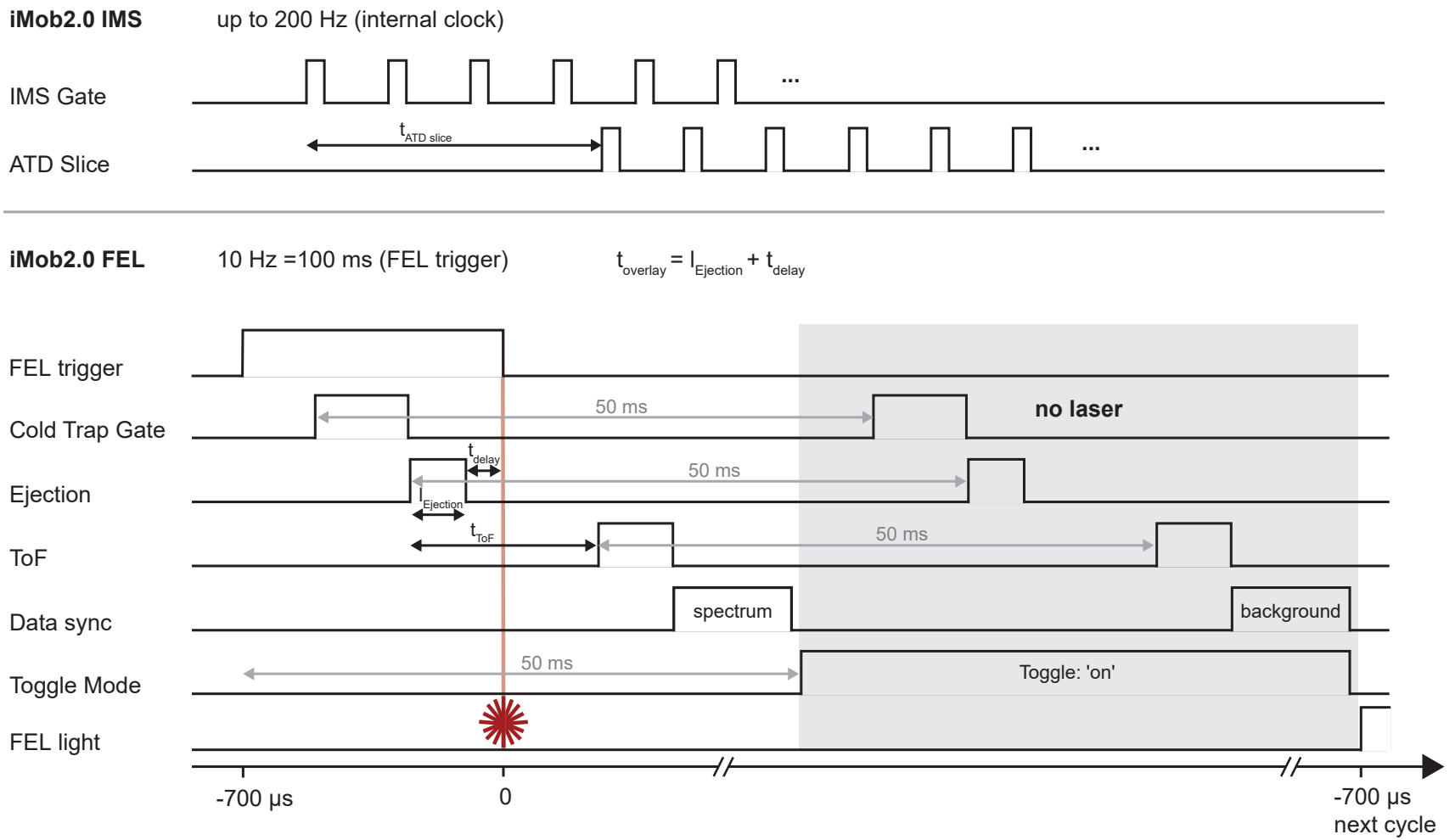

Fig. 5.2.: Updated Timing Scheme for the Spectroscopy Section of iMob 2.0. The referencing for the spectroscopy section of the iMob 2.0 experiment to a 700 µs lead of the laser introduced with Fig. 4.11 was replaced by referencing to $t = 0$, the arrival of the laser in the experiment.

5.2. Operational Practice in Routine Measurements on the iMob 2.0

5.2.1. Operational Pressures in Cryogenic Ion trap

Table 5.1 lists four pressures commonly used to operate the cryogenic ion trap during operation. The pressure is monitored at the high vacuum pressure gauge *L3* and used to conclude the pressure in the cryogenic ion trap as layed out in section 4.8. As a rule of thumb, multiplying the pressure measured at *L3* by 200 gives the pressure in the trapping compartment of the cryogenic ion trap. The pressure in the trapping compartment is in turn two orders of magnitude higher than the pressure in the ejection compartment.

Tab. 5.1.: Conversion of pressures measured at *L3* to pressures used to operate the cryogenic ion trap.

p (***L3***)	p **(Trapping Compartment)**	p **(Ejection Compartment)**
4×10^{-6} mbar	8×10^{-4} mbar	8×10^{-6} mbar
3×10^{-6} mbar	6×10^{-4} mbar	6×10^{-6} mbar
2×10^{-6} mbar	4×10^{-4} mbar	4×10^{-6} mbar
1×10^{-6} mbar	2×10^{-4} mbar	2×10^{-6} mbar

5.2.2. Exemplary Operational Voltages

Table 5.2 gives an exemplary overview over the voltages used for small molecules (LEK and Le^{x}) during operation of the iMob 2.0 instrument. For individual samples, these voltages may vary slightly and during routine operation, the RF amplitudes have to be tuned to the sample under investigation. In addition, different m/z seem to affect the slope of the ejection ramp. Thus, the ejection and acceleration voltages require tuning, too. Even though it is not completely clear how this effects the ejection from the ion trap, ions with larger m/z seem to require a steeper ejection ramp which might be required to overcome a larger moment of inertia for sufficient ejection from the cryogenic ion trap. Since the ejection voltages also vary depending on the pressure in the cryogenic ion trap, the voltages might also depend on the effectiveness of thermalisation upon collision with the buffer gas and the amount of ions trapped in the cryogenic ion trap.
Against common perception, the voltages applied to the quadrupolar deflectors should not discriminate for m/z but may serve as energy filters. This, however, should not be a problem, because the molecular ion species of interest will not have a broad range of energies. In order to avoid discrimination of energies on the edges of the distribution, the width of the energy window which is sufficiently bend, can be adjusted. By choosing a pair of high absolute voltages applied to the two pairs of quarter round rods in the deflectors, the energy window can be widened.

Tab. 5.2.: Exemplary voltages used for routine operation of iMob 2.0.

Voltage	**[V]**
Ion Mobility Part	
Funnel start	10.0
Mid	40.0
Trap	10.6
IMS Gate	15.4
Injection	30.2
Drift Tube	2000.0
Drift End	190.0
Exit End	24.0
Ion guide 1	20.3-17.0-16.0
Ion guide 2	11.2-8.0-6.3
ATD Slice High	200.0
ATD Slice Low	15.0
Deflector 1 -	-50.0
Deflector 1 +	24.0
Cold Trap Section	
Einzel Lens B1 - CT	-40.3
Cold Trap Entry Lens	19.8
Cold Trap Front	18.5
Cold Trap RF	350.0
Cold Trap End	19.2
Cold Trap Gate High	24.5
Cold Trap Gate Low	18.5
Ejection Front	15.8
Ejection End Low	6.2
Ejection End High	40.0
Pre-Acceleration	15.6
Acceleration 1	14.2
Acceleration 2	11.7
Post Acceleration	0.0
Einzel Lens CT - B2	-40.3
Deflector 2 -	-25.0
Deflector 2 +	17.0
Einzel Lens B2 - Hex	-40.4
Hexapole Offset	0.0
Hexapole RF (a.u.)	400.0
Einzel Lens Hex - B3	-40.5
Deflector 3 -	-25.0
Deflector 3 +	17.0
Time of Flight	
Einzel Lenz B3 - ToF	-40.2
ToF Focus	0.0

5.3. Tagging Behaviour

Before the iMob 2.0 experiment was brought into operation, a more or less uniform tagging behaviour for all molecules was expected. Furthermore, data acquisition should have allowed for background corrected spectra to be recorded. In an ideal case, the no-laser and laser data acquisition would capture only ion signals for singly-tagged ions (no-laser trace) and parent ions (laser trace) after depletion of the messenger tag. Small fractions of non-tagged species or species that remain tagged would have been baseline corrected.

However, global tagging behaviour could not be observed and a pragmatic approach towards data analysis has to be implemented. Certainly most striking is the different tagging efficiency observed for leucine-enkephalin and the Lewis X sugar. The molecular weight of the two samples differs only by 27 u (about 5 %) but the observed tagging behaviour during initial trials is completely different. Protonated leucine enkephalin ($[\mathrm{LEK} + \mathrm{H}]^+$) resembles the ideal case of mostly singly tagged ions best for the conditions sampled, depicted in Fig. 5.3a. The small amount of higher tagged species is negligible and can be considered as background for a well set FEL power and focus. In addition, the signal of the parent ion is weak enough to monitor its increase upon messenger tag depletion sufficiently. Contrary, tagging of the protonated Lewis X sugar ($[\mathrm{LeX} + \mathrm{H}]^+$) is hardly achieved. While tagging of LEK was observed without much optimisation needed, $\mathrm{Le^X}$ shows only a low tagging efficiency and the parent ion signal is dominant (compare Fig. 5.3b). Lowering the temperature of the cryogenic ion trap to 35 K overcomes this limitation partially and a 1:1 ratio of singly tagged ions and non-tagged ions could be achieved. However, the remaining high signal of non-tagged ions renders the initial data acquisition strategy unsuitable, because a further increase in the ToF signal cannot be monitored sufficiently. On the other hand, the sodiated adduct of Lewis X ($[\mathrm{LeX} + \mathrm{Na}]^+$) shows very efficient tagging even for higher order tags, rendering the conceived strategy unsuitable, too (Fig. 5.3c).

Considering these three different cases of tagging behaviour, a flexible approach to the calculation of an IR spectrum is needed. Fig. 5.3 illustrates the three different cases of predominant ion signals. The first case refers to the predominant signal of singly tagged ions as observed with LEK. By tuning the time of the ToF trigger and the acceleration voltages after the cryogenic ion trap, the signal of the singly tagged ions in the ToF can be maximised while the ion signal of non-tagged or higher tagged ions can be minimised. Subsequently, the depletion of a messenger tag upon laser irradiation can be monitored by a decrease in the singly messenger tagged ion signal and an increase in the parent ion signal. Therefore, background corrected spectra can be calculated without difficulties. For the second case depicted in Fig. 5.3, the predominance of parent ion signal and hardly any tagged ions is observed. By varying of the tagging conditions (temperature, pressure at *L3* and messenger tagging gas fraction) as well as tuning of the ToF detection for the singly tagged ion should maximise its signal. Because it is difficult to eliminate parent ion signal completely, IR spectra are generated by only monitoring the change in signal upon depletion of the messenger tag.

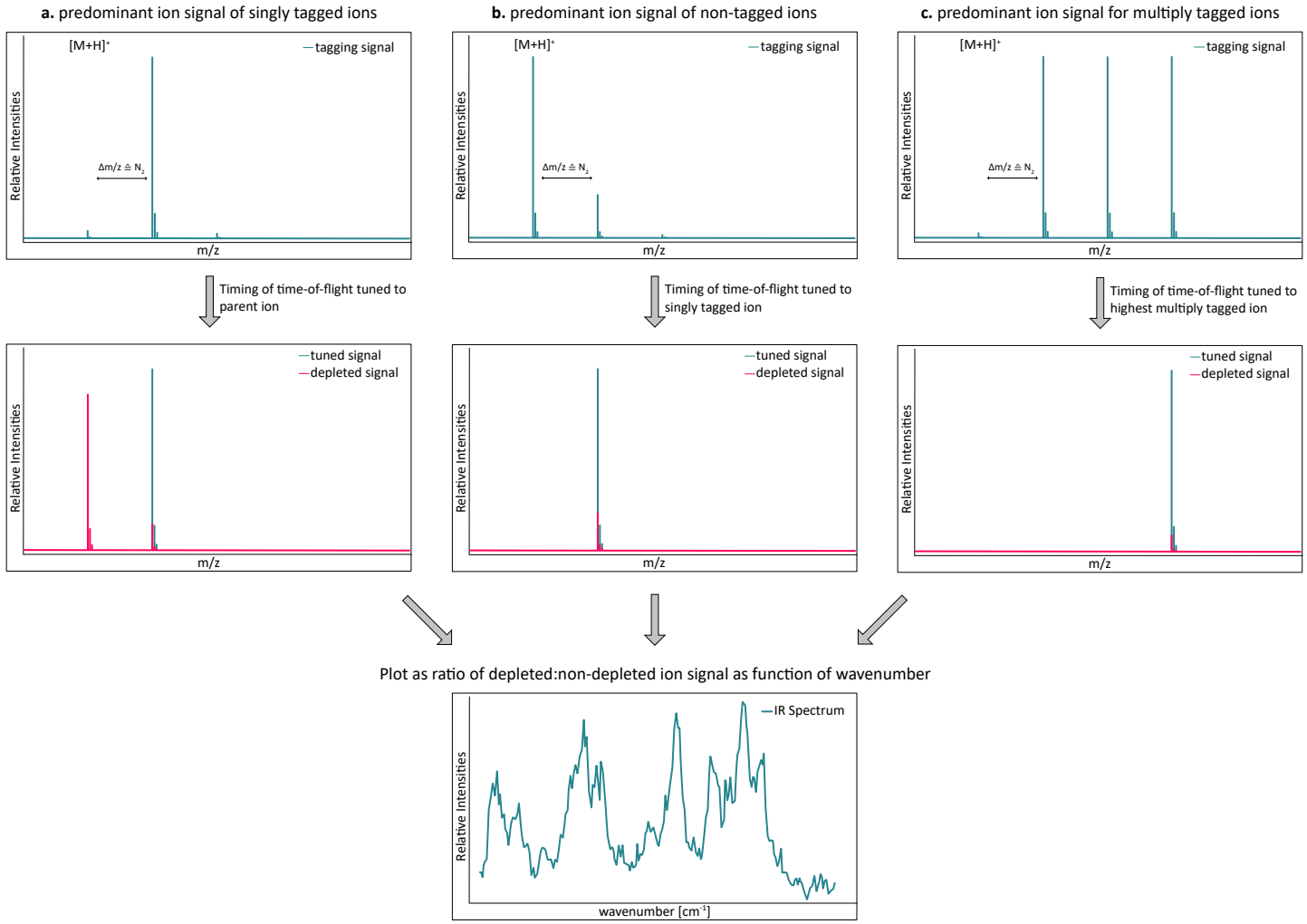

Fig. 5.3.: Variants of tagging spectroscopy. Different molecules and even different adduct ions of the same molecule show different tagging behaviour. In order to sufficiently record IR spectra, it is important to tune the signal in the time-of-flight mass spectrometer.

In a third case, not one predominant ion signal can be observed. Rather, higher tagging is predominant. For suitable spectra acquisition, the detection in the ToF is tuned for the ion signal with the highest number of tags. Similarly to case b. in Fig. 5.3, only the depletion, i.e. the change in the ion signal of highest tagging is monitored and the difference between no-laser and laser trace used to calculate the spectrum.

5.3.1. Evaluation of messenger tagging conditions

Reproducible messenger tagging of the molecules of interest is key to realise the principle of action IR spectroscopy as laid out in section 2.1.3. However, the cryogenic ion trap described above features three different parameters, temperature, pressure in the trapping compartment, and fraction of messenger tagging gas in the buffer gas, which allow for the control of messenger tagging conditions. In addition, the distribution of parent ions and messenger tagged species as observed in the ToF mass spectrometer heavily depends on the trigger which is used to pulse the extraction plates in the ToF mass spectrometer, i.e. they control which slice of the ion cloud is detected after ejection of the ions from the cryogenic ion trap. For all mass spectra evaluated and shown below, a total of 200 scans was added up in the ToF mass spectrometer.

Early during the commissioning of the iMob 2.0 experiment, it was observed, that the tube which is used for the supply of buffer gas to the cryogenic ion trap would get clogged when low temperatures were maintained for a longer time (more than a day). Therefore, the initially used PTFE tubing of 0.5 mm inner diameter was replaced by a PTFE tube of 1 mm inner diameter and the problem did not re-occur thereafter. As a consequence of changing the PTFE tubing, however, altered messenger tagging behaviour of protonated leucine-enkephalin could be observed. Before the remodelling, it was possible to observe multiple messenger tagged ions of protonated LEK in the ToF mass spectrometer as can be seen in Fig. A.3. After the remodelling however, ion signal of multiply messenger tagged ions was no longer predominant but mostly singly messenger tagged ions could be observed (compare Fig. A.4). Compared to the tubing with an inner diameter of 0.5 mm, the new tubing was not wound around the cryostat head. Therefore, differences observed in messenger tagging may result from reduced capacities to precool the buffer gas. The narrow tube was wound around the cryostat and insulated from the vacuum using copper foil. The newly implemented tubing now directly connects the inlet into the vacuum chamber with the inlet into the cryogenic ion trap spanning through vacuum. Even though there are drilled loops in the cryogenic ion trap to precool the gas, this may not suffice and the buffer gas now enters the cryogenic ion trap at a higher temperature than before. Following the difficulties to work in the vacuum chamber, the old tubing is still in place around the cryostat and could be exchanged with the new tubing in case one is interested in elucidating the altered messenger tagging behaviour further. In addition, it might be of interest to explore the messenger tagging behaviour closer to the lower temperature limit of the cryogenic ion trap and sample messenger tagging conditions between 30 and 40 K. Certainly, this can also be due to variations in the ToF trigger controlling the extraction

plates because these deviate slightly from measurement to measurement due to slightly varying voltages of the ToF mass spectrometer. However, it is unlikely to completely miss higher tagged species, because the duration of the trigger signal and thus width of the ion cloud that is extracted into the mass spectrometer is not altered. With regard to the pulsing of the extraction plates, it has to be pointed out, that the high voltage switch for the ToF experienced a malfunctioning component and had to be exchanged for older hardware. This older switch does not act as rapidly to the trigger signal as the broken switch and therefore requires elevated voltages for *V1*, *Pusher*, and *Puller*. This additionally increases the uncertainties to compare tagging conditions observed during different times of the instruments commissioning.

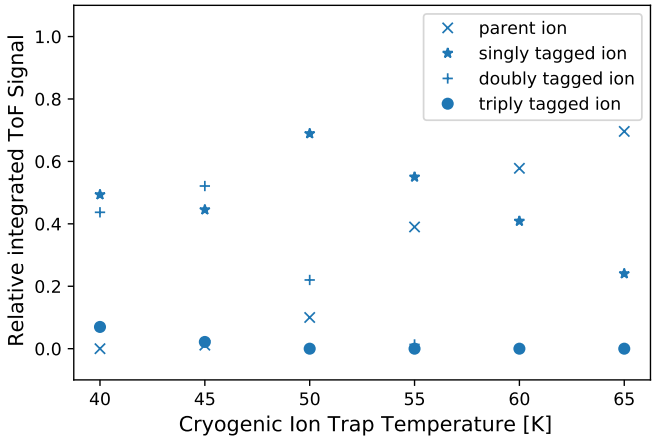

Fig. 5.4.: Temperature influence on the messenger tagging efficiency of protonated leucine-enkephalin. The evaluation is based on Fig. A.3 and was performed for a set of mass spectra acquired for varying temperatures from 40 to 65 K at a pressure of 5×10^{-6} mbar and 4 % N_2 in helium buffer gas.

In general, several trends can be concluded from a plethora of mass spectra recorded over the course of this thesis. All pressures mentioned here refer to the pressures measured in the quadrupole chamber and correspond to higher pressures in the ion trap (see section 5.2 for details). The mass spectra have been evaluated using a Python script to pick signals, integrate these signals, and determine the ratio of the signals in one spectrum.[97]

Fig. 5.4 shows the analysis of the temperature dependency of messenger tagging in the cryogenic ion trap before the remodelling of the buffer gas tubing. While keeping the pressure at a constant 5×10^{-6} mbar and a fraction of 4 % N_2 in helium, the temperature was varied from 40 to 65 K in steps of 5 K. As can be seen, triply messenger tagged ions can only be observed for 40 K and 45 K. Further, the fraction of parent ions increases significantly for temperatures above 50 K while the fraction of singly tagged ions decreases inversely. Doubly messenger tagged ions are also only

observed for temperatures below 55 K. Based on these observation it can be argued, that lower temperatures favour messenger tagging and allow for the detection of multiply tagged species, at least prior to the remodelling of the tubing. Therefore, it would be beneficial to explore the messenger tagging efficiency at temperatures below 40 K, potentially even as low as the lowest possible temperature of 26 K. Contrarily, Fig. A.4, as shown in the appendix, does not confirm the observation of detecting ions with multiple messenger tags after remodelling of the tubing. This can, however, be also due to the implemented changes as raised above.

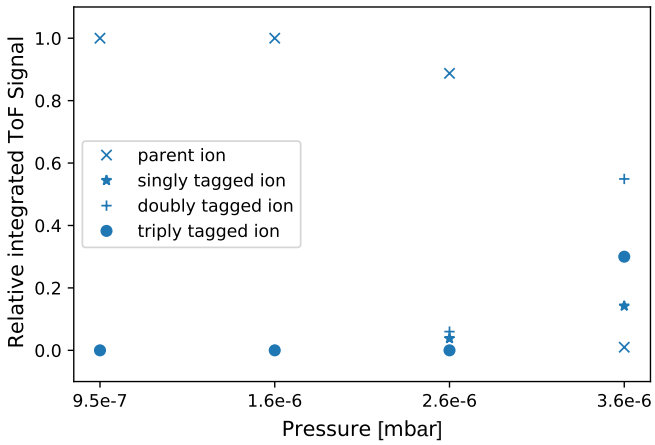

Fig. 5.5.: Messenger tagging efficiency of protonated leucine-enkephalin at varying pressures. Underlying spectra were recorded at 45 K, using 5 % N_2 in helium, and are shown in Fig. A.5.

Similar to the observation of higher messenger tagged species, differences in the optimal pressure to be used for thermalising and messenger tagging of ions in the cryogenic ion trap could be observed throughout the commissioning of iMob 2.0. For the very first measurements at the beginning of this thesis' work, a pressure of 5.6×10^{-6} mbar was found to give the best ion signal in the ToF mass spectrometer. Later on, a pressure from 2 to 4×10^{-6} mbar was employed to facilitate a sufficient operation of the cryogenic ion trap. Fig. 5.5 shows the dependency of messenger tagging as a function of the pressure monitored in the quadrupole chamber. While low pressures only suffice to thermalise the ions, increasing the pressure above 2.6×10^{-6} mbar leads to an increased efficiency of messenger tagging of protonated leucine-enkephalin. The pressure dependency depicted here was explored at a temperature of 45 K, using a fraction of 5 % N_2 in helium. First experiments using larger proteins (RNase) also hint, that slightly higher pressures compared to LEK are required to efficiently thermalise ions of higher m/z values .

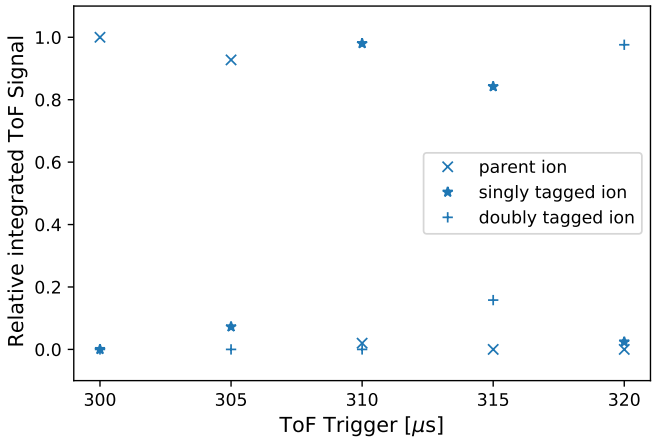

Fig. 5.6.: Messenger tagging observed of protonated leucine-enkephalin depending on the ToF trigger. The evaluation is based on Fig. A.6 and was performed for a set of mass spectra acquired for varying ToF trigger at a pressure of 1.6×10^{-6} mbar and 7.5 % N_2 in helium buffer gas.

As outlined before, the trigger signal used to control the extraction plates in the ToF mass spectrometer allow for different slices of the ion cloud coming from the cryogenic ion trap to be detected. To exemplify the effect of different delays between the ejection from the cryogenic ion trap and the pulsing of the extractor plates, Fig. 5.6 depicts the change in observed species over a delay range of 20 ms for leucine-enkephalin at 45 K, a pressure of 1.6×10^{-6} mbar, and a fraction of 7.5 % in helium.

One motivation to conceive a centrally controlled gas supply for the drift tube and the cryogenic ion trap was the need for instrumentation to finely adjust the fraction of messenger tagging gas in the buffer gas. The aforementioned *Gasbahnhof* allows to prepare buffer gas mixtures doped with a small fraction of messenger tagging gas. Intuitively, it might seem obvious that higher tagging can be observed upon using a higher fraction of messenger tagging gas in the buffer gas mixture. While this certainly could be experienced at the beginning of the work on the iMob 2.0, Fig. 5.7 cannot confirm this dependency. For simplicity, data acquired for higher temperatures is not shown. In order to avoid the tubing getting clogged with frozen N_2, N_2 fractions above 10 % have not been explored to date. The contrary distribution of parent ions and singly tagged ions seen for 2.5 %, 5 %, and 7.5 % N_2 at 40 K and 45 K cannot be explained plausibly.

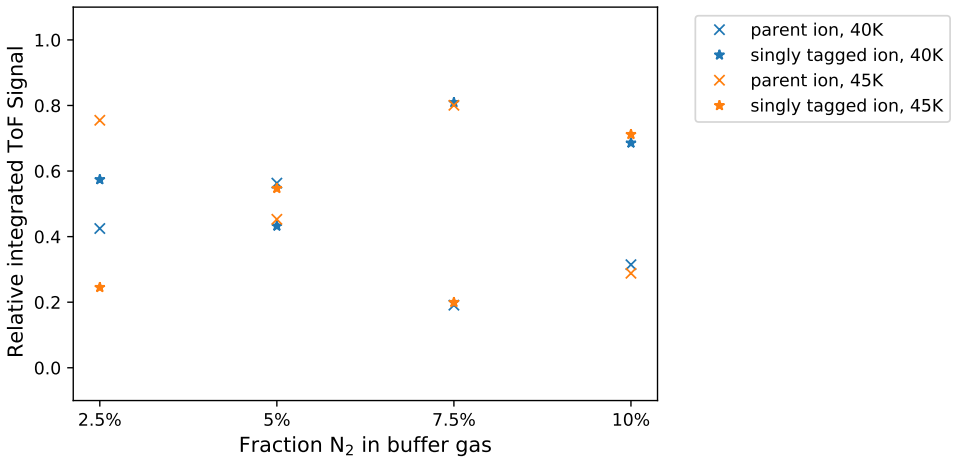

Fig. 5.7.: Messenger tagging efficiency plot of sodiated Lewis X depending on the N_2 fraction. Analysed mass spectra were recorded at 40 K and 45 K, respectively. A pressure of 3×10^{-6} mbar was maintained in the quadrupole region. Fig. A.7 and Fig. A.8 were analysed to evaluate the effect of different messenger tag fractions at different temperatures.

5.3.2. Messenger tagging of bovine cytochrome C

In the course of investigating larger systems, bovine cytochrome C was used to test for the transmission of a 12 kDa protein through all the ion optics to the time of flight mass spectrometer. As Fig. 5.8 nicely illustrates, detecting protonated cytochrome C in a 15+ charge state ([CytC + 15 H]$^{15+}$) in the ToF mass spectrometer was possible after minor optimisation of the ion optic voltages. At a trap temperature of 40 K and 2.5 % N_2 messenger gas in helium, singly and doubly messenger tagged species could be detected as annotated in Fig. 5.8. Intriguingly, even for this high charge state and a difference in $m/z \approx 2$, these three ion species are baseline separated. In order to allow for messenger tagging IR spectroscopy on cytochrome C, the signal intensity as observed in the ToF should be further increased. Furthermore, it is desirable to detect lower charged states of proteins, because high charge states usually do not resemble the native structure of a molecule due to charge repulsion.

5.4. Characterisation of the Cryogenic Ion Trap

Understanding the influence of individual parameters on the performance of the experiment and their effect on the results is highly rewarding. Below, different variables of the iMob 2.0 raised and explained in chapter 4 will be evaluated to improve the understanding of the machine itself but also to facilitate routine measurements.

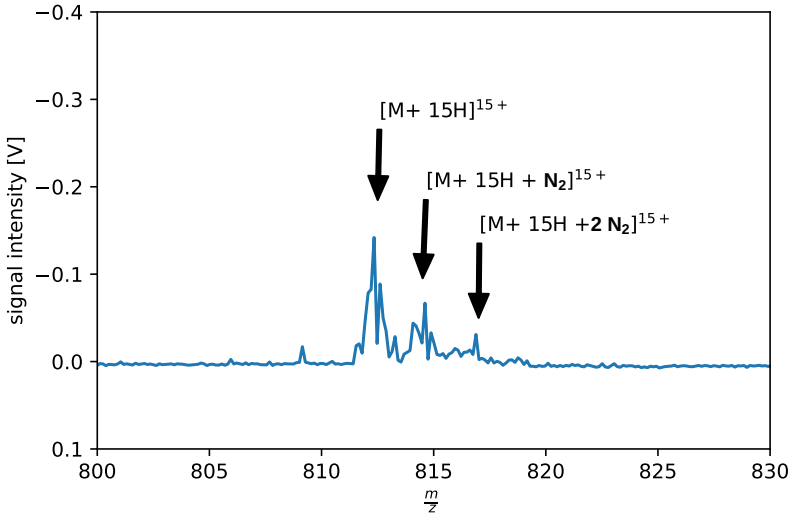

Fig. 5.8.: Mass spectrum of Cytochrome C ($[\mathbf{CytC + 15\ H}]^{\mathbf{15+}}$). The mass spectrum clearly shows baseline separated signals for the parent ion, a singly and doubly tagged species.

Implementing a Cold Trap Voltage Ramp

As outlined above, the instability of the ions in the ejection compartment as well as the long duration of the CT gate trigger required for good ion signal might be due to ions collapsing into the cold trap gate lens[1]. In order to investigate the stability of thermalised ions in the trapping compartment, different combinations of voltages applied to the front and end PCB element are sampled and evaluated based on the integrated ToF signal. Fig. 5.9a depicts the influence of different voltage pairs applied to the front and end of the trapping compartment. The first data point was acquired for an almost flat potential of 18.6 V for CT front and 18.7 V for CT end as the initially conceived operation mode and served as reference. Implementing a voltage ramp with a negative slope, i.e. the voltage applied to the front is larger than the voltage applied to the end, was used to rule out that ions will collapse into the cold trap entry lens. Keeping the voltage applied to the end at 18.7 V, a voltage ramp descending to the end gave even less signal than with an even potential. This already holds true for the minor difference of 0.1 V. Creating a ramped potential rising from front to end, the integrated ToF signal is increased by more than 25 % and no clear preference for an increase by 0.5 V or 1.0 V can be observed. Based on this finding, the voltages applied to the trapping compartment of the cryogenic ion trap can be refined from a flat potential depicted in Fig. 4.8 or Fig. 4.9 respectively to include a slowly rising potential as shown in Fig. 5.9b.

[1] see Fig. 4.4 for details

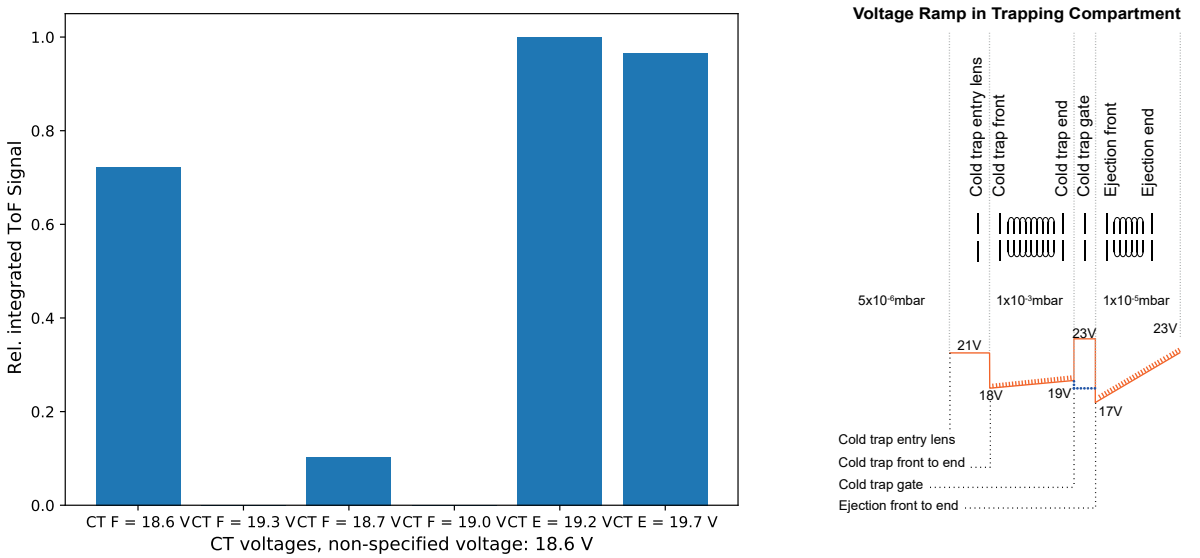

(a) **(b)**

Fig. 5.9.: Cryogenic Ion Trap - CT voltage ramp. Monitoring the ion signal in the ToF mass spectrometer, the effect of different voltage potentials applied to the trapping compartment is evaluated. For the first four settings of Cold Trap Front (CT F), Cold Trap End (CT E) was kept at 18.7 V. When varying CT E, CT F was kept at 18.6 V. A slowly rising potential from front to end results in a higher ToF signal.

Varying the Ejection Rate

Despite the predetermined repetition rate of the FHI FEL of 10 Hz which is used to run the spectroscopy section of the iMob 2.0 in routine operation, it is interesting to observe how the ToF signal changes with slower or faster trigger rates while keeping a rate of 80 Hz to inject ions into the drift tube, i.e. fill the cryogenic ion trap. Varying the trigger rate on an external delay generator allowed to probe the stability of ions in the cryogenic ion trap. Repetition rates as low as 0.25 Hz were used to evaluate stability on the second time-scale. Fig. 5.10 demonstrates that ions remain stable for periods up to one second when looking at the orange and blue traces for a constant and a rising CT potential. The almost linear slope of last three data points up to a trapping time of 4 s of the green trace suggests that either the space charge limit in the ion trap has been reached or the detector amplifier was saturated due to very high ion signal (>5 V) in the ToF mass spectrometer. Since the signal integrals are normalised for the three data individually, comparison of the integrals is possible only to a limited extend. However, it is intriguing that the traces for a rising and a constant CT potential behave similarly.

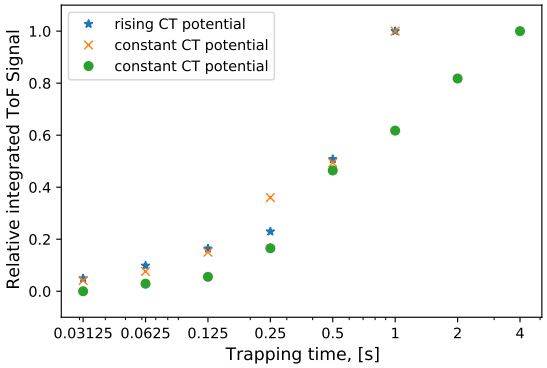

Fig. 5.10.: Investigation of the stability of ions in the cryogenic ion trap. Variation of the trigger signal governing CT gate and the ejection ramp allows to investigate the stability of ions in the cryogenic ion trap.

Duration of Cold Trap Gate Trigger

During the initial commissioning of the experiment, parameters were primarily chosen to yield good signal in the ToF spectrometer. The duration of the cold trap gate trigger, i.e. the trigger responsible for the transfer of messenger-tagged ions from one cryogenic ion trap compartment to the other, was set to 400 µs. For most ions below $^{m}/_{z} = 1000$, this is longer than the time required for IR spectroscopy and detection, as the trigger for the ToF is delayed from the start of the ejection trigger by up to 400 µs. The effect of a shorter duration of the cold trap trigger is monitored by comparing the integrated ToF signal of the sodiated LeX ions ([LeX + Na^+]). Fig. 5.11a shows that upon bisecting the duration to 200 µs, no ions can be detected in the ToF spectrometer anymore. Even reduction of the trigger length by only 100 µs to 300 µs yields a significant reduction in signal as can be seen in Fig. 5.11a. While transfer of ions should be rapid, a low space charge in the trapping compartment might be causing the slow transfer. However, this seems rather unlikely as many ions should enter the ion trap given the high rate of 80 Hz at which the IMS stage of the instrument is operated. The long time scale required might also be due to the limited diffusion of thermalised ions from the trapping compartment to the ejection compartment, as the orifice of the CT gate lens is narrow (diameter: 6 mm) in order to allow for the operation with two different pressures (see section 4.8). This narrow orifice might cause a collapse of ions into the copper plate used as CT gate.

Delayed Ejection Trigger

To test the stability of ions in the ejection compartment of the cryogenic ion trap, a delay between the end of the trigger controlling CT gate and the start of the trigger controlling ejection is implemented. Fig. 5.11b clearly shows, that a delay of 25 µs does not allow for detection of ions in the ToF mass spectrometer. Therefore, the delay is too long for ions to remain stably in the

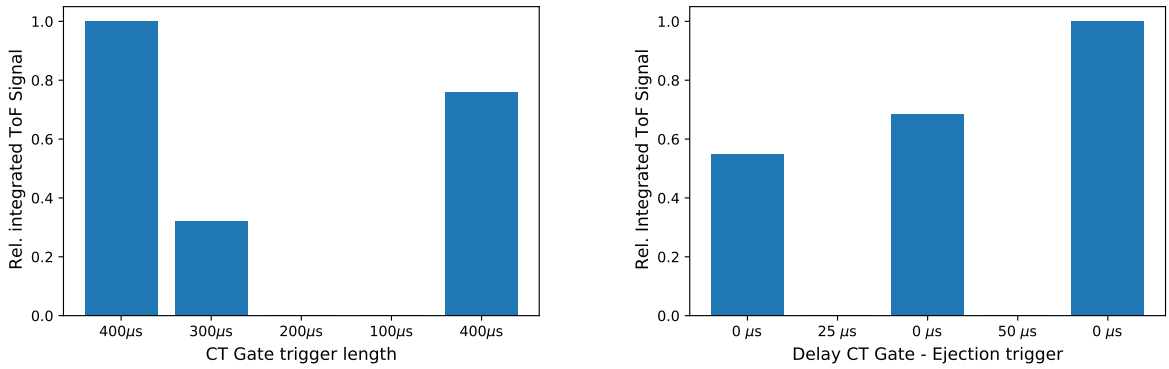

Fig. 5.11.: Parameters for ion transfer in the cryogenic ion trap monitored *via* the ToF Signal. a) The integrated ToF signal is monitored while varying the length of the cold trap (CT) gate trigger length. For times below 400 µs an instant loss in signal can be observed. b) The effect of a delay between CT gate and the ejection trigger is analysed by following the ToF signal. The loss in signal observed for any delay indicates poor stability of the ions in the ejection compartment of the cryogenic ion trap.

ejection compartment. This instability is unexpected, given the RF voltage applied and the ion stability seen in the trapping compartment. It might be caused by a rather steep voltage ramp applied in routine operation with $\Delta V \approx 20\,\mathrm{V}$ between ejection front and ejection end, causing the ions to collapse into CT gate. It is, however, unlikely that ion loss results from a collision of ions with the CT gate lens, as there is no overlap of the two triggers (compare Fig. 5.2) and the CT gate potential is high (24.5 V) when ejection is triggered.

It may be possible to circumvent the ion loss and increase the stability by including a gated potential in the setup as it is illustrated in Fig. 5.12. This might allow for a flatter potential of the ejection ramp. However, technical realisation will prove to be difficult due to the limited space between cryogenic ion trap end and the acceleration lens stack. Here, it is conceivable to convert the pre-acceleration lens into a gated lens and make use of the post-acceleration lens which remains mostly unused at the moment. If the cryogenic ion trap would be accessible more readily, it would also be possible to use the last PCB element as gate and operate it independently from the resistor chain.

5.5. The Influence of Laser Power on Messenger Tag Depletion

Compared to other flavours of action spectroscopy, a low photon flux is sufficient for messenger tag IR spectroscopy. As the IR radiation provided by the FHI FEL offers a high photon flux, the IR beam can be attenuated before entering the experimental hall to fit the needs of the different

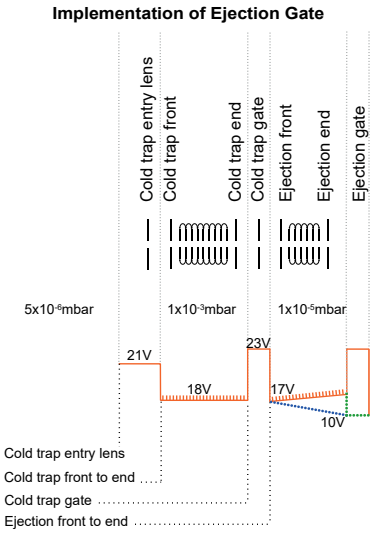

Fig. 5.12.: Suggested gated ejection potential in the cryogenic ion trap. Although the technical implementation would be challenging, a gated potential at the end of the ejection voltage ramp might facilitate a flatter ramp and increase the stability of ions in the ejection compartment.

experiments. In case the photon flux is too high, more than one photon are absorbed by the molecular ions and the inciding energy is too large to be dissipated by the loss of a messenger tag alone. In this case, IRPD is replaced by IRMPD and fragmentation of the ions can be observed. However, if the inciding flux is too low, depletion of the messenger tag as IRPD process is also not possible. To reveal the dependency of the observed ToF signal on the inciding energy, the ion signal in the ToF mass spectrometer was monitored at three different wavenumbers while varying the digital attenuation. The wavenumbers were chosen to correspond to absorption bands of LEK: 1512, 1662 and 1704 cm^{-1}. Fig. 5.13 shows the increasing depletion of messenger tags with increasing relative laser power at 1704 cm^{-1}. For the dependency at 1512 and 1662 cm^{-1} the respective plots are shown in Fig. A.2. A linear approximation of the correlation fits well as the R^2 value of 0.993 highlights. Similar plots for the two remaining wavelengths can be found in chapter A. The linear increase seen in the ratio between parent ion signal, $[\mathrm{LEK} + \mathrm{H}]^+$, and tagged ion signal, $[\mathrm{LEK} + \mathrm{H} + \mathrm{N_2}]^+$, indicates the increasing depletion of messenger tags. However, the data does not indicate the transition from IRPD to IRMPD and it remains unclear if the observed signal corresponds to the maximal achievable tag depletion. Therefore, less attenuation should be used to explore this trend further.

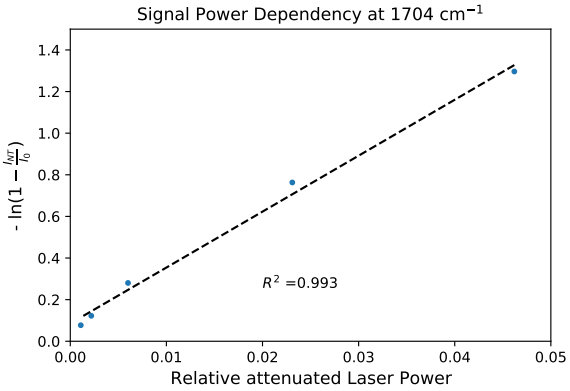

Fig. 5.13.: The Influence of Laser Intensity on the Ion Signal in the ToF Spectrometer at 1704 cm^{-1}. The depletion of messenger tags from ions is monitored as fraction of the total observed ion signal relative to the attenuated laser power. The quality of the linear correlation is estimated by the coefficient of determination R^2.

5.6. Benchmarking IR Messenger Tagging Spectroscopy using Leucine-enkephalin

The study of molecules in the gas phase avoids disturbing effects of the solvent on the molecular structure or arrangement in solution. Due to its well known behaviour in the gas phase, Leucine-enkephalin (Fig. 4.12) has been widely used as model system to probe the performance of novel instrumentation or calibrate an experiment.[14,30,98] As a pentapeptide, LEK is small compared to other biologically important samples but large enough to be a representative model (m/z ([LEK + H]$^+$) = 556).

During the comissioning of iMob 2.0, LEK was employed as standard to test for ion transmission throughout the different parts of the instrument, to sample messenger tagging conditions, tune the ToF mass spectrometer, and to detect malfunctions eventually. Fig. 5.14 shows the ATD of mass-selected LEK with and without IMS selection. The two peaks seen in the ATD for LEK without IMS selection can be attributed to the monomer and the dimer of LEK respectively. As they have the same m/z ratio, they cannot be separated by MS alone and IMS selection is required to select for the monomer. The orthogonal character of these two techniques comes in handy for spectroscopy of (bio)molecules in the gas phase. By m/z and IMS selection, only well defined ions enter the cryogenic ion trap, and are submitted to IR spectroscopy subsequently.

As a consequence of the difficulties seen with regard to ion transmission and messenger tagging, LEK was employed during the first FHI FEL experiments on the iMob 2.0 instrument to establish the messenger tagging IR spectroscopy experiment. In the course of this thesis, several sets of parameters have been tested to, eventually, find a set for sufficient acquisition of IR spectra. Fig. 5.15 depicts one of the very early spectra acquired with the ion trap cooled to 40 K, using helium with 5 % nitrogen as buffer gas, a voltage applied to the pneumatic mirror of 6 V, and the

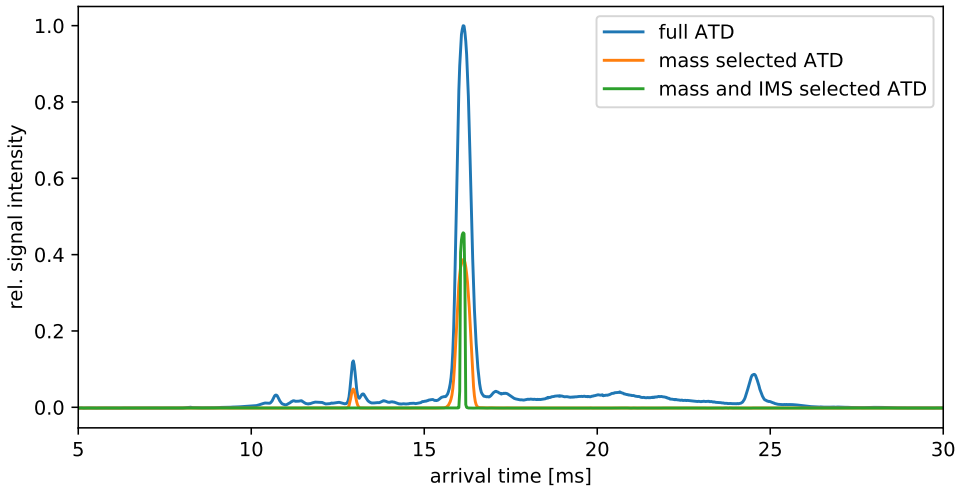

Fig. 5.14.: Arrival time distribution of Leucine-enkephalin. A 50 µM solution of Leucine-enkephalin was analysed by ion mobility spectrometry. The full ATD (blue), after mass selection of $[LEK + H]^+$ ($m/z = 556$) (orange) and with mass and ion mobility selection (green) were recorded.

FEL power digitally attenuated to 1.8 mJ. The blue trace resembles the averaged spectrum of the two spectra shown as red and black dashed lines. For every FEL scan, 100 mass spectra were recorded for the individual wavenumbers.
In addition to the little difficulties seen when subjecting LEK to IR spectroscopy, LEK also served as a benchmark of the performance of the iMob 2.0 instrument. Not only can IR spectra be reproduced by different experiments[14,30], but also compared to spectra obtained by different flavours of action spectroscopy. Gonzáles Flórez *et al.*[14] performed their study on the structure of LEK in helium nanodroplets. The major advantage of their approach is the very low temperature of the helium matrix of 0.4 K resulting in very narrow and sharp vibrational bands without thermal contributions. Fig. 5.16a depicts their IR spectrum measured over a wider spectral range compared to Fig. 5.15 which was measured only for the spectral range above 1400 cm^{-1}. Both spectra feature the same vibrational bands in the range from 1400 to 1800 cm^{-1}. In the amide I region from 1600 to 1800 cm^{-1} the spectrum acquired on the helium droplet features five bands attributed to C=O stretch virbrations which can be seen in Fig. 5.15 as well. The amide II region (1400 to 1600 cm^{-1}) features one strong band in Fig. 5.16a and several significantly weaker bands. In contrast, Fig. 5.15 shows not only the band at 1520 cm^{-1} as a strong band but additional strong bands from 1400 to 1450 cm^{-1}. These bands can be attributed to the N-H bending and vibrations seen in the aromatic rings of the phenylalanine and tyrosine side chains.

A second spectrum recorded on the iMob 2.0 machine confirms the vibrational bands seen in Fig. 5.15. The vibrations in the amide I region are not as nicely resolved, though. The parameters used for acquisition of the spectrum were slightly different; 10 % N_2 in He were used as messenger tag doped buffer gas, the measured laser intensity was determined to be 10.3 mJ and 8 V were

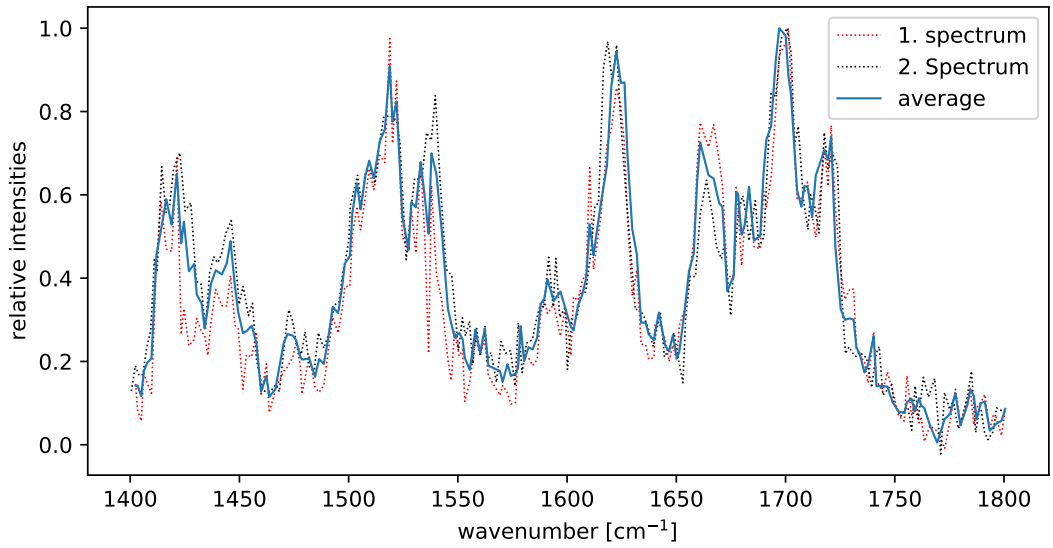

Fig. 5.15.: Messenger Tagging IR Spectrum of Leucine-enkephalin. The blue solid line resembles the averaged spectrum of the two measured spectra depicted as dashed lines in red and black. Acquired at a temperature of the ion trap of 40 K, using 5 % N_2 in He for messenger tagging, and a laser power of 1.8 mJ. 6 V were applied to the pneumatic mirror.

applied to the pneumatic mirror. Extending the recorded spectral range down to 1200 cm^{-1}, Fig. 5.17 resolves the vibrational band in the amide III region around 1280 cm^{-1} better than Fig. 5.16 and reveals two weaker bands around 1330 and 1370 cm^{-1}.

Two aspects become evident quickly: first, the signal-to-noise ratio of the spectra obtained at the iMob 2.0 is worse compared to the spectrum acquired on the helium nanodroplet machine, and second, the vibrational bands are broader. While the latter may certainly be attributed to the temperature difference of about 40 K leading to thermal contributions of the detected vibrations for the IR spectrum acquired on iMob 2.0, the former may be resolved by measuring a higher number of scans in the ToF mass spectrometer for every wavenumber sampled. Another aspect worth noting are the different intensity ratios observed using the two different measurement principles. While it is hard to judge which flavour of action spectroscopy is over-estimating a vibrational band in the respective spectrum, this might certainly be the case. In addition, it can be assumed that the focal point of the FEL is not perfectly tuned to the centre of the interaction region of the iMob 2.0 machine yet. Combined with the potential of improving the timing between ejection from the second compartment of the cryogenic ion trap, this determines at which point the molecular ion beam is overlaid with the IR laser pulse. In fact, a well tuned timing seems to be crucial for IVR to result in the depletion of a messenger tag prior to detection in the ToF mass spectrometer.

Furthermore, routine checks of the beamline alignment prior to the beam times revealed that the laser beam would incide slightly differently for every beam time. It can be assumed that the long

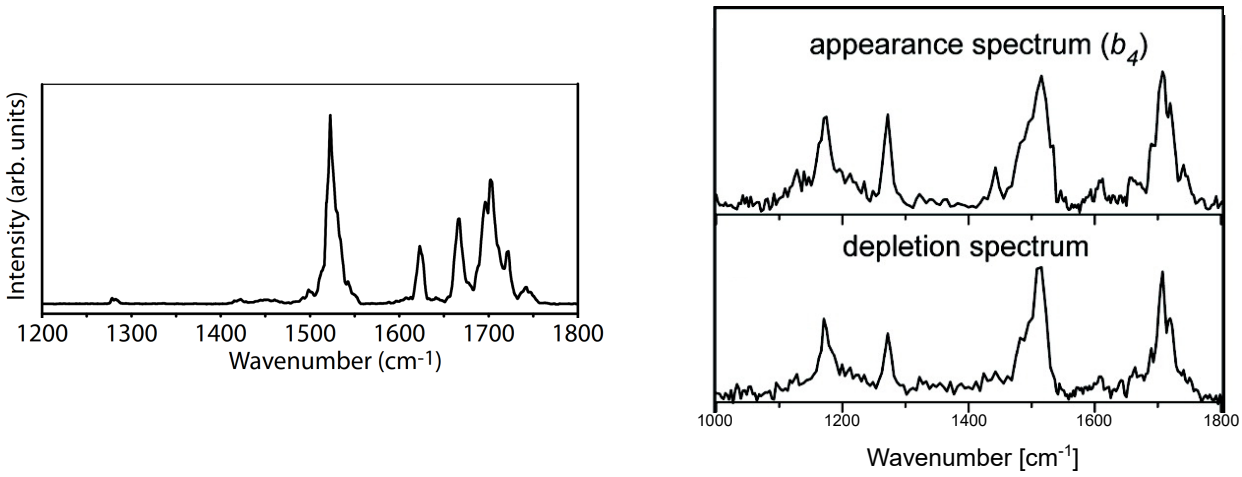

(a) **(b)**

Fig. 5.16.: IR action spectra of Leucine-enkephalin obtained by different flavours of action spectroscopy. a) IR spectrum obtained from the helium droplet machine, adapted from González Flórez *et al.*[14]. b) IRMPD spectrum adapted from Polfer *et al.*[30].

optical path through the experimental hall causes minor differences to be noticed more heavily at experiments further away. Subsequently, the alignment of the FEL laser beam onto the optical table of the iMob 2.0 had to be adjusted prior to experiments for every beam time using the two fixed 90° mirrors. This re-alignment will certainly complicate the estimation of laser intensities for different beam times and might be compensated best for by including a powermeter at the end of the interaction region on the housing of the third quadrupolar deflector or by employing a beam splitter that allows to continuously monitor the FEL intensity on the optical table.

At a first glance, it might seem apparent that different combinations of voltages to control the ion's trajectory and energies of the FEL leaving the diagnostic table might cause differences in the two messenger tagging IR spectra seen in Fig. 5.15 and Fig. 5.17 respectively. However, this conclusion will certainly prove erroneous. Before the remodelling and upgrading of the quadrupolar deflectors (described in detail in section 5.1.1), clipping of the helium-neon laser used for alignment on the edges of the deflector chambers and the hexapole interaction region could be observed. After levelling of the optical elements starting with the first quadrupolar deflector all the way through to the third quadrupolar deflector, no clipping is observed anymore and it can be assumed that the molecular ion and the laser beam traverse the interaction co-linearly. In addition, higher voltages applied to the pneumatic mirror shift the focus of laser further to the back of the interaction region. While the absence of clipping should allow for less laser power to successfully perform IRPD spectroscopy experiments, the higher power used in Fig. 5.17 might result from the relatively high voltage applied to the pneumatic mirror. Because the FEL is focused to the back of the interaction region, more photons might be required to detect depletion of messenger tags, because IVR might be too slow. To complicate things further, the timing of ejection of ions from the cryogenic ion

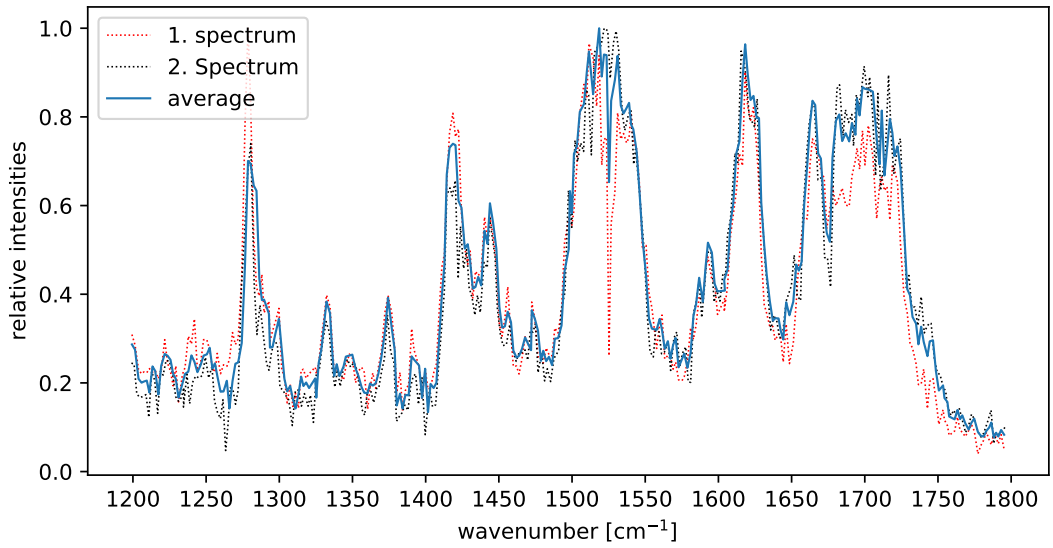

Fig. 5.17.: Messenger Tagging IR Spectrum of Leucine-enkephalin after Re-Alignment of the Ion Trajectory along the Interaction Region. The height of the second and third quadropular deflectors were adjusted to the hexapole for unhindered traversing of the FEL. The blue solid line resembles the averaged spectrum of the two measured spectra depicted as dashed lines in red and black. Acquired at a temperature of the ion trap of 40 K, using 10 % N_2 in He for messenger tagging, and a laser power of 10.3 mJ. 8 V were applied to the pneumatic mirror.

trap relative to the FEL pulse allows to synchronise the overlap of the ion pulse and the laser pulse at the focal point of the laser.

A second type of action spectroscopy which has been employed to assess the structure of LEK is IRMPD spectroscopy. In a study from 2007, Polfer *et al.*[30] investigated the mobility of the proton in protonated LEK and performed IRMPD experiments on protonated LEK ions. A corresponding photodissociation appearance spectrum ($\Sigma_{\text{(Photofragments)}}/\sum_{\text{(All Ions)}}$) is shown in the top panel of Fig. 5.16b. In addition, they also studied a_4 and b_4 fragment ions after collision-induced dissociation (CID) shown in the lower panel of Fig. 5.16b. Compared to the messenger tagging IR spectrum in Fig. 5.15, Fig. 5.16b features the same spectral bands. In general, however, the spectral bands are not as nicely resolved as seen in the two messenger tagging IR spectra. The increased width of the bands can be attributed to thermal contributions in the IRMPD spectrum which are less significant at the lower temperature employed for the attachment of the messenger tags in Fig. 5.15 and Fig. 5.17.

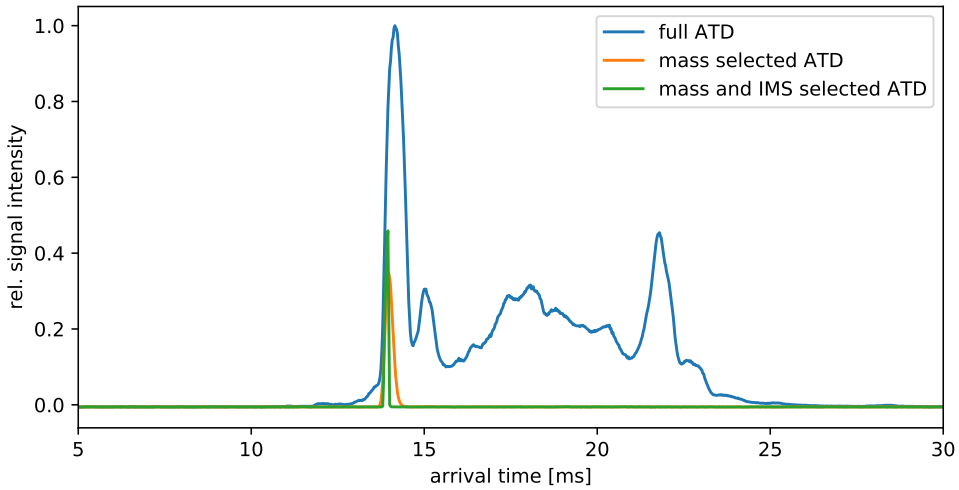

Fig. 5.18.: Arrival time distribution (ATD) of Le^x. A 500 µM solution of Le^x was analysed by ion mobility spectrometry. A full ATD (blue), after mass selection of $[LeX + Na]^+$ ($m/z = 552$) (orange) and with mass and ion mobility selection (green) were recorded.

5.7. Advancing the Mechanistic Understanding of Fucose Migration

In line to previous studies performed in the group, attempts to unravel the puzzle of fucose migration have been taken during this work. As laid out in section 2.3.2, mobile protons can be considered a prerequisite for fucose residues to be subject of IRL. Therefore, the protonated species of Le^x and BG-H2 were chosen as a system to further investigate fucose migration.

During preliminary work on the iMob machine and in contrast to earlier findings, it was observed that protonated samples of equally handled Le^x and BG-H2 exhibit slightly different CCS in helium.[99] Upon activation of the BG-H2 sample in the trapping compartment of the entrance funnel, its CCS could be altered to match the CCS of Le^x. This observation would allow for the IR spectroscopic investigation of the two species, BG-H2 and activated BG-H2, after ion mobility selection on the iMob 2.0. If the assimilation in CCS values of BG-H2 after activation in the entrance funnel and Le^x would go hand in hand with assimilation of the spectral signatures, it would prove the conversion of BG-H2 to Le^x. In contrast, measurements performed accordingly for the sodiated species of BG-H2 should not reveal a change in the spectral signature. Same applies for spectra of Le^x.

The major challenge on the new iMob 2.0 setup is the difficulty of having a strong signal of one tagged species in the ToF mass spectrometer which can be selected as a precursor ion for the IRPD experiments. While it was possible to investigate the protonated species of BG-H2 and Le^x on the IMS stage of the iMob 2.0 machine, it was very difficult to observe messenger tagging of the protonated species after the cryogenic ion trap (see section 5.3).

Attempts to carry out messenger tagging IR spectroscopy on the signal obtained in the ToF mass spectrometer did not give useful spectral data (compare Fig. A.1).
In order to further explore the potential of the iMob 2.0 for messenger tagging IR spectroscopy and whether saccharides of the Lewis family are amenable for IR spectroscopy, the sodiated species of Le^x ($[Le^x + Na]^+$) was ion mobility and mass selected as can be seen in Fig. 5.18.

Upon defined selection of $[Le^x + Na]^+$, the ions were trapped and cooled to 40 K in the cryogenic ion trap. 2.5 % N_2 in the buffer gas were used to tag the ions and the pulsed ion beam was overlaid with the FEL radiation in the interaction region. Using only little attenuation to 33 % of the laser power, an IRPD spectrum of sodiated Le^x from 1000 to 1200 cm^{-1} could be recorded and is shown in Fig. 5.19.

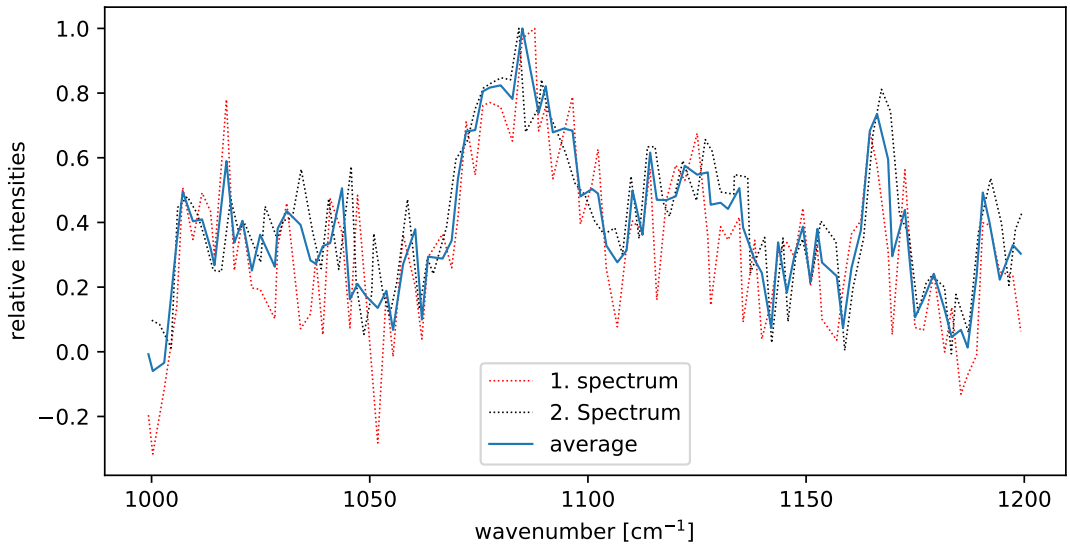

Fig. 5.19.: IRPD Spectrum of sodiated Le^x obtained at the iMob 2.0 experiment. The IRPD experiment was performed at 40 K using 2.5 % N_2 as messenger tag in helium. Two spectra were recorded and averaged. Despite the low signal-to-noise ration, the average spectrum resembles the features seen in the data acquired on the helium nanodroplet machine.

Compared to the spectral data recorded by Mucha *et al.*[12] and shown in Fig. 5.20, the spectral features can be reproduced in Fig. 5.19. Especially, the strong C-O stretch vibration just under 1100 cm^{-1} can be reproduced. The feature seen around 1170 cm^{-1} might correspond to a normal mode, which, similar to the LEK spectrum, could not be resolved by the helium nanodroplet approach. The poor signal-to-noise ratio observed in the spectrum measured on the iMob 2.0 machine can be attributed to several aspects. First, the thermal contributions in Fig. 5.19 are more prominent. Second, the difficulties to select only one ion species in time and space for IR

spectroscopy prevent for a background free spectrum. In addition, the absolute ToF signal which can be achieved for the trisaccharides does not seem to be strong enough to allow for sufficient IR spectroscopy.

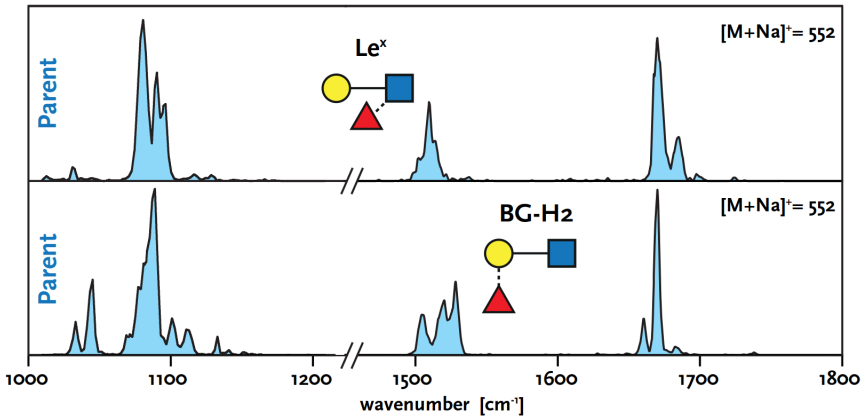

Fig. 5.20.: IR spectra of mass selected sodiated Le^x (top) and BG-H2 trisaccharides (bottom) in helium nanodroplets depicted in SNFG.[64] The spectra for the two individual trisaccharides show distinct signatures. Figure adapted from Mucha *et al.*[12].

6. Conclusion and Outlook

In the course of this thesis, a novel instrumentation for messenger tagging IR spectroscopy has been put into operation successfully. The herein reported instrument *iMob 2.0* is based on a previously established experimental setup for ion mobility spectrometry[27] which was later extended to facilitate infrared multiphoton dissociation (IRMPD) experiments[13].

After a brief overview of the existing parts of the instrument, the individual components to allow for messenger tagging spectroscopy were introduced and explained. Here, the unique design of a segmented cryogenic ion trap which does not rely on a duty cycle but rather allows for independent filling, trapping, messenger tagging, and ejection was of special interest. With regard to the instrumentation, several improvements have been implemented to improve the ease of use and the quality of spectral data achievable. In this line of work, a central control plate for the gas supply to the iMob 2.0 experiment has been purchased. Commonly referred to as the *Gasbahnhof*, it allows to mix buffer gas with fractions of messenger tagging gas and at the same time also supplies the drift gas to the IMS stage of the instrument. Further, the alignment of the ion trajectory has been optimised to yield better transmission. The voltage supplies for the three quadrupolar deflectors used to bend the ion beam through the device have been replaced by individual voltage supplies for the quarter round rods. This new mode of operation follows the logic described by Randall E. Pedder[93] and now allows for the chamber of the deflectors, as well as entrance and exit lenses to be operated at a defined potential, too. In addition, the temporal control of the voltages manoeuvring the ions through the different sections of the instrument has been adjusted such that the arrival of the laser light to the interaction region of the iMob 2.0 is used as reference point.

On the experimental side, first insights into the messenger tagging behaviour of different molecules could be gained. It could be observed, that leucine-enkephalin and Le^x show different tagging behaviours, also depending on the nature of the attached ion. Furthermore, messenger tagging differed substantially between the sodiated and the protonated adduct ions of Le^x. Here, it is conceivable, that the positive charge of the sodium ion is more evenly spread throughout the trisaccharide ion and therefore allows for more efficient and higher tagging. In contrast, the rather hard and small positive charge of the proton may not as well spread over the molecule, thus rendering tagging less advantageous. Furthermore, it can be noted that the tagging behaviour in general changed over the second half of this master thesis. As such, primarily singly tagged ions are observed currently.

Another central aspect of this thesis was to evaluate the cryogenic ion trap. Up to date, no comparable ion trap design for the use in messenger tagging IR spectroscopy has been reported. For commissioning, the parameters controlling the taps have been set to plausible yet arbitrary values. As it increased the ion signal in the ToF, it proofed to be beneficial to implement a slightly rising potential in the trapping compartment of the cryogenic ion trap. By varying the rate at which the spectroscopy section of the iMob 2.0 is operated, it could be shown, that ions are stable in the trapping compartment of the cryogenic ion trap on a second timescale. In contrast, they seem to be unstable in the ejection compartment as a delay between the transfer from the trapping compartment and the ejection shows a significant signal loss in the ToF mass spectrometer. Furthermore, the transfer of ions between the two compartments of the cryogenic ion trap takes longer than intuitively thought. This either points to very slow diffusion of ions through the narrow orifice connecting the two compartments. In the same line as the rising potential applied to the first compartment of the cryogenic ion trap, this might indicate ions collapsing into the cold trap gating lens.

The relative low stability of ions in the ejection compartment of the cryogenic ion trap could be corrected for by implementing a gating element similar to the cold trap gate at the end of the ejection potential ramp (compare Fig. 5.12). This additional element might eventually allow for a less steep ejection ramp and potentially increased stability of ions in the ejection compartment. Even though the implementation will be a delicate extension of the ion optics, it is conceivable to either use the last PCB of the cryogenic ion trap if the trap is to be taken out at one point. It would then have to be disconnected from the voltage ramp and a gated voltage supply implemented. Alternatively, the stack of acceleration voltages could be adapted: either by implementing a gating voltage for the first acceleration lens (*pre-acceleration*) or adding an additional gating lens as the *ejection gate*. Realising both of these options could be achieved by either adding more teflon spacers to the flange between cryogenic ion trap and quadrupolar bender 2 or by reducing the length of the cylinder making up the post-acceleration lens.

Even though preliminary tests to correlate signal intensity in the ToF mass spectrometer with the laser intensity have been made and show a linear correlation, a non-linear continuation of this is trend is to expected for higher laser intensities when going from IRPD to IRMPD. In-depth evaluation of the correlation between signal intensity in the ToF mass spectrometer and the laser intensity will be possible after a recently purchased powermeter is included in the optical table which directs the FEL beam into the interaction region of the iMob 2.0 experiment. In addition to measuring the laser intensity more reliably than by holding the powermeter to the end of the interaction region, the realignment of the optical path and the newly levelled ion trajectory through all four quadrupolar deflectors also rule out clipping of the laser beam. In addition to the laser intensity, the role of the spatial position of the FEL laser in the interaction region should be optimised, i.e. its effect should be explored. It seems very plausible, that the temporal and spatial overlap of molecular ion and laser beam are crucial for the quality of the IRPD spectra recorded using the ToF mass spectrometer. That is, ideally only one photon is to interact with

one molecular ion to deplete the messenger tag but a certain time is needed for the energy to be dissipated by IVR and the loss of the messenger tag.

In addition to the upgrade of the voltage supply for the quadrupolar deflectors, their inherent function to serve as an energy filter could be utilised. According to documentation for quadrupolar deflectors by Ardara Technologies L.P., the absolute values of every pair of voltages applied to the two pairs of quarter round rods not only deflects the molecular ion beam but also defines the width of the energy regime that is sufficiently deflected. In this context, higher absolute values result in less discrimination of energies, i.e. a broader window of energies is permitted through the bender. This does not mean that the deflectors posses an inherent property to discriminate for different masses. The possibility to discriminate for different energies might prove to be useful to reduce background signal in the ToF mass spectrometer by trying to discriminate for only one ion species. Thereby, it should be possible to compare the ToF signal with and without laser more readily and resolve a cleaner spectrum.

Another aspect to improve the quality of the spectral data acquired by IRPD spectroscopy on the iMob 2.0 experiment could be the implementation of a sophisticated laser power correction during data analysis of FEL beamtimes. Attempts to include a power correction similar to the power correction preformed by some users of the helium nanodroplet machine, have yielded worse spectra compared to no power correction. However, other than for the helium nanodroplet experiment and its multi-photon-process, a simple first order power correction of the measured ToF signal seems more feasible for the iMob 2.0 data because IRPD resembles a one-photon-process.

To evaluate the performance and potential of the iMob 2.0 experiment to (re)produce spectral data, the pentapeptide leucine-enkephalin was used as a benchmark. Compared to spectral data published earlier, most spectral bands are not as well resolved as with the helium nanodroplet approach.[14] However, the IRPD spectrum acquired by the iMob 2.0 experiment resolves potentially underestimated vibrational bands in the amide II and III region better. An IRMPD spectrum used for comparison shows similarly broad vibrational bands, however, individual vibrational modes seem to be resolved better.

Attempts to further elucidate the phenomenon of fucose migration were hindered by the difficulties to sufficiently monitor messenger tagged ions of protonated trisaccharides, Le^x and BG-H2, in the ToF mass spectrometer. As pointed out above, messenger tagging behaviour seems to be dependent on the charge distribution in the molecules of interest. Despite these difficulties to observe messenger tagged protonated trisaccharides of the Lewis family, IR spectra of the sodiated Le^x have been recorded. The observed bands correspond nicely to the spectral features observed on the helium nanodroplet machine and prove that spectroscopy on trisaccharides is possible on the iMob 2.0 machine.

In order to assess the potential for larger molecular systems in the future, the 12 kDa bovine protein cytochrome C has been exposed to messenger tagging. Although biologically less relevant, the 15+ charge state of the molecule could be observed with one, two and three tags baseline separated in the ToF mass spectrometer.

In summary, a novel instrumentation for messenger tagging IR spectroscopy has been successfully commissioned over the course of this thesis. The transmission of ions through the different parts of the experiment has been accomplished and optimised in different aspects. Starting with small molecules of biological relevance, messenger tagging IR spectroscopy could be benchmarked and different experimental parameters evaluated. Without doubt, the machine holds great potential for the investigation of (bio)molecular structure by means of IR spectroscopy and complements the instrumentation resources available in the group.

7. References

[1] Jaskolski, M.; Dauter, Z.; Wlodawer, A. A brief history of macromolecular crystallography, illustrated by a family tree and its Nobel fruits. *FEBS Journal* **2014**, *281*, 3985–4009.

[2] Wüthrich, K. The way to NMR structures of proteins. *Nature Structural Biology* **2001**, *8*, 923–925.

[3] Cressey, D.; Callaway, E. Cryo-electron microscopy wins chemistry Nobel. 2017; https://www.nature.com/articles/nature.2017.22738.

[4] Fenn, J. B.; Mann, M.; Meng, C. K.; Wong, S. F.; Whitehouse, C. M. Electrospray ionization for mass spectrometry of large biomolecules. *Science* **1989**, *246*, 64–71.

[5] Bahr, U.; Karas, M.; Hillenkamp, F. Analysis of biopolymers by matrix-assisted laser desorption/ionization (MALDI) mass spectrometry. *Fresenius' Journal of Analytical Chemistry* **1994**, *348*, 783–791.

[6] Ruotolo, B. T.; Robinson, C. V. Aspects of native proteins are retained in vacuum. *Current Opinion in Chemical Biology* **2006**, *10*, 402–408.

[7] Wyttenbach, T.; Bowers, M. T. Intermolecular interactions in biomolecular systems examined by mass spectrometry. *Annual Review of Physical Chemistry* **2007**, *58*, 511–533.

[8] Ruhaak, L. R.; Xu, G.; Li, Q.; Goonatilleke, E.; Lebrilla, C. B. Mass Spectrometry Approaches to Glycomic and Glycoproteomic Analyses. *Chemical Reviews* **2018**, *118*, 7886–7930.

[9] Barth, A.; Zscherp, C. What vibrations tell us about proteins. *Quarterly Reviews of Biophysics* **2002**, *35*, 369–430.

[10] Oomens, J.; Polfer, N.; Moore, D. T.; Van Der Meer, L.; Marshall, A. G.; Eyler, J. R.; Meijer, G.; Von Helden, G. Charge-state resolved mid-infrared spectroscopy of a gas-phase protein. *Physical Chemistry Chemical Physics* **2005**, *7*, 1345–1348.

[11] González Flórez, A. I.; Mucha, E.; Ahn, D. S.; Gewinner, S.; Schöllkopf, W.; Pagel, K.; Von Helden, G. Charge-Induced Unzipping of Isolated Proteins to a Defined Secondary Structure. *Angewandte Chemie - International Edition* **2016**, *55*, 3295–3299.

[12] Mucha, E.; Lettow, M.; Marianski, M.; Thomas, D. A.; Struwe, W. B.; Harvey, D. J.; Meijer, G.; Seeberger, P. H.; von Helden, G.; Pagel, K. Fucose Migration in Intact Protonated Glycan Ions: A Universal Phenomenon in Mass Spectrometry. *Angewandte Chemie - International Edition* **2018**, *57*, 7440–7443.

[13] Warnke, S. A Gas-Phase Approach to Biomolecular Structure: Combining Ion Mobility-Mass Spectrometry with Spectroscopy. Ph.D. thesis, Freie Universität Berlin, 2015.

[14] González Flórez, A. I.; Ahn, D. S.; Gewinner, S.; Schöllkopf, W.; Von Helden, G. IR spectroscopy of protonated leu-enkephalin and its 18-crown-6 complex embedded in helium droplets. *Physical Chemistry Chemical Physics* **2015**, *17*, 21902–21911.

[15] Masson, A.; Kamrath, M. Z.; Perez, M. A. S.; Glover, M. S.; Rothlisberger, U.; Clemmer, D. E.; Rizzo, T. R. Infrared Spectroscopy of Mobility-Selected H+-Gly-Pro-Gly-Gly (GPGG). *Journal of the American Society for Mass Spectrometry* **2015**, *26*, 1444–1454.

[16] Lorenz, U. J.; Rizzo, T. R. Planar multipole ion trap/time-of-flight mass spectrometer. *Analytical Chemistry* **2011**, *83*, 7895–7901.

[17] Bohrer, B. C.; Merenbloom, S. I.; Koeniger, S. L.; Hilderbrand, A. E.; Clemmer, D. E. Biomolecule analysis by Ion mobility spectrometry. *Annual Review of Analytical Chemistry* **2008**, *1*, 293–327.

[18] Manz, C.; Pagel, K. Glycan analysis by ion mobility-mass spectrometry and gas-phase spectroscopy. *Current Opinion in Chemical Biology* **2018**, *42*, 16 – 24.

[19] Revercomb, H. E.; Mason, E. A. Theory of Plasma Chromatography/Gaseous Electrophoresis. A Review. *Analytical Chemistry* **1975**, *47*, 970–983.

[20] Thomson, J. J.; Rutherford, E. XL. On the passage of electricity through gases exposed to Röntgen rays. *The London, Edinburgh, and Dublin Philosophical Magazine and Journal of Science* **1896**, *42*, 392–407.

[21] Langevin, P. Sur la the orie du mouvement brownien. *Annales de Chimie et de Physique* **1905**, *5*, 245–288.

[22] Atkins, P.; Paula, J. D. *Physical Chemistry*, ninth ed.; 2010.

[23] Oomens, J.; Sartakov, B. G.; Meijer, G.; von Helden, G. Gas-phase infrared multiple photon dissociation spectroscopy of mass-selected molecular ions. **2006**, *254*, 1–19.

[24] Polfer, N. C. Infrared multiple photon dissociation spectroscopy of trapped ions. *Chemical Society Reviews* **2011**, *40*, 2211–2221.

[25] Okumura, M.; Yeh, L. I.; Myers, J. D.; Lee, Y. T. Infrared spectra of the cluster ions $H_7O_3^+ \cdot H_2$ and $H_9O_4^+ \cdot H_2$. *The Journal of Chemical Physics* **1986**, *85*, 2328–2329.

[26] Wolk, A. B.; Leavitt, C. M.; Garand, E.; Johnson, M. A. Cryogenic ion chemistry and spectroscopy. *Accounts of Chemical Research* **2014**, *47*, 202–210.

[27] Warnke, S. Ein Ionenmobilitätsspektrometer zur Spektroskopie an konformations- und massenselektierten Biomolekülen. M.Sc. thesis, Eberhard Karls Universität Tübingen, 2010.

[28] Little, D. P.; Speir, J. P.; Senko, M. W.; O'Connor, P. B.; McLafferty, F. W. Infrared Multiphoton Dissociation of Large Multiply Charged Ions for Biomolecule Sequencing. *Analytical Chemistry* **1994**, *66*, 2809–2815.

[29] Bagratashvili, V. N.; Letokov, V. S.; A., M. A.; Ryabov, E. A. *Multiple Photon Infrared Laser Photophysics and Photochemistry*; Harwood: Chichester, 1985.

[30] Polfer, N. C.; Oomens, J.; Suhai, S.; Paizs, B. Infrared spectroscopy and theoretical studies on gas-phase protonated Leu-enkephalin and its fragments: Direct experimental evidence for the mobile proton. *Journal of the American Chemical Society* **2007**, *129*, 5887–5897.

[31] Lehmann, K. K.; Scoles, G.; Pate, B. H. Intramolecular dynamics from eigenstate-resolved infrared spectra. *Annual Review of Physical Chemistry* **1994**, *45*, 241–274.

[32] Filsinger, F.; Ahn, D. S.; Meijer, G.; Von Helden, G. Photoexcitation of mass/charge selected hemin +, caught in helium nanodroplets. *Physical Chemistry Chemical Physics* **2012**, *14*, 13370–13377.

[33] Mucha, E.; González Flórez, A. I.; Marianski, M.; Thomas, D. A.; Hoffmann, W.; Struwe, W. B.; Hahm, H. S.; Gewinner, S.; Schöllkopf, W.; Seeberger, P. H.; von Helden, G.; Pagel, K. Glycan Fingerprinting via Cold-Ion Infrared Spectroscopy. *Angewandte Chemie International Edition* **2017**, *56*, 11248–11251.

[34] Bierau, F.; Kupser, P.; Meijer, G.; von Helden, G. Catching Proteins in Liquid Helium Droplets. *Phys. Rev. Lett.* **2010**, *105*, 133402.

[35] Lisy, J. M. Infrared studies of ionic clusters: The influence of Yuan T. Lee. *Journal of Chemical Physics* **2006**, *125*, 132302.

[36] Bieske, E. J.; Dopfer, O. High-Resolution Spectroscopy of Cluster Ions. *Chemical Reviews* **2000**, *100*, 3963–3998.

[37] Dopfer, O. Spectroscopic and theoretical studies of CH^+_3-Rg_n clusters (Rg=He, Ne, Ar): From weak intermolecular forces to chemical reaction mechanisms. *International Reviews in Physical Chemistry* **2003**, *22*, 437–495.

[38] Geistlinger, K.; Dahlmann, F.; Michaelsen, T.; Ončák, M.; Endres, E.; Wester, R. Multiple helium tagging and OH vibrational spectroscopy of cold protonated glycine ions. *Journal of Molecular Spectroscopy* **2021**, *379*, 111479.

[39] Cismesia, A. P.; Bailey, L. S.; Bell, M. R.; Tesler, L. F.; Polfer, N. C. Making Mass Spectrometry See the Light: The Promises and Challenges of Cryogenic Infrared Ion Spectroscopy as a Bioanalytical Technique. *Journal of the American Society for Mass Spectrometry* **2016**, *27*, 757–766.

[40] Fenn, J. B.; Mann, M.; Meng, C. K.; Wong, S. F.; Whitehouse, C. M. Electrospray ionization–principles and practice. *Mass Spectrometry Reviews* **1990**, *9*, 37–70.

[41] Leavitt, C. M.; Wolk, A. B.; Kamrath, M. Z.; Garand, E.; Van Stipdonk, M. J.; Johnson, M. A. Characterizing the intramolecular H-bond and secondary structure in methylated GlyGlyH + with H 2 predissociation spectroscopy. *Journal of the American Society for Mass Spectrometry* **2011**, *22*, 1941–1952.

[42] Paul, W. Electromagnetic traps for charged and neutral particles. *Reviews of Modern Physics* **1990**, *62*, 531–540.

[43] Dehmelt, H. G. Radiofrequency Spectroscopy of Stored Ions I: Storage. *Advances in Atomic, Molecular and Optical Physics* **1968**, *3*, 53–72.

[44] Kamrath, M. Z.; Relph, R. A.; Guasco, T. L.; Leavitt, C. M.; Johnson, M. A. Vibrational predissociation spectroscopy of the H2-tagged mono- and dicarboxylate anions of dodecanedioic acid. *International Journal of Mass Spectrometry* **2011**, *300*, 91–98.

[45] Wang, X. B.; Wang, L. S. Development of a low-temperature photoelectron spectroscopy instrument using an electrospray ion source and a cryogenically controlled ion trap. *Review of Scientific Instruments* **2008**, *79*, 073108.

[46] Gerlich, D. Ion-neutral collisions in a 22-pole trap at very low energies. *Physica Scripta* **1995**, *1995*, 256–263.

[47] Gerlich, D.; Horning, S. Experimental Investigations of Radiative Association Processes as Related to Interstellar Chemistry. *Chemical Reviews* **1992**, *92*, 1509–1539.

[48] Boyarkin, O. V.; Mercier, S. R.; Kamariotis, A.; Rizzo, T. R. Electronic spectroscopy of cold, protonated tryptophan and tyrosine. *Journal of the American Chemical Society* **2006**, *128*, 2816–2817.

[49] Asvany, O.; Bielau, F.; Moratschke, D.; Krause, J.; Schlemmer, S. Note: New design of a cryogenic linear radio frequency multipole trap. *Review of Scientific Instruments* **2010**, *81*, 076102.

[50] Jusko, P.; Brünken, S.; Asvany, O.; Thorwirth, S.; Stoffels, A.; Van Der Meer, L.; Berden, G.; Redlich, B.; Oomens, J.; Schlemmer, S. The FELion cryogenic ion trap beam line at the FELIX free-electron laser laboratory: Infrared signatures of primary alcohol cations. *Faraday Discussions* **2019**, *217*, 172–202.

[51] Asmis, K. R.; Brümmer, M.; Kaposta, C.; Santambrogio, G.; von Helden, G.; Meijer, G.; Rademann, K.; Wöste, L. Mass-selected infrared photodissociation spectroscopy of $V_4O_{10}^+$. *Physical Chemistry Chemical Physics* **2002**, *4*, 1101–1104.

[52] Luca, A.; Schlemmer, S.; Čermák, I.; Gerlich, D. On the combination of a linear field free trap with a time-of-flight mass spectrometer. *Review of Scientific Instruments* **2001**, *72*, 2900–2908.

[53] Goebbert, D. J.; Meijer, G.; Asmis, K. R. 10K ring electrode trap - Tandem mass spectrometer for infrared spectroscopy of mass selected ions. AIP Conference Proceedings. 2009; pp 22–29.

[54] Heine, N.; Asmis, K. R. Cryogenic ion trap vibrational spectroscopy of hydrogen-bonded clusters relevant to atmospheric chemistry. *International Reviews in Physical Chemistry* **2015**, *34*, 1–34.

[55] Roithová, J.; Gray, A.; Andris, E.; Jašík, J.; Gerlich, D. Helium Tagging Infrared Photodissociation Spectroscopy of Reactive Ions. *Accounts of Chemical Research* **2016**, *49*, 223–230.

[56] Khanal, N.; Masellis, C.; Kamrath, M. Z.; Clemmer, D. E.; Rizzo, T. R. Cryogenic IR spectroscopy combined with ion mobility spectrometry for the analysis of human milk oligosaccharides. *Analyst* **2018**, *143*, 1846–1852.

[57] Motz, H.; Thon, W.; Whitehurst, R. N. Experiments on radiation by fast electron beams. *Journal of Applied Physics* **1953**, *24*, 826–833.

[58] Madey, J. M. Stimulated emission of bremsstrahlung in a periodic magnetic field. *Journal of Applied Physics* **1971**, *42*, 1906–1913.

[59] Schöllkopf, W.; Gewinner, S.; Todd, A. M. M.; Colson, W. B.; De Pas, M.; Dowell, D.; Gottschalk, S. C.; Junkes, H.; Rathke, J. W.; Schultheiss, T. J.; Young, L. M.; von Helden, G.; Meijer, G. The FHI FEL Upgrade Design. 39th International Free-Electron Laser Conference. 2019.

[60] Schöllkopf, W.; Gewinner, S.; Junkes, H.; Paarmann, A.; von Helden, G.; Bluem, H.; Todd, A. M. M. The new IR and THz FEL facility at the Fritz Haber Institute in Berlin. Advances in X-ray Free-Electron Lasers Instrumentation III. 2015.

[61] Gottschalk, S. C.; DeHart, T. E.; Kelly, R. N.; Offenbacker, M. A.; Valla, A. S.; Bluem, H.; Dowell, D.; Rathke, J.; Todd, A. M.; Gewinnner, S.; Junkes, H.; Meijer, G.; Schöllkopf, W.; Zhang, W. Q.; Lehnert, U. Design and performance of the wedged pole hybrid undulator for the Fritz-Haber-Institut IR FEL. 34th International Free Electron Laser Conference. 2012.

[62] McNaught, A. D.; Wilkinson, A. *IUPAC. Compendium of Chemical Terminology, 2nd ed. (the Gold Book)*; Blackwell Scientific Publications, 1997.

[63] Moss, G. P.; Smith, P. A.; Tavernier, D. Glossary of class names of organic compounds and reactive intermediates based on structure (IUPAC recommendations 1995). *Pure and Applied Chemistry* **1995**, *67*, 1307–1375.

[64] Neelamegham, S.; Aoki-Kinoshita, K.; Bolton, E.; Frank, M.; Lisacek, F.; Lütteke, T.; O'Boyle, N.; Packer, N. H.; Stanley, P.; Toukach, P.; Varki, A.; Woods, R. J. Updates to the Symbol Nomenclature for Glycans guidelines. *Glycobiology* **2019**, *29*, 620–624.

[65] National Research Council, *Transforming Glycoscience: A Roadmap for the Future*; National Academies Press, 2012; pp 1–192.

[66] Schneider, M.; Al-Shareffi, E.; Haltiwanger, R. S. Biological functions of fucose in mammals. *Glycobiology* **2017**, *27*, 601–618.

[67] Molinari, M. N-glycan structure dictates extension of protein folding or onset of disposal. *Nature Chemical Biology* **2007**, *3*, 313–320.

[68] Watanabe, Y.; Berndsen, Z. T.; Raghwani, J.; Seabright, G. E.; Allen, J. D.; Pybus, O. G.; McLellan, J. S.; Wilson, I. A.; Bowden, T. A.; Ward, A. B.; Crispin, M. Vulnerabilities in coronavirus glycan shields despite extensive glycosylation. *Nature Communications* **2020**, *11*, 1–10.

[69] Shajahan, A.; Supekar, N. T.; Gleinich, A. S.; Azadi, P. Deducing the N- And O-glycosylation profile of the spike protein of novel coronavirus SARS-CoV-2. *Glycobiology* **2020**, *30*, 981–988.

[70] Watkins, W. M. The ABO blood group system: Historical background. *Transfusion Medicine* **2001**, *11*, 243–265.

[71] Yin, B. W. T.; Finstad, C. L.; Kitamura, K.; Federici, M. G.; Welshinger, M.; Kudryashov, V.; Hoskins, W. J.; Welt, S.; Lloyd, K. O. Serological and immunochemical analysis of Lewis Y (Le^y) blood group antigen expression in epithelial ovarian cancer. *International Journal of Cancer* **1996**, *65*, 406–412.

[72] Myers, R. B.; Srivastava, S.; Grizzle, W. E. Lewis Y Antigen as Detected by the Monoclonal Antibody BR96 is Expressed Strongly in Prostatic Adenocarcinoma. *The Journal of Urology* **1995**, *153*, 1572–1574.

[73] Werz, D. B.; Ranzinger, R.; Herget, S.; Adibekian, A.; von der Lieth, C.-W.; Seeberger, P. H. Exploring the Structural Diversity of Mammalian Carbohydrates ("Glycospace") by Statistical Databank Analysis. *ACS Chemical Biology* **2007**, *2*, 685–691.

[74] Leymarie, N.; Zaia, J. Effective use of mass spectrometry for glycan and glycopeptide structural analysis. *Analytical Chemistry* **2012**, *84*, 3040–3048.

[75] Sheeley, D. M.; Reinhold, V. N. Structural Characterization of Carbohydrate Sequence, Linkage, and Branching in a Quadrupole Ion Trap Mass Spectrometer: Neutral Oligosaccharides and N-Linked Glycans. *Analytical Chemistry* **1998**, *70*, 3053–3059.

[76] Hofmann, J.; Hahm, H. S.; Seeberger, P. H.; Pagel, K. Identification of carbohydrate anomers using ion mobility–mass spectrometry. *Nature* **2015**, *526*, 241–244.

[77] Vachet, R. W.; Bishop, B. M.; Erickson, B. W.; Glish, G. L. Novel Peptide Dissociation: Gas-Phase Intramolecular Rearrangement of Internal Amino Acid Residues. *Journal of the American Chemical Society* **1997**, *119*, 5481–5488.

[78] McLafferty, F. W. Mass Spectrometric Analysis. Molecular Rearrangements. *Analytical Chemistry* **1959**, *31*, 82–87.

[79] Chawner, R.; Holman, S. W.; Gaskell, S. J.; Eyers, C. E. Peptide Scrambling During Collision-Induced Dissociation is Influenced by N-terminal Residue Basicity. *Journal of the American Society for Mass Spectrometry* **2014**, *25*, 1927–1938.

[80] Erlekam, U.; Bythell, B. J.; Scuderi, D.; Van Stipdonk, M.; Paizs, B.; Maître, P. Infrared spectroscopy of fragments of protonated peptides: Direct evidence for macrocyclic structures of b_5 ions. *Journal of the American Chemical Society* **2009**, *131*, 11503–11508.

[81] McNeil, M. Elimination of internal glycosyl residues during chemical ionization-mass spectrometry of per-O-alkylated oligosaccharide-alditols. *Carbohydrate Research* **1983**, *123*, 31–40.

[82] Harvey, D. J.; Mattu, T. S.; Wormald, M. R.; Royle, L.; Dwek, R. A.; Rudd, P. M. "Internal residue loss": Rearrangements occurring during the fragmentation of carbohydrates derivatized at the reducing terminus. *Analytical Chemistry* **2002**, *74*, 734–740.

[83] Kováčik, V.; Hirsch, J.; Kováč, P.; Heerma, W.; Thomas-Oates, J.; Haverkamp, J. Oligosaccharide characterization using collision-induced dissociation fast atom bombardment mass spectrometry: Evidence for internal monosaccharide residue loss. *Journal of Mass Spectrometry* **1995**, *30*, 949–958.

[84] Brüll, L. P.; Heerma, W.; Thomas-Oates, J.; Haverkamp, J.; Kovácik, V.; Kovác, P. Loss of internal $1 \rightarrow 6$ substituted monosaccharide residues from underivatized and per-O-methylated trisaccharides. *Journal of the American Society for Mass Spectrometry* **1997**, *8*, 43–49.

[85] Franz, A. H.; Lebrilla, C. B. Evidence for long-range glycosyl transfer reactions in the gas phase. *Journal of the American Society for Mass Spectrometry* **2002**, *13*, 325–337.

[86] Ernst, B.; Müller, D. R.; Richter, W. J. False sugar sequence ions in electrospray tandem mass spectrometry of underivatized sialyl-Lewis-type oligosaccharides. *International Journal of Mass Spectrometry and Ion Processes* **1997**, *160*, 283–290.

[87] Jia, C.; Wu, Z.; Lietz, C. B.; Liang, Z.; Cui, Q.; Li, L. Gas-phase ion isomer analysis reveals the mechanism of peptide sequence scrambling. *Analytical Chemistry* **2014**, *86*, 2917–2924.

[88] Riba Garcia, I.; Giles, K.; Bateman, R. H.; Gaskell, S. J. Studies of Peptide a- and b-Type Fragment Ions Using Stable Isotope Labeling and Integrated Ion Mobility/Tandem Mass Spectrometry. *Journal of the American Society for Mass Spectrometry* **2008**, *19*, 1781–1787.

[89] Hofmann, J.; Stuckmann, A.; Crispin, M.; Harvey, D. J.; Pagel, K.; Struwe, W. B. Identification of Lewis and Blood Group Carbohydrate Epitopes by Ion Mobility-Tandem-Mass Spectrometry Fingerprinting. *Analytical Chemistry* **2017**, *89*, 2318–2325.

[90] Lettow, M.; Mucha, E.; Manz, C.; Thomas, D. A.; Marianski, M.; Meijer, G.; von Helden, G.; Pagel, K. The role of the mobile proton in fucose migration. *Analytical and Bioanalytical Chemistry* **2019**, *411*, 4637–4645.

[91] Kemper, P. R.; Dupuis, N. F.; Bowers, M. T. A new, higher resolution, ion mobility mass spectrometer. *International Journal of Mass Spectrometry* **2009**, *287*, 46–57.

[92] Baker, E. S.; Clowers, B. H.; Li, F.; Tang, K.; Tolmachev, A. V.; Prior, D. C.; Belov, M. E.; Smith, R. D. Ion Mobility Spectrometry-Mass Spectrometry Performance Using Electrodynamic Ion Funnels and Elevated Drift Gas Pressures. *Journal of the American Society for Mass Spectrometry* **2007**, *18*, 1176–1187.

[93] Pedder, R. E. Fundamental Studies in Quadrupole Ion Trap Mass Spectrometry. Ph.D. thesis, University of Florida, 1992.

[94] Zeman, H. D. Deflection of an ion beam in the two-dimensional electrostatic quadrupole field. *Review of Scientific Instruments* **1977**, *48*, 1079–1085.

[95] Dawson, P. H. *Quadrupole Mass Spectrometry and its Applications*; Elsevier, 1976; pp 95–119.

[96] Burke, N. L.; Redwine, J. G.; Dean, J. C.; Mcluckey, S. A.; Zwier, T. S. UV and IR spectroscopy of cold protonated leucine enkephalin. *International Journal of Mass Spectrometry* **2015**, *378*, 196–205.

[97] Van Rossum, G.; Drake Jr, F. L. *Python reference manual*; Centrum voor Wiskunde en Informatica Amsterdam, 1995.

[98] Sztáray, J.; Memboeuf, A.; Drahos, L.; Vékey, K. Leucine enkephalin—A mass spectrometry standard. *Mass Spectrometry Reviews* **2011**, *30*, 298–320.

[99] Manz, C.; Grabarics, M.; Hoberg, F.; Pugini, M.; Stuckmann, A.; Struwe, W. B.; Pagel, K. Separation of isomeric glycans by ion mobility spectrometry – the impact of fluorescent labelling. *Analyst* **2019**, *144*, 5292–5298.

Acknowledgement

Das Anfertigen dieser Arbeit wäre mir nicht möglich gewesen, hätten mich nicht viele Menschen auf dem Weg zur Abgabe so bereitwillig begleitet und wohlwollend unterstützt.

Ich möchte mich bei Prof. Dr. Gert von Helden für das Vertrauen bedanken, dass ich als Masterand bei der Inbetriebnahme des iMob 2.0 dabei sein durfte. Danke für die Weitergabe des technischen Wissen, das Motivieren, die Unterstützung, wenn ich mich ungeschickt angestellt habe und die freundschaftliche Atmosphäre in der Gruppe! Besonderer Dank gilt auch Prof. Dr. Kevin Pagel, der sich bereit erklärt hat, für diese Arbeit als Zweitgutachter zu fungieren und teilweise unbewusst auf unterschiedlichen Wegen spannende Proben an mich herangetragen hat. Prof. Dr. Gerard Meijer möchte ich für die Aufnahme in die Abteilung Molekülphysik des Fritz Haber Institut der Max Planck Gesellschaft und das Bereitstellen der Infrastruktur danken.

Ein besonders großer Dank geht an Maike Lettow. Danke für das unermüdliche und zeitintensive Einarbeiten am iMob 2.0, für die vielen Stunden Gerät tunen, fürs Fragen beantworten und das Nach-Hause-Schicken. Trotz der knappen Zeit, gab es immer Raum für nette, freundschaftliche Gespräche!

Danke an das Team um Dr. Wieland Schöllkopf und Sandy Gewinner für das Bereitstellen von vielen Photonen während der FHI FEL Strahlzeiten oder des HeNe-Lasers zum Aufsetzen des Strahlengangs in unser Gerät.

Außerdem möchte ich mich bei Klaus-Peter Vogelgesang, Sebastian Kray und Stefan Schlichting für die große Hilfsbereitschaft bei technischen Problemen und Anliegen bedanken.

Jerome war mir eine große Hilfe bei der Auswertung der vielen Massenspektren zum Tagging-Verhalten; danke!
A big thank you also to Martín for cheering me up, when I was talking about problems only and him regarding to them as challenges or puzzles rather than problems. Thanks to Gergő for his patience to see if we can get proteins through all the ion optics.
Vielen Dank an Carla, Katja, Gergő, Katharina, Kim, Maike, Markó und Martín in der MP Enklave in der Haber Villa für die nette und konstruktive Atmosphäre und das Kekse-Teilen! Allen anderen Mitgliedern der Helden-Pagel Gruppe und der MP danke ich für eine unvergessliche Zeit und eine tolle, hilfsbereite Atmosphäre.

Alex, Daniel, Jan, Justus, Paul und meiner Uppsala Gang möchte ich für die freundschaftliche Unterstützung, das Aufmuntern und den sportlichen Ausgleich danken!

Besonderer Dank gilt meinen Eltern, die mir meine studentische Laufbahn in finanzieller und ideeller Hinsicht überhaupt erst ermöglicht haben. Meinem Bruder Christoph danke ich für sein offenes Ohr und unseren reflektierten Austausch.

Ganz zum Schluss möchte ich meinem *partner in crime* Charlotte danken; für die immerwährende Unterstützung, das Ertragen meiner Prioritäten und den Ausgleich neben der Wissenschaft.

A. Appendix

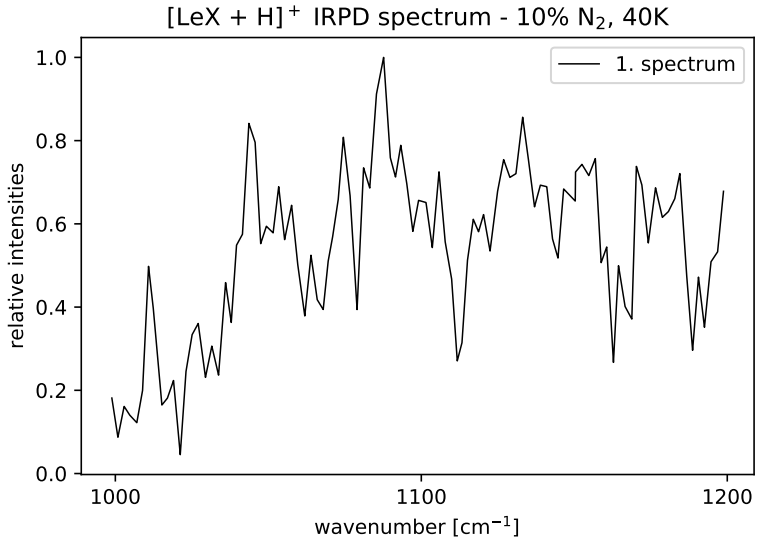

Fig. A.1.: IRPD spectrum of protonated Le^{x}. Spectral features only faintly remind of the IR spectra obtained using the helium nanodroplet experiment.[12]

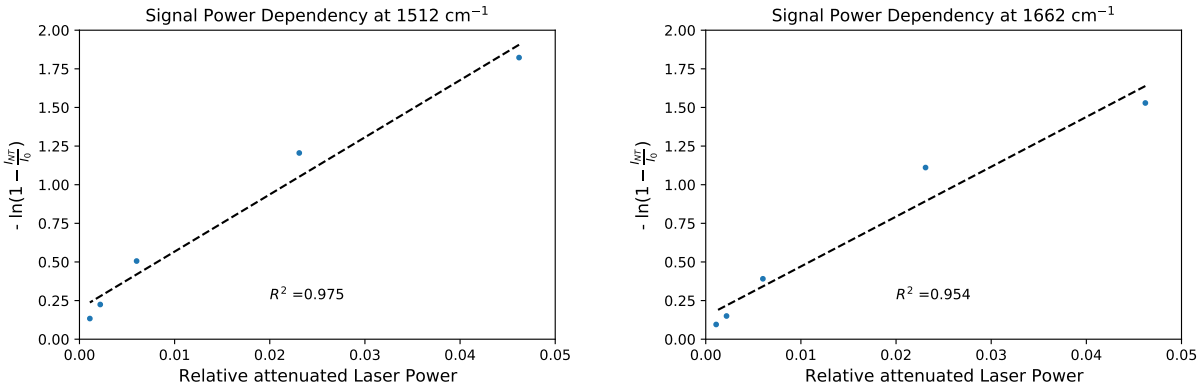

(a) **(b)**

Fig. A.2.: The Influence of the Laser Intensity on the Ion Signal in the ToF mass spectrometer at 1512 cm^{-1} and 1662 cm^{-1}. The depletion of messenger tags from ions is monitored as fraction of the total observed ion signal relative to the attenuated laser power.

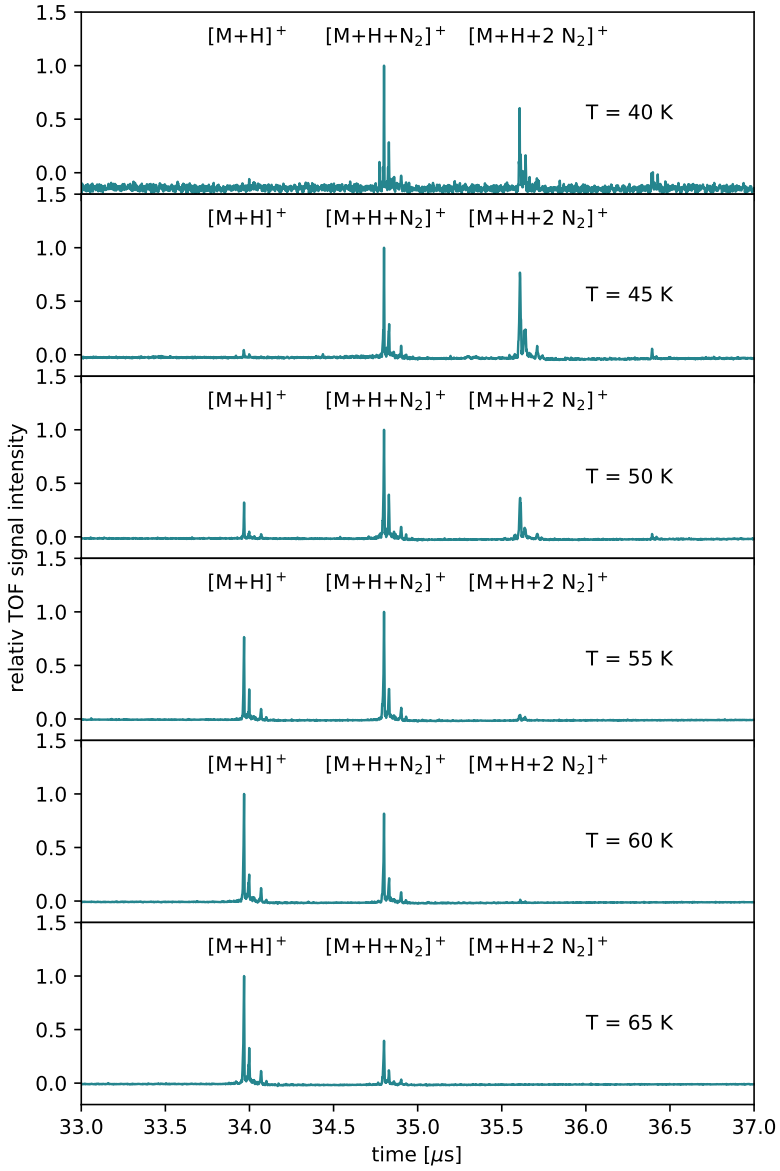

Fig. A.3.: Mass spectra of protonated leucine-enkephalin to evaluate the temperature dependency of messenger tagging. Spectra acquired for the temperatures indicated at a pressure of 5×10^{-6} mbar, and 4 % of N_2 in the buffer gas mixture.

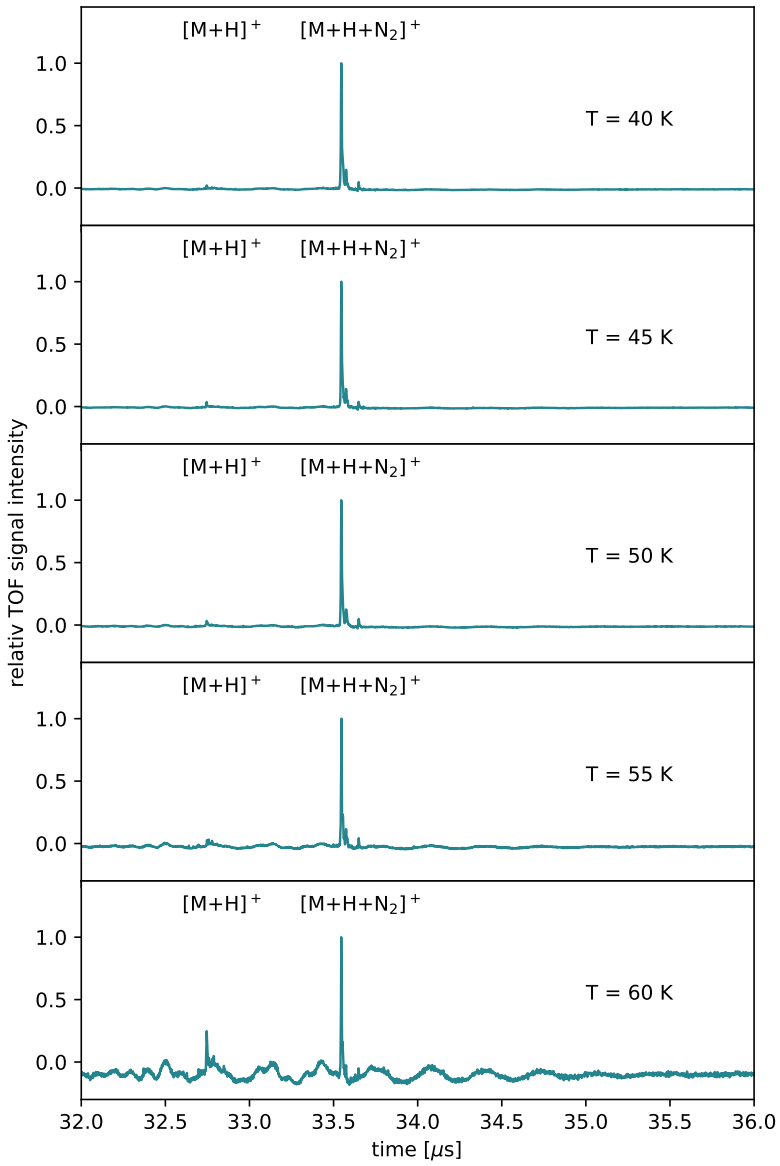

Fig. A.4.: Mass spectra of protonated leucine-enkephalin to evaluate the temperature dependency of messenger tagging after remodelling of the buffer gas tubing. Spectra acquired for the temperatures indicated at a pressure of 1.6×10^{-6} mbar, and 5 % of N_2 in the buffer gas mixture.

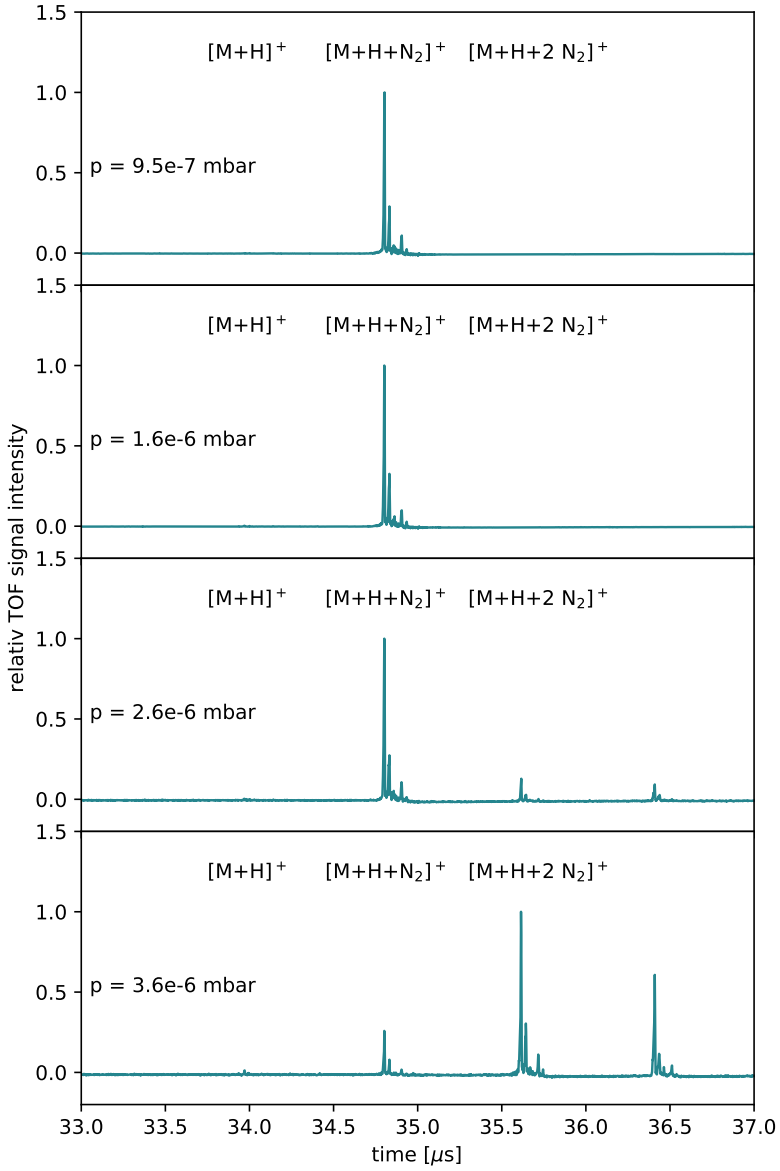

Fig. A.5.: Mass spectra of protonated leucine-enkephalin to evaluate the pressure dependency of messenger tagging. Spectra for the pressures indicated were acquired at 45 K, using 5 % N_2 in helium as buffer gas.

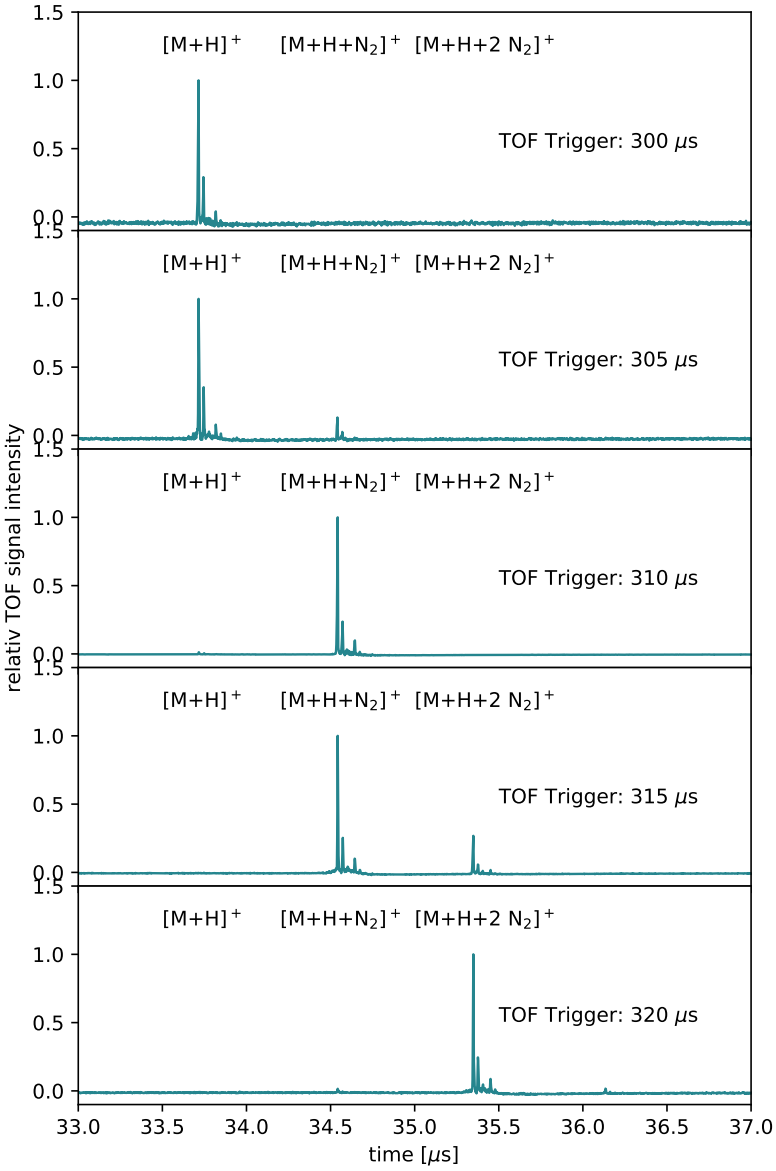

Fig. A.6.: Mass spectra of protonated leucine-enkephalin to evaluate the trigger dependency of the observed messenger tagged species. Spectra were acquired at a temperature of 45 K, a pressure 1.6×10^{-6} mbar, and 7.5 % N_2.

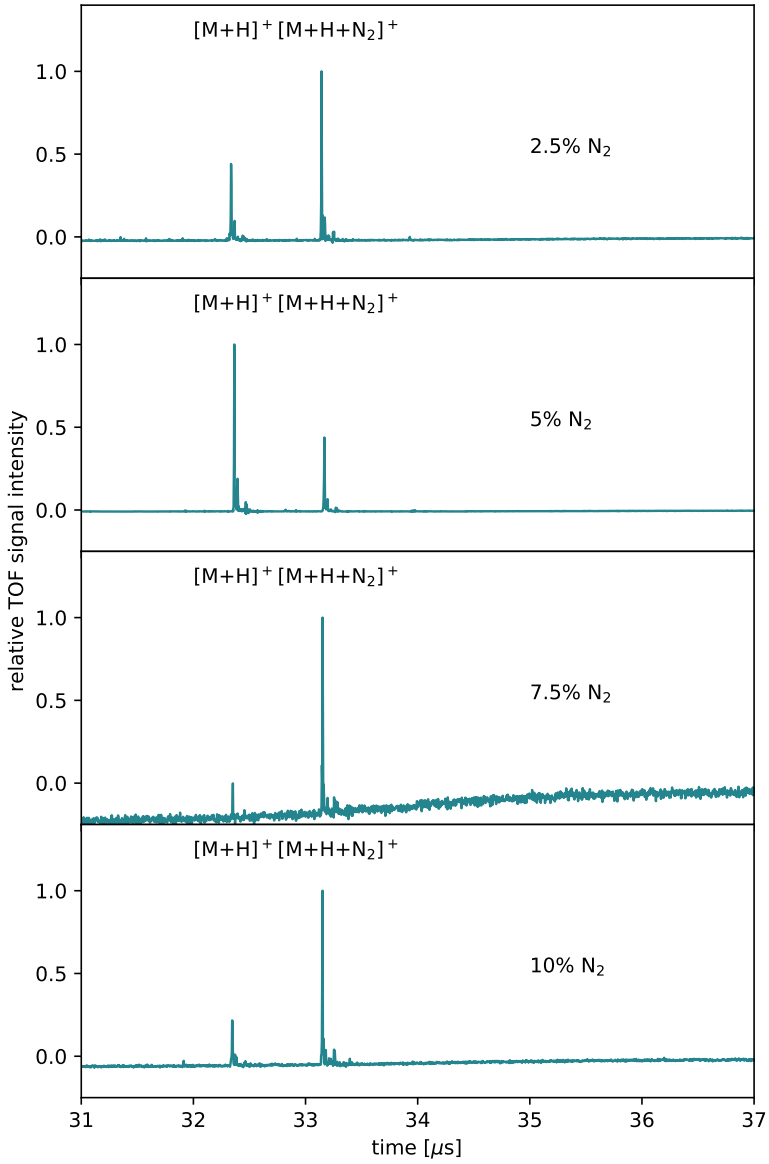

Fig. A.7.: Mass spectra of sodiated Lewis X to evaluate the N_2 dependency of messenger tagging. Spectra were recorded at 40 K and a pressure of 3×10^{-6} mbar.

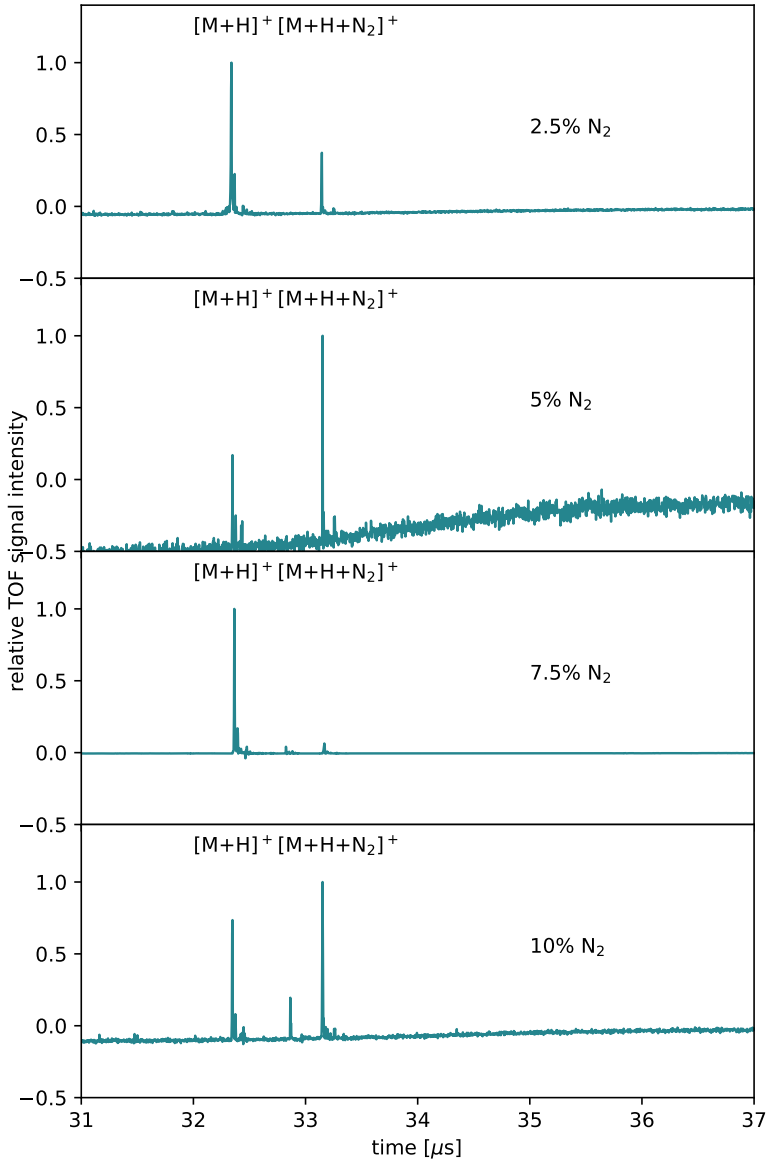

Fig. A.8.: Mass spectra of sodiated Lewis X to evaluate the N_2 dependency of messenger tagging. Spectra were recorded at 45 K and a pressure of 3×10^{-6} mbar.